THE UNIVERSITY OF ADELAIDE

DEPARTMENT OF MECHANICAL ENGINEERING

AN INVESTIGATION INTO THE CHARACTERISTICS

of

TAPERED AND STEPPED LAND HYDROSTATIC JOURNAL BEARINGS

by

ALLAN L. CARPENTER B.E.

Thesis for the Degree

of

DOCTOR OF PHILOSOPHY

November, 1969

TABLE OF CONTENTS

SUMMARY

This thesis deals with an investigation initiated in the Mech-
anical Engineering Department of the University of Adelaide to ex-
amine the characteristics of two types of externally pressurised
journal bearings.   The journal configurations investigated were

(a)   journal with tapered lands, and

(b)   journal with stepped lands.

The effects of varying the journal geometry and the operating
conditions on the load carrying capacity, leakage flow and angular
stiffness were examined.   The effects of pressure ratio, fluid
inertia and flow choking, encountered in initial experimental test-
ing, were also thoroughly investigated, both theoretically and ex-
perimentally.

The theoretical analyses showed that both the tapered and the
stepped land forms were subject to a significant degree of circum-
ferential (short circuiting) flow, the effect of which is to de-
crease the load carrying capacity.   An invesigation of this phen-
omenon showed that the load carrying capacity of both tapered and
stepped land configurations can be improved by adding flow-straight-
ening vanes to the lands.

The results of the theoretical analysis, which are closely
confirmed by experimental evidence, lead to the conclusions that:-

(1)   The Reynold's equation can be used to evaluate the performance
characteristics (load capacity, leakage flow and righting torque)

of the bearing configurations discussed in this thesis, provided
that, in the compressible flow case, the lubricant flow does not
become choked. If it is required to determine these character-
istics for choked flow conditions, corrections must be applied to
the 'Reynolds' analysis. However, it is considered that bearings
would rarely be required to operate in the choked condition in
practice.

(2)   The assumption of isothermal flow in the clearance space is
valid for both incompressible and compressible flows, except (in
the compressible flow case) when choked flow conditions occur.

(3)   The effect of lubricant compressibility is to decrease the
load carrying capacity and to increase the leakage flow and the
righting torque.

(4)   The effect of the pressure ratio ($PR = \dfrac{P_{INLET}}{P_{OUTLET}}$) with incompress-
ible lubricants is negligible. With compressible lubricants, an
increase in the pressure ratio results in a decrease in the load
coefficient (C_f) and an increase in the flow and moment coefficients
(C_q and C_m) from the values obtained for incompressible flow. At
very low pressure ratios ($PR \rightarrow 1$) the values of these coefficients
closely approach the values obtained for incompressible flow.

(5)   The load coefficient (C_f) varies approximately linearly with
eccentricity ratio (E), both for incompressible flow and for
compressible flow at a given pressure ratio. The radial stiffness
of the bearing (K_r) is therefore constant throughout the clearance.

(6)   The maximum load coefficient (C_f) for tapered land bearings
with length ratios (L) in the range 0.5 to 2.0 is developed at a
taper ratio (T) in the region of 1. The maximum values of the
load coefficient, for length ratio L = 1, are:-

(a) C_f = 0.20 for incompressible flow

(b) C_f = 0.16 for compressible flow

The maximum load coefficient for stepped land bearings is
developed when the step length ratio (SLR) is in the range 0.1 to
0.2, with the step depth ratio (SDR) in the range 1.0 to 2.0. The
maximum values of the load coefficient, for length ratio L = 1,
are:-

(c) C_f = 0.28 for incompressible flow

(d) C_f = 0.20 for compressible flow

(7)   The angular stiffness (K_a) of both tapered and stepped land
bearings is less than that of a parallel land configuration.
However, the parallel land bearing has no radial load carrying
capacity.

(8)   The load carrying capacity of both tapered and stepped land
configurations can be improved by adding flow straightening vanes
to the lands. For bearings with length ratio L = 2.0, improve-
ments in the load capacity of the order of 30% for tapered land
and 80% for stepped land configurations were recorded.

(9)   The tapered and stepped land bearing configurations are
characterised by ease of manufacture (these bearings have been

moulded in plastic), operation (an industrial compressed air supply was used to operate prototype instruments fitted with these bearings), and maintenance (the component parts are simple, and require no specialised servicing equipment). It is considered therefore that bearings of these types are suitable for industrial applications.

(10)   There is an optimum configuration, whether tapered or stepped land, for any application. Adequate information has been presented for any such configuration to be determined.

STATEMENT OF ORIGINALITY

This thesis contains no material which has been
accepted for the award of any other degree or
diploma in any University.   To the best of the
author's knowledge and belief, this thesis
contains no material previously published or
written by another person, except where due
reference is made in the text.

Allan L. Carpenter

November, 1969

ACKNOWLEDGEMENTS

1   INTRODUCTION

In many industrial applications, fluid film bearings are unable to support the required load because of the low relative speed between the journal and the bearing surfaces. To overcome this situation, external pressurisation is employed, the lubricant being supplied under pressure to the clearance space.

In the case of oil lubricated bearings the hydrodynamic lift generated at the operating speed is normally sufficient to carry the design load. External pressurization is then required only during starting and stopping. However, when a gas is used as the lubricant its low viscosity results in low aerodynamic lift, even at high speeds. External pressurization is then often found to be necessary over the full operating range of speeds.

Hitherto, various workers in this field have reported on investigations carried out on externally pressurised bearings of a design now referred to as the externally compensated type. These bearing assemblies consisted of a cylindrical journal and a bearing shell having a set of orifices machined into it, through which the lubricant was supplied to the clearance space (1).

During an investigation (2) into the stiction of piston type hydraulic control valves, an interesting phenomenon was observed. In this investigation the effect of high pressure oil fed to the centre of a dumb-bell shaped piston enclosed in a cylinder was examined. The lands of the piston were tapered so as to produce a converging clearance in the direction of flow. A maldistribution of pressure was noted

in the clearance, which produced an out of balance force tending to centralise the piston. It was thought that this phenomenon could be adapted profitably to hydrostatic bearings. For this reason a theoretical and experimental investigation was initiated in the Mechanical Engineering Department of the University of Adelaide to examine the characteristics of a bearing enclosing a tapered land journal.

The effects of varying the bearing geometry and the operating conditions on the load carrying capacity, leakage flow and angular stiffness were examined.

A similar investigation was also undertaken of a bearing in which the taper along the land was replaced by a single step. The reason for this was that the stepped land configuration, being the closest approximation to the tapered land form, was easier to manufacture.

2   NOMENCLATURE

Variables

c	Radial clearance
d	Nominal bearing diameter
e	Eccentricity
f	Elemental force or load
F	Total force or load on one land
G	External force field/unit mass
K	Bearing stiffness = (load/unit angular displacement)
h	Clearance at position (x, y)
l	Land length = 1/2 bearing length
m	Mass flow/unit circumference, or elemental moment
p	Pressure at position (x, y)
p_1	Supply pressure
p_2	Discharge pressure
Δp	Pressure drop = $p_1 - p_2$
q	Elemental leakage flow
Q	Total leakage flow over one land
r	Nominal bearing radius
s	Radial step depth
t	Radial taper decrement over length of land
u	x-component of fluid velocity
v	y-component of fluid velocity
w	z-component of fluid velocity
U	Bearing or journal surface velocity in x direction

V	Bearing or journal surface velocity in y direction
W	Bearing or journal surface velocity in z direction
x	Axial location co-ordinate
y	Circumferential location co-ordinate
z	Radial location co-ordinate
δ	Finite difference interval
μ	Dynamic viscosity of lubricant
ρ	Density of lubricant
θ	Polar circumferential location
ϕ	Transformed pressure variable $= p^2$, or angle of tilt

Dimensionless Ratios and Coefficients

A	Angularity ratio $= \dfrac{\theta}{c}$
C_f	Load coefficient $= \dfrac{F}{\Delta p.l.d}$
C_m	Moment coefficient $= \dfrac{M}{\Delta p.l.d}$
C_q	Flow coefficient $= \dfrac{Q.\mu.l}{\Delta p.d.C}$
E	Eccentricity ratio $= \dfrac{e}{c}$
H	Dimensionless clearance $= \dfrac{h}{c}$
L	Length ratio $= \dfrac{l}{r} = \dfrac{2l}{d}$
P	Dimensionless pressure $= \dfrac{p}{\Delta p}$
PR	Pressure ratio $= \dfrac{p_1}{p_2}$
SDR	Step depth ratio $= \dfrac{s}{c}$
SLR	Step length ratio $= \dfrac{l'}{l}$

T   Taper ratio $= \dfrac{t}{c}$

X   Dimensionless axial location parameter $= \dfrac{x}{l}$

Y   Dimensionless circumferential location parameters $= \dfrac{y}{2\pi r}$

3   THEORETICAL CONSIDERATIONS

3.1   General

Figure 1 shows the configuration of an externally pressurised bearing of the tapered land type. The assembly consists of a cylindrical bearing shell and a journal of dumb-bell form, tapered to produce a converging clearance in the direction of flow. The lubricant is fed to a central annulus at a pressure p_1 and allowed to flow through the clearance to a pressure p_2. If the journal is concentric with the bearing, then the pressure in any plane normal to the axis will be constant around the clearance, and no out of balance force will exist. However, if the journal is displaced radially in the bearing, then the circumferential pressure distribution in such a plane will no longer be constant, and an out of balance force will be set up tending to centralise the journal. For given pressures p_1 and p_2 the magnitude of this force will depend on the position of the journal within the shell, and will be a maximum when it contacts the bore. It should perhaps be mentioned that the same effect would be produced if the tapers were provided in the shell and the journal was made cylindrical. However, practical considerations favour the former arrangement.

In order to derive the load and flow characteristics of the bearing it was first necessary to determine the pressure distribution in the clearance space. This required the solution of the equation describing the flow regime in the clearance space, viz.

FIGURE 1   Tapered land journal bearing (parallel alignment)

$$\frac{\partial}{\partial x}\left(\frac{\rho h^3}{\mu}\cdot\frac{\partial p}{\partial x}\right) + \frac{\partial}{\partial y}\left(\frac{\rho h^3}{\mu}\cdot\frac{\partial p}{\partial y}\right) = 0 \qquad \ldots(1)$$

subject, of course, to the appropriate boundary conditions. The derivation of equation (1) is given in Appendix I.

In subsequent sections both incompressible and compressible flow cases are considered.

3.2   Incompressible flow

For incompressible flow, isothermal conditions (and hence constant viscosity) and constant density may be assumed (3). Equation (1) therefore reduces to

$$\frac{\partial}{\partial x}\left(h^3\cdot\frac{\partial p}{\partial x}\right) + \frac{\partial}{\partial y}\left(h^3\cdot\frac{\partial p}{\partial y}\right) = 0 \qquad \ldots(2)$$

which in non-dimensional form can be written as

$$\frac{\partial}{\partial X}\left(H^3\,\frac{\partial P}{\partial X}\right) + \left(\frac{L}{2\pi}\right)^2\cdot\frac{\partial}{\partial Y}\left(H^3\cdot\frac{\partial P}{\partial Y}\right) = 0 \qquad \ldots(3)$$

The solution of equation (3) gives the non-dimensional pressure (P) at any point (X, Y) in the clearance space.

A general analytical solution to satisfy the appropriate boundary conditions was not possible, and it was necessary for recourse to be had to approximate methods. However, it was possible to

obtain exact solutions for the two limiting cases of (a) very short bearings (L = 0), and (b) very long bearings (L = ∞).

3.2.1 Case 1. Short bearing (L = 0)

With L = 0 the second term in equation (3) becomes zero, and equation (3) reduces to:-

$$\frac{\partial}{\partial X}(H^3 . \frac{\partial P}{\partial X}) = 0 \qquad \qquad ...(4)$$

Expanding equation (4) gives

$$\frac{\partial P}{\partial X} . \frac{3 \partial H}{H \partial X} - \frac{\partial^2 P}{\partial X^2} = 0 \qquad \qquad ...(5)$$

Replacing $\frac{\partial P}{\partial X}$ by a and $\frac{\partial^2 P}{\partial X^2}$ by $\frac{\partial a}{\partial X}$, equation (5) can be written, after re-arranging,

$$\frac{\partial a}{a} = \frac{-3 \partial H}{H} \qquad \qquad ...(6)$$

Integrating equation (6) twice, and replacing the terms in a by their equivalents in P yields

$$P = \frac{f_1(Y)}{2H^2 . H^1} + f_2(Y) \qquad \qquad ...(7)$$

where $f_1(Y)$ and $f_2(Y)$ are functions of Y only.

Applying the boundary conditions

$$P = P_2 \; \left(= \frac{P_2}{\Delta p}\right) \text{ at } X = 0$$

and

$$P = P_1 \; \left(= \frac{P_1}{\Delta p}\right) \text{ at } X = 1$$

to equation (7), and writing

$$H = H_2 \text{ at } X = 0$$

and

$$H = H_1 \text{ at } X = 1$$

the following two equations are obtained.

$$P_2 \; = \frac{-f_1(Y)}{2H_2^2 \cdot H'} + f_2(Y) \qquad\qquad \ldots (8a)$$

$$P_1 \; = \frac{-f_1(Y)}{2H_1^2 \cdot H'} + f_2(Y) \qquad\qquad \ldots (8b)$$

Combining equations (8a) and (8b) yields

$$P_2 + \frac{f_1(Y)}{2H_o^2 \cdot H'} = P_1 + \frac{f_1(Y)}{2H_i^2 \cdot H'}$$

which reduces to

$$f_1(Y) = 2\left(\frac{H_i^2 \cdot H_o^2}{H_o^2 - H_i^2}\right) H' \cdot \Delta P \qquad \ldots(9)$$

and substituting for $f_1(Y)$ in equation (8a) gives

$$f_2(Y) = P_2 - \left(\frac{H_i^2}{H_o^2 - H_i^2}\right) \Delta P \qquad \ldots(10)$$

Substituting for $f_1(Y)$ and $f_2(Y)$ in equation (7), an expression for the pressure (P) is obtained, viz.

$$P = \left(\frac{H_i^2}{H_o^2 - H_i^2}\right)\left(\frac{H_o^2}{H^2} - 1\right) \cdot \Delta P + P_2 \qquad \ldots(11)$$

An expression for the radial clearance, h, at any point x, y, on the bearing surface is derived in Appendix II, viz.

$$h = c + \frac{x}{1} \cdot t - e \cdot \cos\theta \qquad \ldots(12)$$

which, in dimensionless form, can be expressed as

$$H = 1 + X \cdot T - E \cdot \cos(2\pi Y) \qquad \ldots(13)$$

12

Substituting for the non-dimensional location co-ordinate (X) at the boundaries (X = 0 and X = 1) in equation (13) yields

$$H_o = 1 - E.\cos(2\pi Y) \qquad \qquad ...(14)$$

and

$$H_1 = 1 + T - E.\cos(2\pi Y) \qquad \qquad ...(15)$$

and using the expressions for H, H_o and H_1 from equations (13), (14) and (15), equation (11) may be expanded to give the following expression for the pressure (P).

$$P = \left(\frac{(1 + T - E.\cos(2\pi Y))^2}{T(T + 2(1 - E.\cos(2\pi Y)))} \right) ...$$

$$... \left(1 - \frac{(1 - E.\cos(2\pi Y))^2}{(1 + X.T - E.\cos(2\pi Y))^2} \right) + P_2 \qquad ...(16)$$

An expression for the load capacity (F) of the bearing is derived in Appendix III, viz.

$$F = \Delta p.l.d.\pi \int_0^1 \int_0^1 P.\cos(2\pi Y).dX.dY \qquad ...(17)$$

Substituting for P from equation (16) into equation (17) gives

$$F = \Delta p.l.d.\pi \int_0^1 \int_0^1 \left[P + \left(\frac{(1 + T - E.\cos(2\pi Y))^2}{T(T + 2(1 - E.\cos(2\pi Y)))} \right) \cdots \right.$$

$$\left. \cdots \left(1 - \frac{(1 - E.\cos(2\pi Y))^2}{(1+X.T - E.\cos(2\pi Y))^2} \right) \right].\cos(2\pi Y).dX.dY \quad \dots(18)$$

The integration of equation (18) is carried out in Appendix IV and yields for the load capacity the expression

$$F = \frac{\Delta p.l.d.\pi.T}{4E} \left[\frac{T + 2}{\sqrt{(T + 2)^2 - 4E^2}} - 1 \right] \quad \dots(19)$$

The maximum load capacity occurs at full eccentricity when $E = 1$, and thus from equation (19)

$$F_{MAX} = \frac{\Delta p.l.d.\pi.T}{4} \left[\frac{T + 2}{\sqrt{(T + 2)^2 - 4}} - 1 \right] \quad \dots(20)$$

3.2.2   Case 2.   Long bearing (L =∞)

When $L = \infty$ the first term in equation (3), $p\theta$, becomes negligible, and equation (3) reduces to

$$\frac{\partial}{\partial Y}(H^3 \frac{\partial P}{\partial Y}) = 0 \quad \dots(21)$$

Expanding equation (21) and integrating gives

$$\frac{\partial P}{\partial Y} = \frac{f_1(X)}{H^3} \quad \dots(22)$$

and further integration gives an expression for the pressure (P), namely

$$P = \frac{f_1(X)}{H^3} + f_2(X) \qquad \qquad ...(23)$$

where $f_1(X)$ and $f_2(X)$ are functions of X only.

Since the flow will be entirely axial in the plane of symmetry (at $Y = 0$ and $Y = 0.5$) it follows that in that plane $\frac{\partial P}{\partial Y} = 0$. To satisfy this condition in equation (22), $f_1(X)$ must be zero. Hence equation (23), reduces to

$$P = f_2(X) \qquad \qquad ...(24)$$

It will be observed from equation (25) that the pressure at any point in the clearance is independent of Y and dependent only on X. The pressure distribution will therefore have axial symmetry, and no radial out of balance force will be generated. The load coefficient for the bearing with $L = \infty$ will therefore be zero.

3.2.3   Case 3. Finite bearing

As already mentioned, an exact solution of equation (12) is not possible for the finite bearing, and recourse must be had to approximate methods. The relaxation method was used (see Appendix IV) and this yielded a set of pressure values at pre-determined points over the bearing surface.

The load capacity (F) and the leakage flow (Q) can then be
evaluated from the expressions given in Appendix III, viz.

$$F = \Delta p.l.d.\pi \iint_0^1 \int_0^1 P.\cos(2\pi Y).dX.dY \qquad \qquad ...(25)$$

and

$$Q = \frac{\Delta p.d.c^3.\pi}{12\mu.l} \int_0^1 H^3.\frac{\partial P}{\partial X}.dY \bigg|_{X=0} \qquad \qquad ...(26)$$

3.2.4   Angular Stiffness

In many practical applications a journal bearing may not only
be required to support radial load, but also to keep angular
alignment of the journal and bearing within specified limits. A
knowledge of the bearing's ability to resist these angular
deflections (called here the angular stiffness) is of con-
siderable importance. It was decided therefore to examine the
effect of the taper ratio and length ratio on the angular stiff-
ness of tapered land bearings.

For a given journal/bearing configuration, the value of the
angular stiffness will depend on the angle between the journal
and bearing axes. This will be a maximum when the two lands of
the journal contact the bearing shell, as shown in Figure 2.
This position was therefore chosen for the analysis.

An expression for the clearance (h_i) under tilted conditions
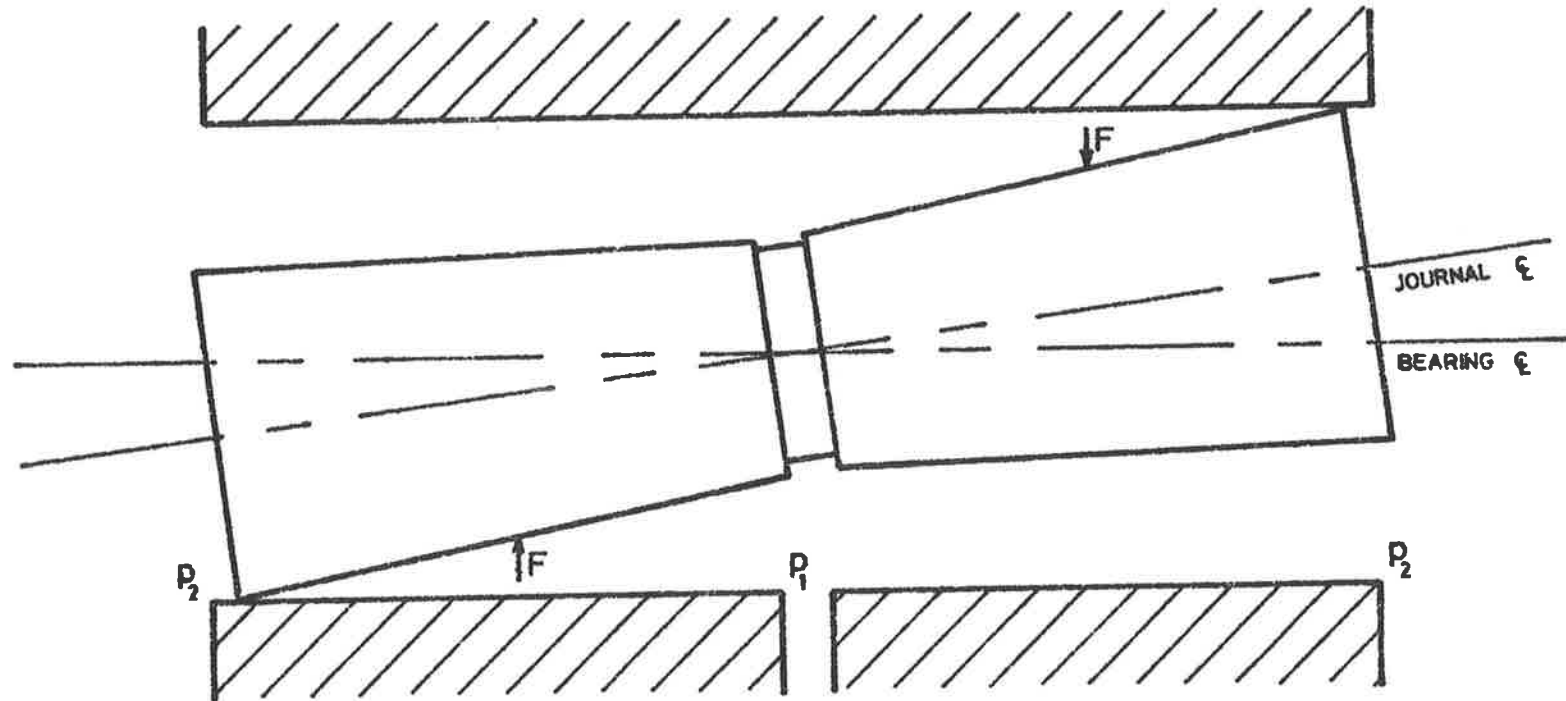is derived in Appendix II, viz.

FIGURE 2   Tapered land journal bearing (tilted alignment)

$$h_{\iota} = c + \frac{x}{l} \cdot t - \frac{(1 - x) \cdot A \cdot c}{l} \cdot \cos\theta$$

which, in dimensionless form, can be expressed as

$$H_{\iota} = 1 + X.T - A.(1 - X).\cos(2\pi Y)$$

With the clearance $H = H_{\iota}$, equation (3), p8, is then solved for the pressure as before.

The righting moment (M) given (Appendix III) by

$$M = \Delta p.l^2.d.\pi \iint (1 - X).P.\cos(2\pi Y).dX.dY \qquad \ldots(27)$$

can then be evaluated numerically.

3.2.5 Incompressible flow results

The results of the analysis are presented in Figures 3 to 9. Typical pressure distributions are shown in Figures 3, 4 and 5. In Figure 3 is shown a pressure field with the pressure represented by the non-dimensional form

$$P = \frac{p}{\Delta p}$$

Computed values at each of the mesh points are given, with the constant pressure lines interpolated. It will be observed that
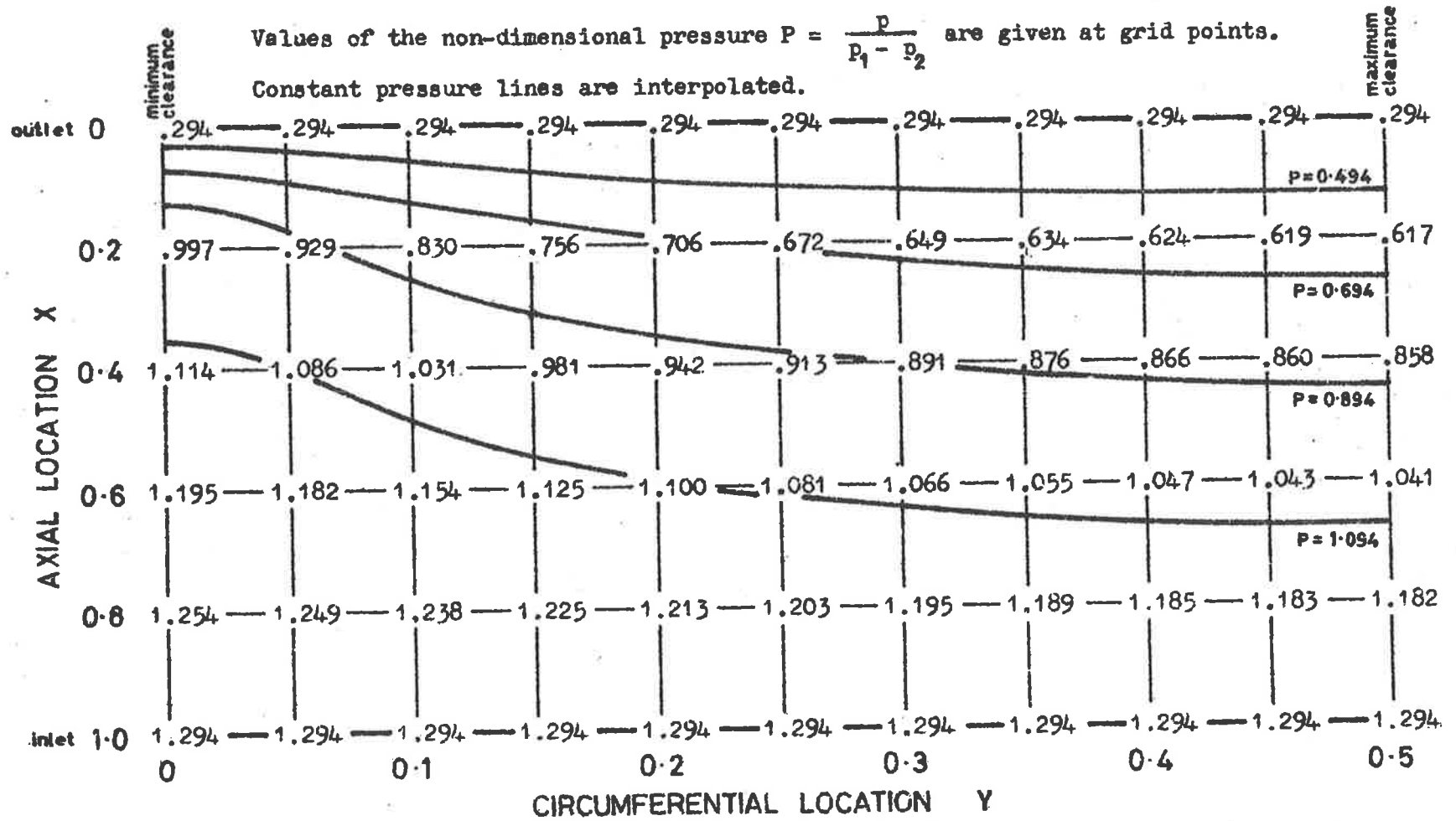
Values of the non-dimensional pressure $P = \dfrac{p}{p_1 - p_2}$ are given at grid points.

Constant pressure lines are interpolated.

minimum clearance | maximum clearance

outlet 0   .294 —— .294 —— .294 —— .294 —— .294 —— .294 —— .294 —— .294 —— .294 —— .294 —— .294

P = 0.494

0.2   .997 —— .929 —— .830 —— .756 —— .706 —— .672 —— .649 —— .634 —— .624 —— .619 —— .617

P = 0.694

AXIAL LOCATION X

0.4   1.114 —— 1.086 —— 1.031 —— .981 —— .942 —— .913 —— .891 —— .876 —— .866 —— .860 —— .858

P = 0.894

0.6   1.195 —— 1.182 —— 1.154 —— 1.125 —— 1.100 —— 1.081 —— 1.066 —— 1.055 —— 1.047 —— 1.043 —— 1.041

P = 1.094

0.8   1.254 —— 1.249 —— 1.238 —— 1.225 —— 1.213 —— 1.203 —— 1.195 —— 1.189 —— 1.185 —— 1.183 —— 1.182

inlet 1.0   1.294 —— 1.294 —— 1.294 —— 1.294 —— 1.294 —— 1.294 —— 1.294 —— 1.294 —— 1.294 —— 1.294 —— 1.294

0   0.1   0.2   0.3   0.4   0.5

CIRCUMFERENTIAL LOCATION   Y

FIGURE 3   Pressure distribution over half the journal land (for L = 2.0, T = 1.0, E = 1.0)
Incompressible flow

18

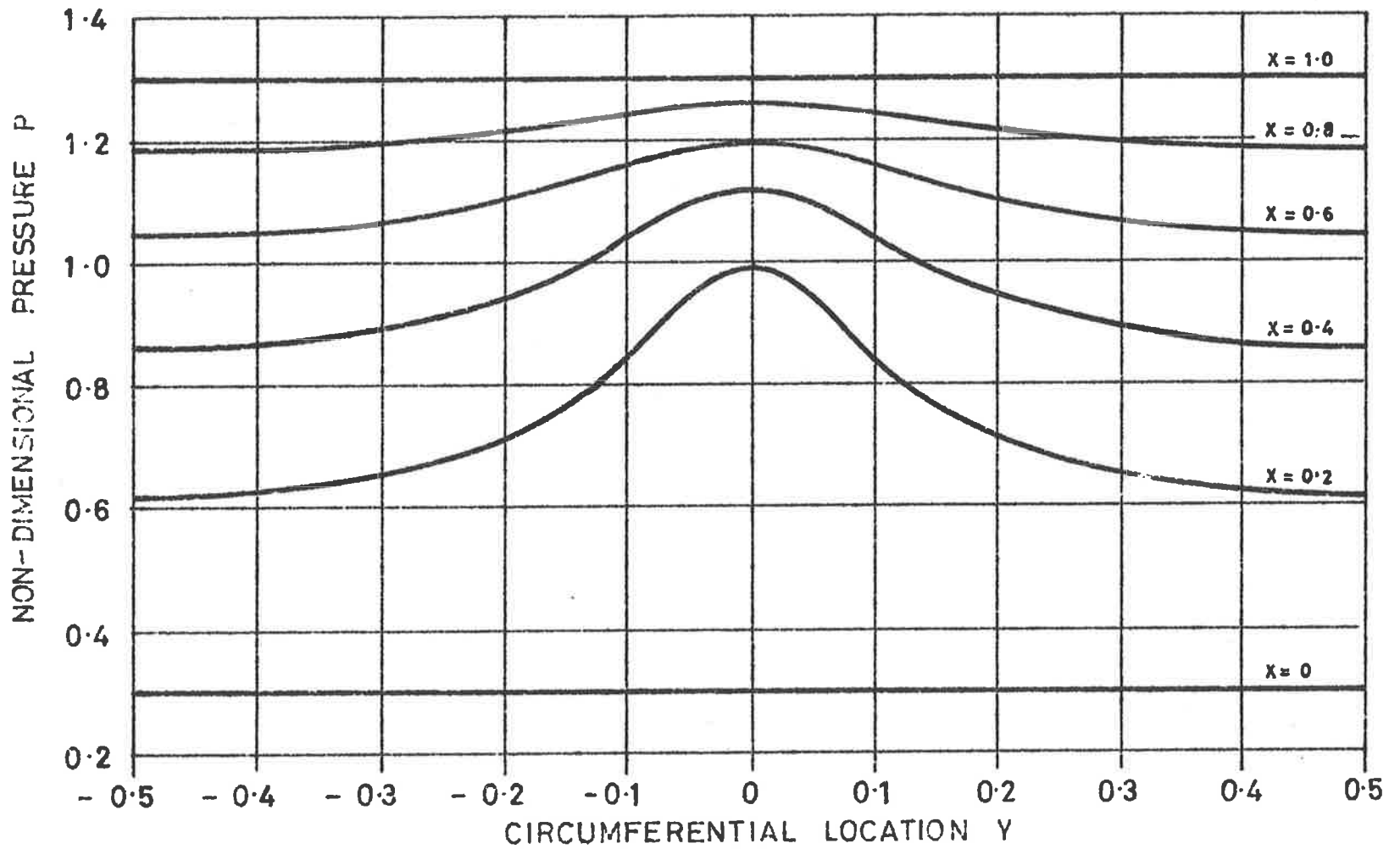FIGURE 4 Circumferential pressure distributions at several transverse stations (for L=2·0, T=1·0, E=1·0) Incompressible flow
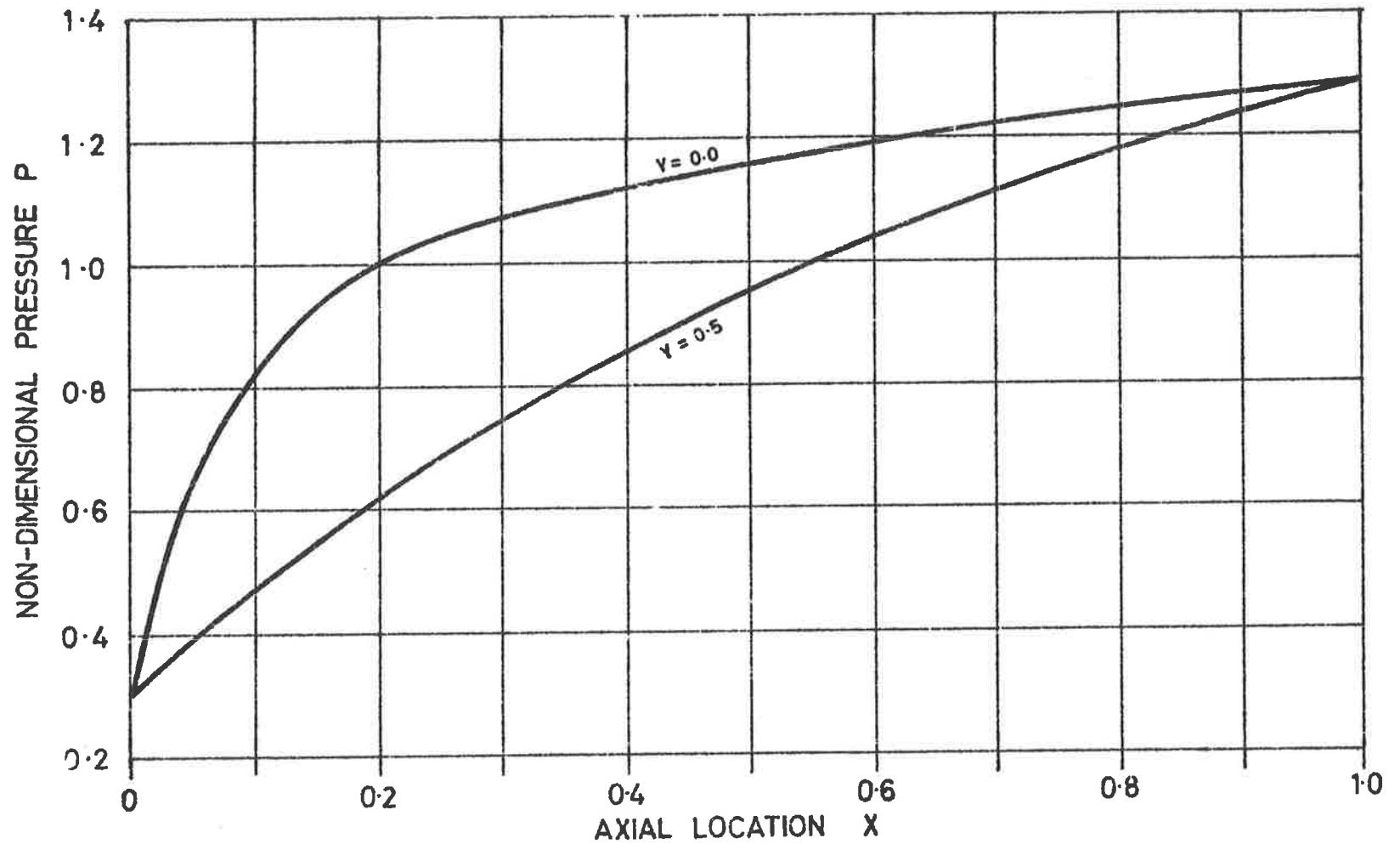
FIGURE 5   Axial pressure distributions in the plane of symmetry
(for L=2·0, T=1·0, E=1·0)   Incompressible flow

the slope of the constant pressure contours is zero at the
boundaries $Y = 0$ ($\theta = 0$) and $Y = 0.5$ ($\theta = 180$) owing to the fact
that the flow at those boundaries is entirely axial. A similar
consideration applies to the curves of Figure 4, where the
circumferential distribution of pressure is presented at a
number of transverse stations. Figure 5 shows the axial
distribution of pressure at two   circumferential stations.

The relationship between the load capacity and the taper ratio
(T) for selected values of the length ratio (L) is shown in Figure
6 where the load capacity is represented by the non-dimensional
load coefficient (C_f). It will be observed that for a given
length ratio the load coefficient reaches a maximum at a part-
icular value of the taper ratio. For length ratios in the range
$0 < L \leqslant 2.0$ (the range covering most practical applications) this
value is in the region of 1.0 and increases as the length ratio
is increased. Also it will be seen that, for a given taper ratio,
the load coefficient decreases as the length ratio increases.
This may be explained as follows.

In very short bearings the friction path of the fluid in the
axial direction is very short compared with that in the circum-
ferential direction. Therefore the circumferential flow will
tend to be negligible compared with the axial flow. In the
limiting case, as the length ratio (L) approaches zero, the ratio
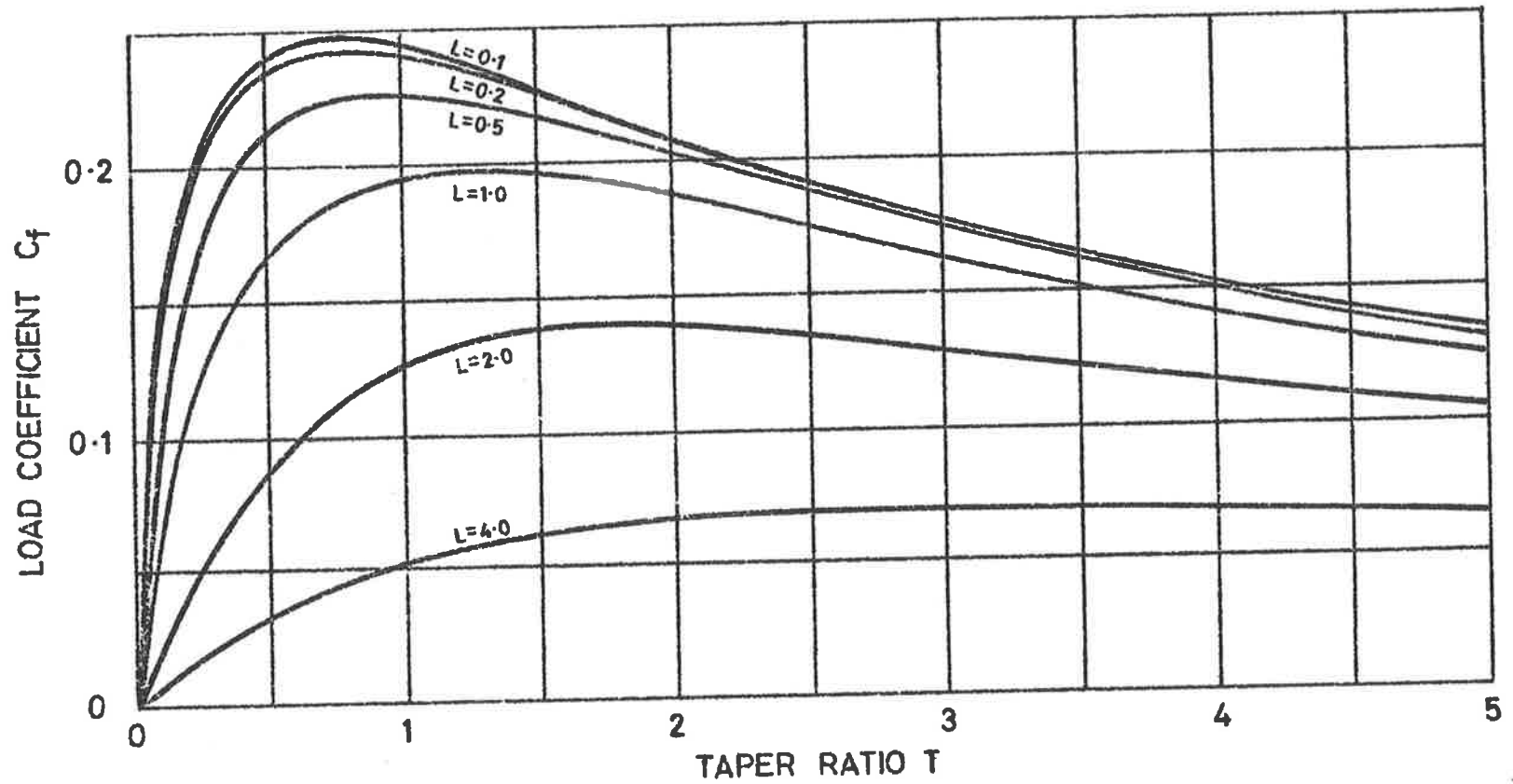of these flows will also tend to zero.

FIGURE 6   Load coefficient against taper ratio (for L=0·1 to 4·0, E=1·0)

Incompressible flow

However, as the length ratio is increased the axial friction path becomes more comparable with the circumferential friction path. This will have the effect of increasing the ratio of the circumferential to axial flows, thus decreasing the pressure in the region of small clearance and increasing it in the large clearance region. This in turn will reduce the load carrying capacity by an amount which will depend on the length ratio. The effect of eccentricity on the load capacity is illustrated in Figure 7 where the load coefficient (C_f) for two journal configurations $(L = 1.0, 2.0: T = 1.0)$ is plotted against eccentricity ratio (E). The trend of these curves indicates that the stiffness (load/unit radial displacement) of this type of bearing increases slightly with increasing eccentricity. This result is at variance with the stiffness characteristic of the externally compensated type of bearing, where the stiffness falls off considerably with eccentricity ratios greater than 0.6. Figure 8 shows the effect of the taper ratio (T) on the leakage flow for selected values of the length ratio (L), where the leakage flow is represented by the non-dimensional flow coefficient (C_q). It will be observed that, within the range analysed, the flow coefficient is almost independent of the length ratio, and varies linearly with the taper ratio.

The effect of eccentricity on the leakage flow is shown in Figure 9 where the flow coefficient (C_q) is plotted against the eccen-
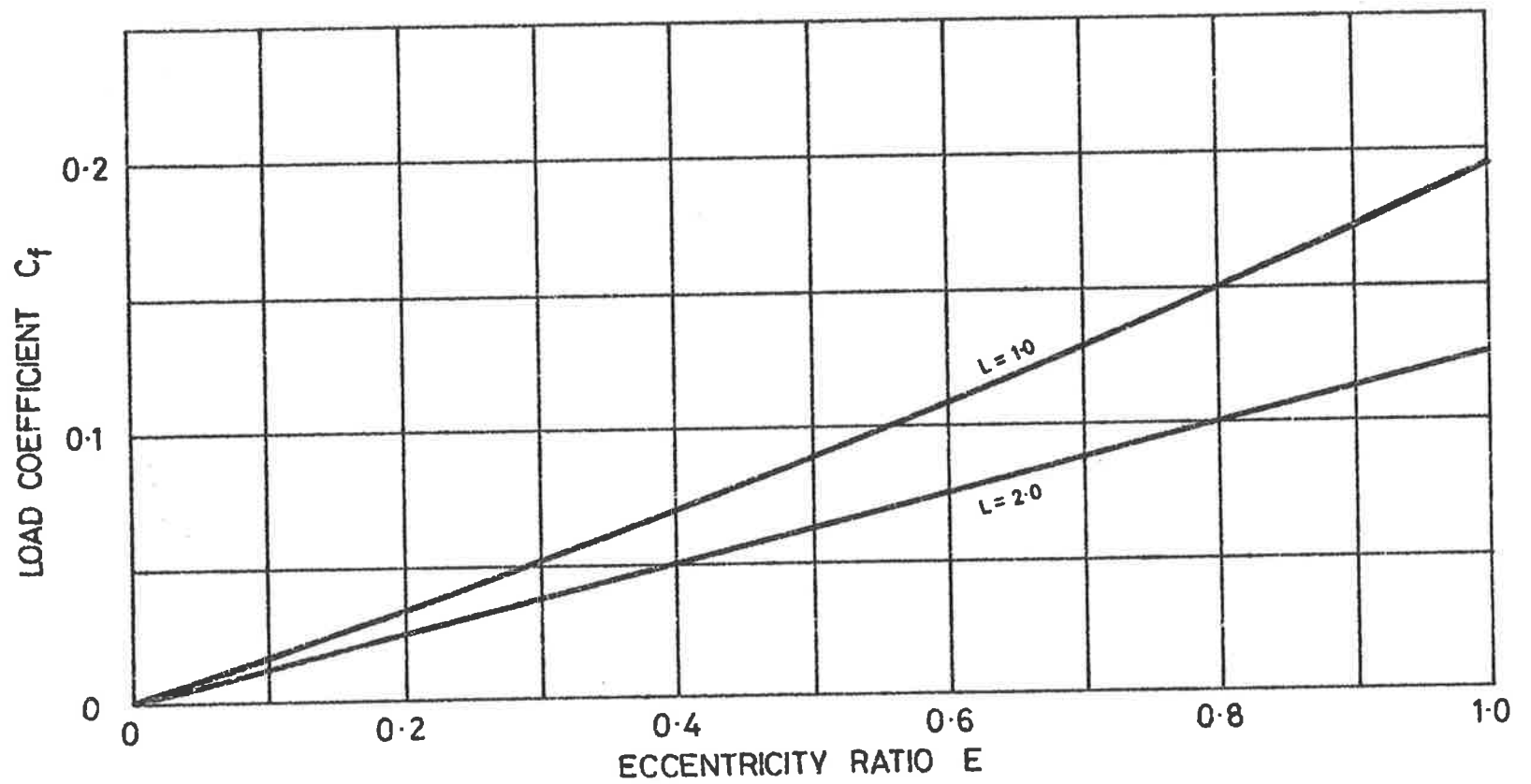
FIGURE 7 Load coefficient against eccentricity ratio (for L=1·0 and 2·0, T=1·0)

Incompressible flow
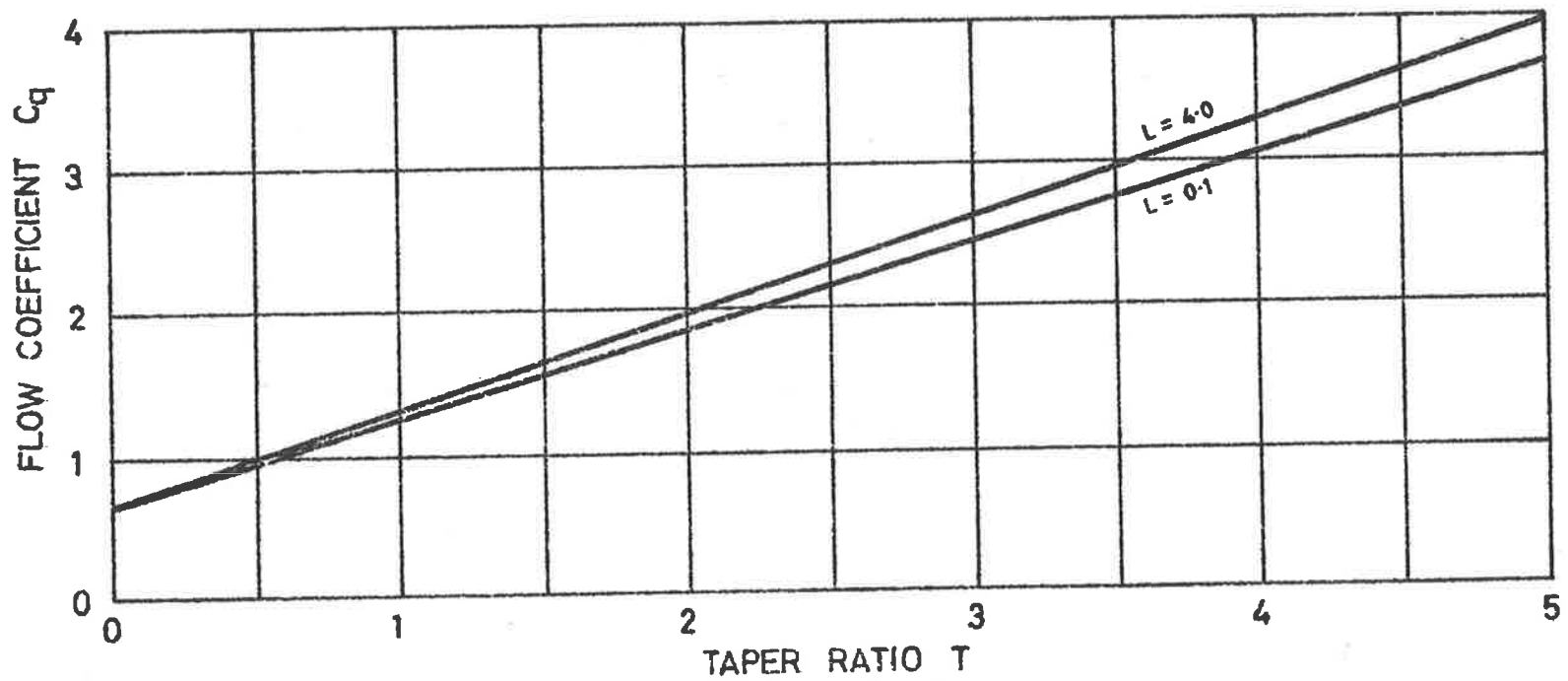
FIGURE 8   Flow coefficient against taper ratio (for L=0·1 and 4·0, E=1·0)

Incompressible flow
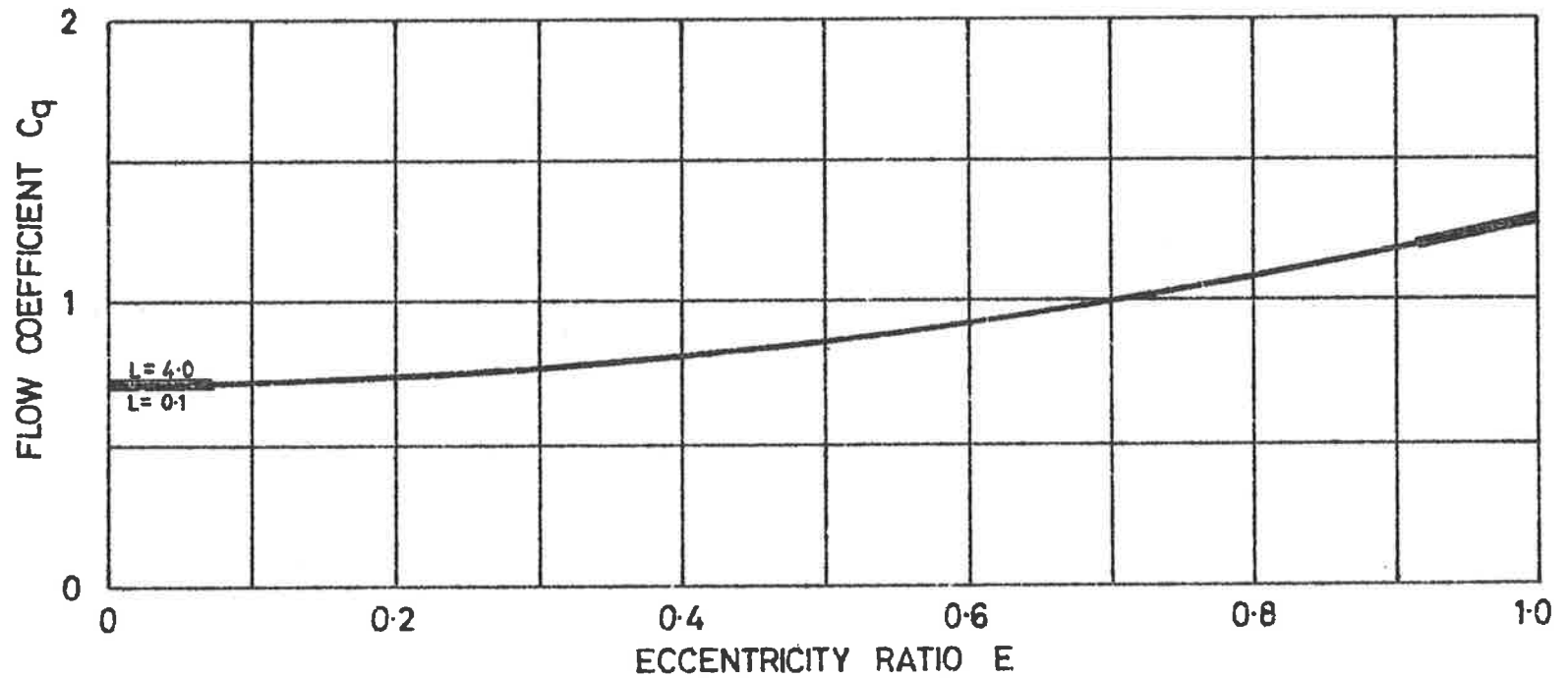
FIGURE 9 Flow coefficient against eccentricity ratio (for L=0·1 to 4·0, T=1·0)
Incompressible flow

tricity ratio (E) for the two journals previously considered
(L = 1.0, 2.0: T = 1.0). As was expected, the leakage increases
with eccentricity up to a maximum at the fully eccentric position
(E = 1.0).

Figure 10 shows axial pressure distributions at two circum-
ferential stations for a fully tilted bearing (see Figure II-2,
Appendix II). It will be observed that both the curve at Y = 0
(the position of minimum clearance), and that at Y = 0.5 (the
position of maximum clearance) are lower than the equivalent
curves for the non-tilted configuration shown in Figure 5.

The relationship between the righting moment (M) and the
taper ratio (T) is shown in Figure 11 for selected values of
the length ratio (L), where the righting moment is represented
by the non-dimensional moment coefficient (C_m). It will be ob-
served that for a given length ratio the moment coefficient de-
creases with increasing taper ratio, and that the maximum moment
coefficient occurs when the taper ratio equals zero - that is,
for a parallel land journal.

3.3 Compressible flow

For compressible flow the assumption that the density is con-
stant is no longer valid. However the assumption that isothermal
conditions prevail in the clearance space is true, as has already
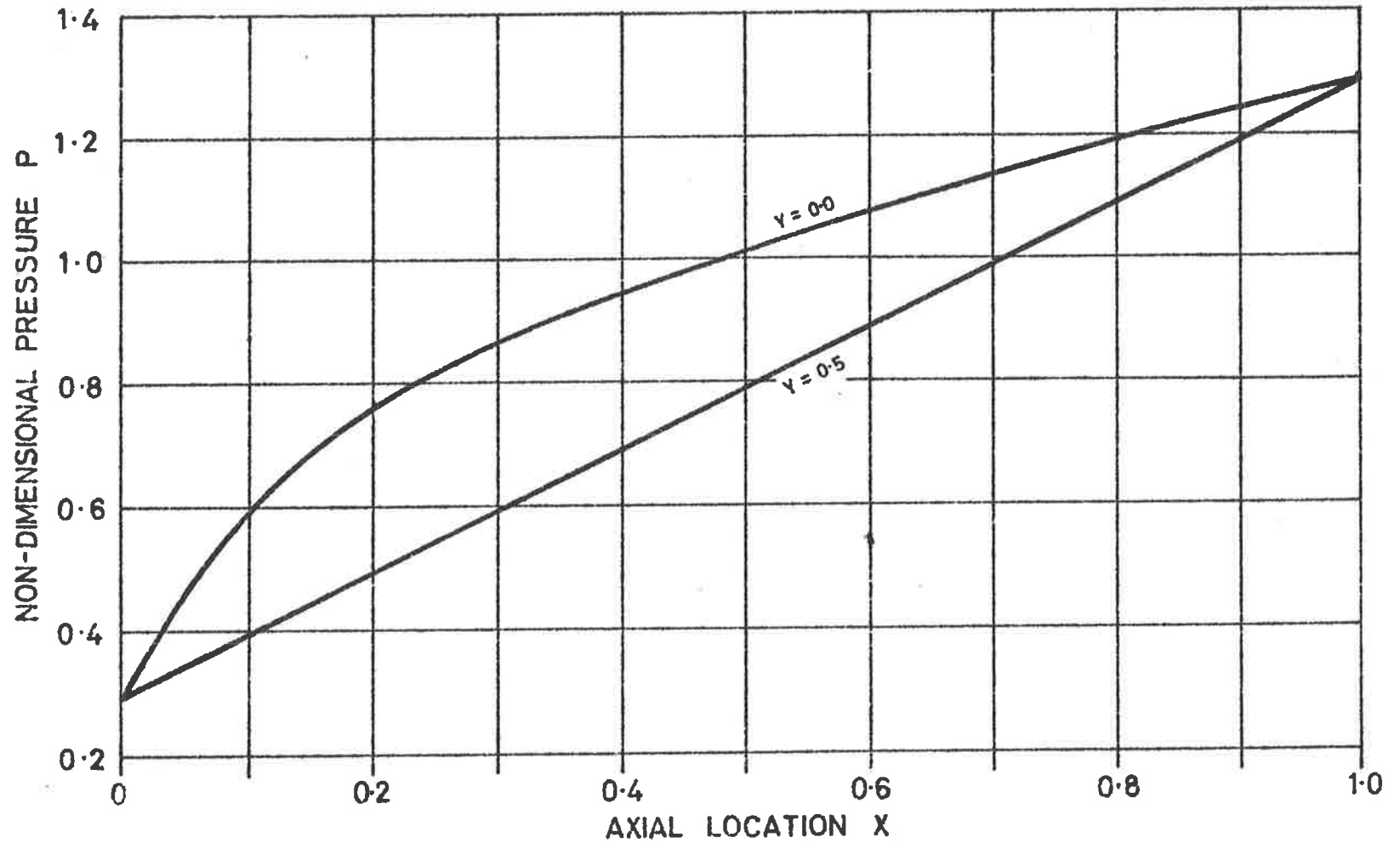
FIGURE 10   Axial pressure distributions in the plane of symmetry – tilted journal (for L= 2·0, T= 1·0, E= 1·0), Incompressible flow.
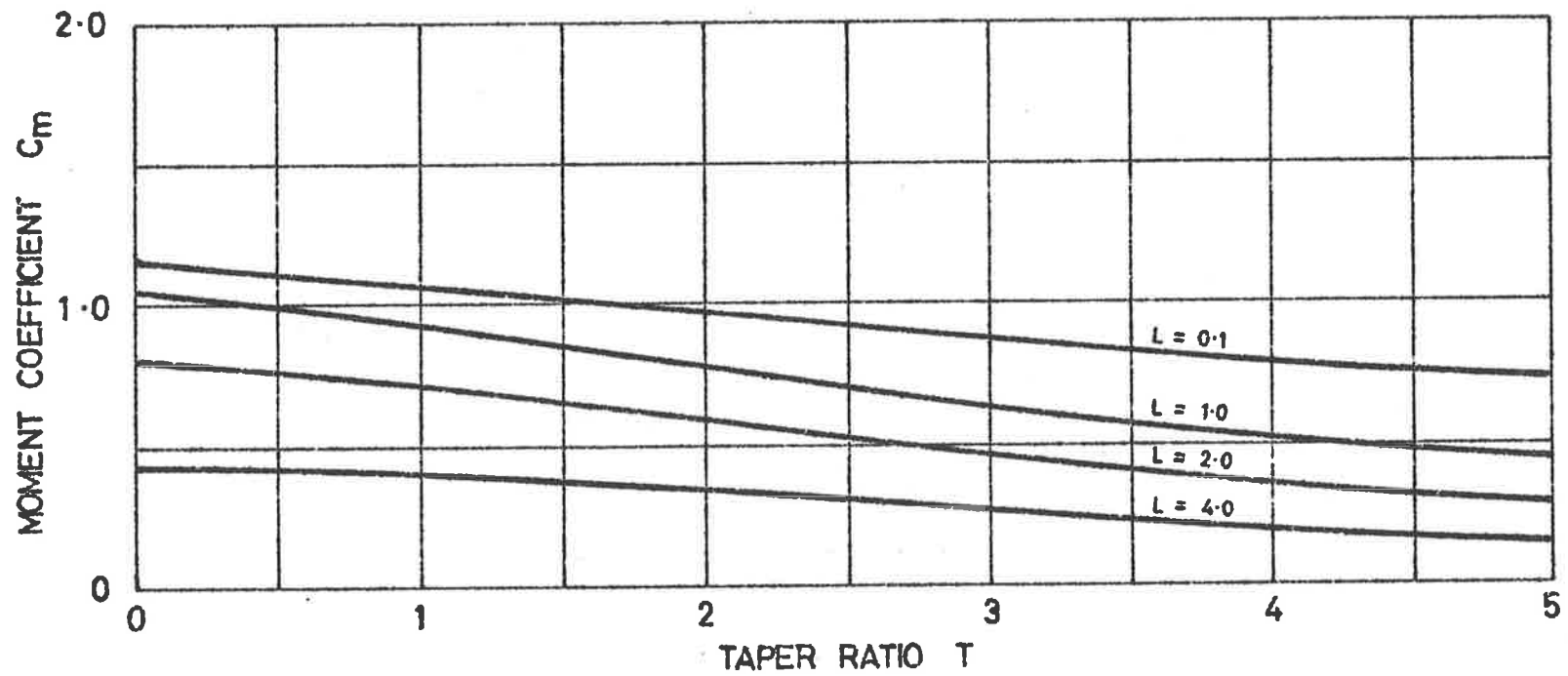
FIGURE 11   Moment coefficient against taper ratio (for L = 0·1 to 4·0, E = 1·0) Incompressible flow

been established by previous investigators (4). For this reason, over a wide range of operating conditions, the viscosity may be taken to be constant.

Using the isothermal relation

$$\frac{p}{\rho} = \text{Constant} \qquad \qquad ...(28)$$

equation (1), p8 , can be expressed as

$$\frac{\partial}{\partial x}\left(ph^3 \cdot \frac{\partial p}{\partial x}\right) + \frac{\partial}{\partial y}\left(ph^3 \cdot \frac{\partial p}{\partial y}\right) = 0$$

which can be written as

$$\frac{\partial}{\partial x}\left(h^3 \cdot \frac{\partial p^2}{\partial x}\right) + \frac{\partial}{\partial y}\left(h^3 \cdot \frac{\partial p^2}{\partial y}\right) = 0 \qquad \qquad ...(29)$$

Attention is drawn to the similarity between equation (29) and equation (2), p8 . The term p in the incompressible case has been replaced by the term p^2 in the equation for compressible flow. The substitution

$$\phi = p^2$$

in equation (29) results in a form identical to that of equation (2),

namely,

$$\frac{\partial}{\partial x}\left(h^3 \cdot \frac{\partial \phi}{\partial x}\right) + \frac{\partial}{\partial y}\left(h^3 \cdot \frac{\partial \phi}{\partial y}\right) = 0 \qquad \ldots(30)$$

The method of solution of equation (2) can then be applied directly to equation (30).

The solution of equation (30) with boundary values given by

$$\phi = (p_2^2) \quad \text{at } x = 0$$
$$\phi = (p_1^2) \quad \text{at } x = 1$$

results in a field of values of ϕ. Values of p are then obtained from

$$p = \sqrt{\phi}$$

A general analytical solution of equation (30) is not possible, but solutions for the two limiting cases of (a) very short bearings ($L = 0$), and (b) very long bearings ($L = \infty$) can be obtained.

3.3.1   Case 1. Short bearing ($L = 0$)

An analysis similar to that used for incompressible flow (Section 3.2.1, p9), when applied to equation (30), results in an expression for a non-dimensional pressure (P_c) identical to

that for incompressible flow (equation (16), p12). The non-dimensional pressure (P_c) is defined by

$$P_c = \frac{\phi}{\phi_1 - \phi_2}$$

$$= \frac{p^2}{p_1^2 - p_2^2} \qquad \ldots(31)$$

Substituting for P from equation (31) into equation (16) gives an expression for the pressure (p),

$$p = \sqrt{p_2^2 + (p_1^2 - p_2^2)\left[\left(\frac{(1 + T - E.\cos(2\pi Y))^2}{T(T + 2(1 - E.\cos(2\pi Y)))}\right). \ldots \ldots \left(1 - \frac{(1 - E.\cos(2\pi Y))^2}{(1 + X.T - E.\cos(2\pi Y))^2}\right)\right]} \qquad \ldots(32)$$

Re-defining the pressure in terms of the non-dimensional expression previously used, ($P = \frac{p}{\Delta p}$) and substituting into the expression for the load capacity of the bearing (equation (17), p12), gives

$$F = l.d.\pi \iint_0^1 \int_0^1 \frac{1}{\Delta p}\sqrt{}.\cos(2\pi Y).dX.dY \qquad \ldots(33)$$

where the term contained by the radical sign is the right hand side of equation (32).

The analytical evaluation of the integral of equation (33) was

found to be too difficult. The integral was subsequently
evaluated numerically.

3.3.2   Case 2. Long bearing $(L = \infty)$

An analysis similar to that used in Section 3.2.2, when
applied to equation (30), p31, yields an expression for the
non-dimensional pressure (P_c), viz.

$$P_c = f_3(X)$$

where the pressure (P_c) is defined in terms of the transformed
pressure variable (ϕ) as

$$P_c = \frac{\phi}{\phi_1 - \phi_2}$$

$$= \frac{p^2}{p_1^2 - p_2^2}$$

Re-writing the expression for P_c in terms of the pressure (p),
gives

$$p = \sqrt{(p_1^2 - p_2^2).f_3(X)}$$

which can be expressed as

$$p = f_4(X) \qquad\qquad \ldots(34)$$

where $f_4(X)$ is a function of X only.

As stated previously (Section 3.2.2) the pressure at any point in the clearance is independent of the circumferential location (Y) and dependent only on the axial location (X). The pressure distribution defined by equation (34) will therefore have axial symmetry, and no out of balance force will be generated. The load coefficient (C_4) of the bearing with $L = \infty$ will therefore be zero.

3.3.3 Case 3. Finite bearing

The solution for the bearing of finite length was obtained by numerical analysis. Equation (30) was solved using the same computer program, with minor modifications, as that used for the incompressible flow case (Appendix VII). The load capacity (F), the leakage flow (Q) and the righting moment (M) of the bearing were determined, as before, by the evaluation of equations (25), (26) and (27), pp 15 and 17. The above computations were carried out for boundary pressure values:-

$p_1 = 50$ p.s.i.g.

$p_2 = 0$ p.s.i.g.

i.e., for a pressure ratio (PR) of 4.4
which were values considered to be easily reproduced in the

experimental testing. However, it was realised that at other pressure ratios, different values of the load, flow and moment coefficients would be obtained, due to the effects of the compressibility of the lubricant. The effect of pressure ratio was therefore investigated by computing these performance coefficients for inlet pressures ranging from 5 to 150 p.s.i.g., with the outlet pressure held at zero p.s.i.g.

There was no such effect apparent in the incompressible flow case, where the performance characteristics proved to be independent of the pressure ratio.

3.3.4   Compressible flow results

The results of the compressible flow analysis are shown in Figures 12 to 23. It can be seen that these curves exhibit the same general shape as do those for incompressible flow (Figures 3 to 11, pp 18 to 28). Furthermore, it can be seen that the effect of compressibility is to reduce the load coefficient and to increase the flow and moment coefficients.

Typical pressure distributions are shown in Figures 12, 13 and 14. Comparison of these with the incompressible flow distributions of Figures 3, 4 and 5, pp 18 to 20, show that higher pressures are maintained in the clearance space with compressible flow, particularly in the region of small clearance. As a consequence, the slopes of the pressure distributions in the axial direction are steeper at exit in the case of compressible flow,
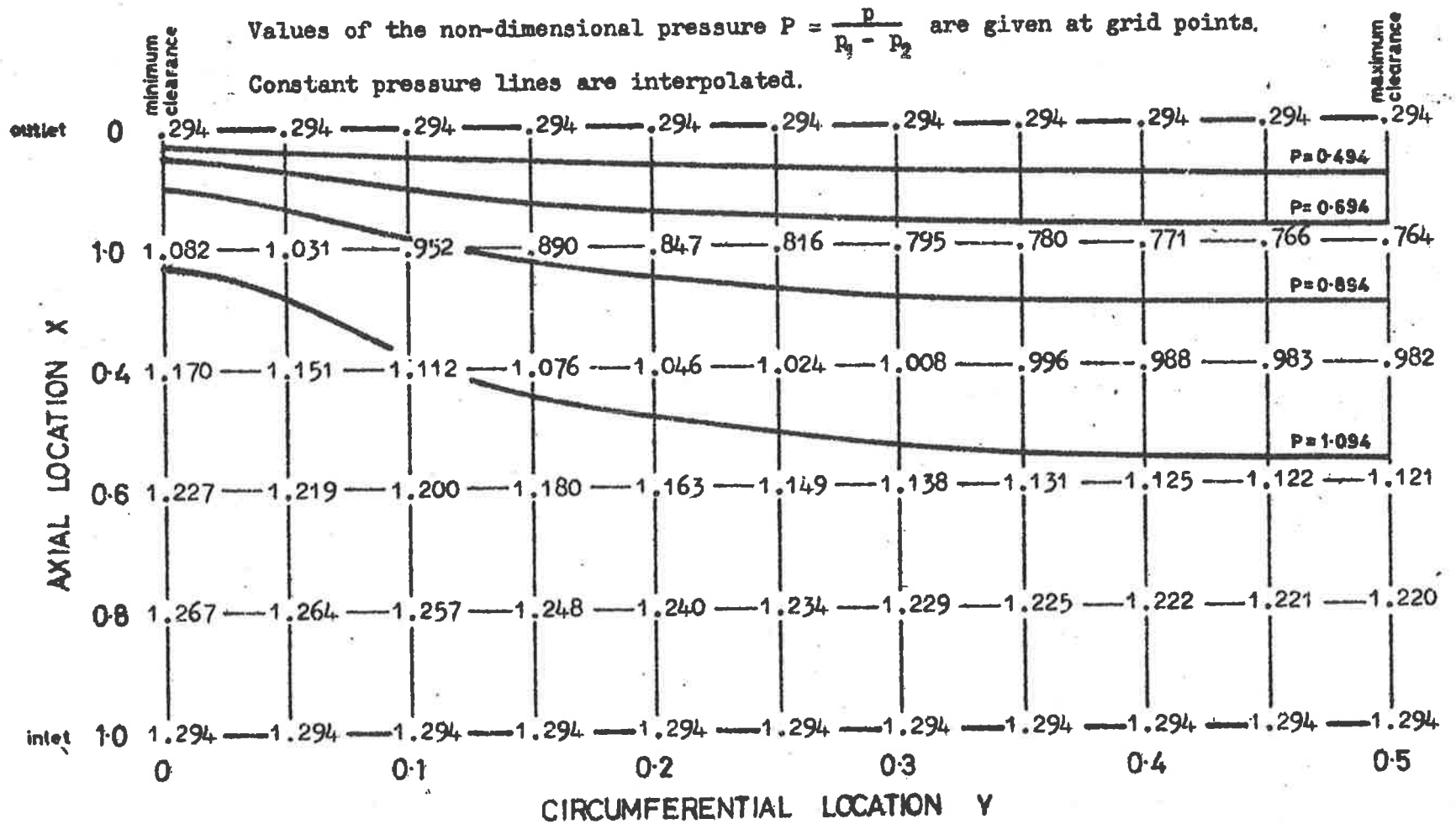
FIGURE 12   Pressure distribution over half the journal land (for L=2·0, T=1·0, E=1·0)
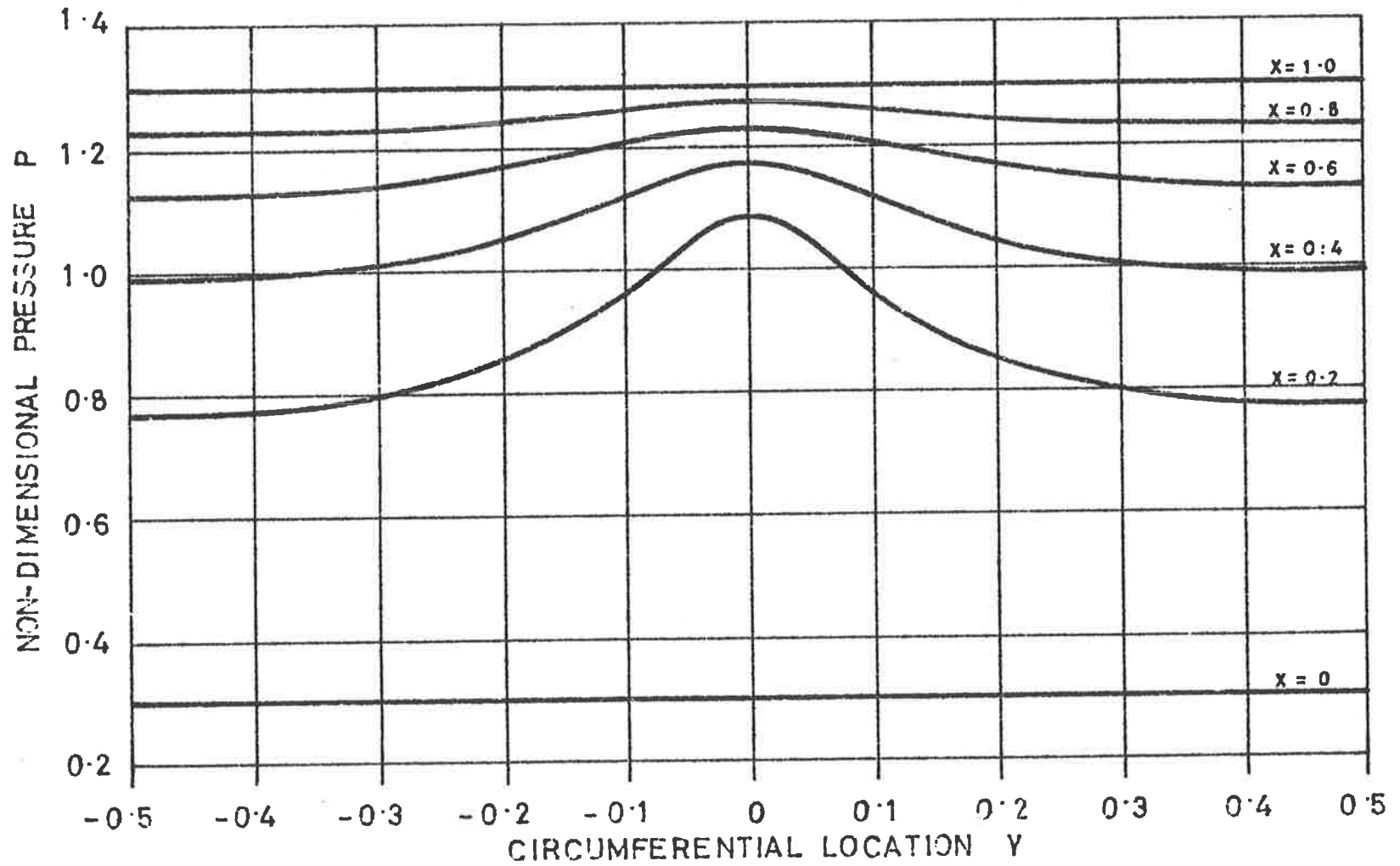Compressible flow (PR = 4·4)

FIGURE 13 Circumferential pressure distributions at several transverse stations (for L=2·0, T=1·0, E=1·0) Compressible flow (PR=4·4)
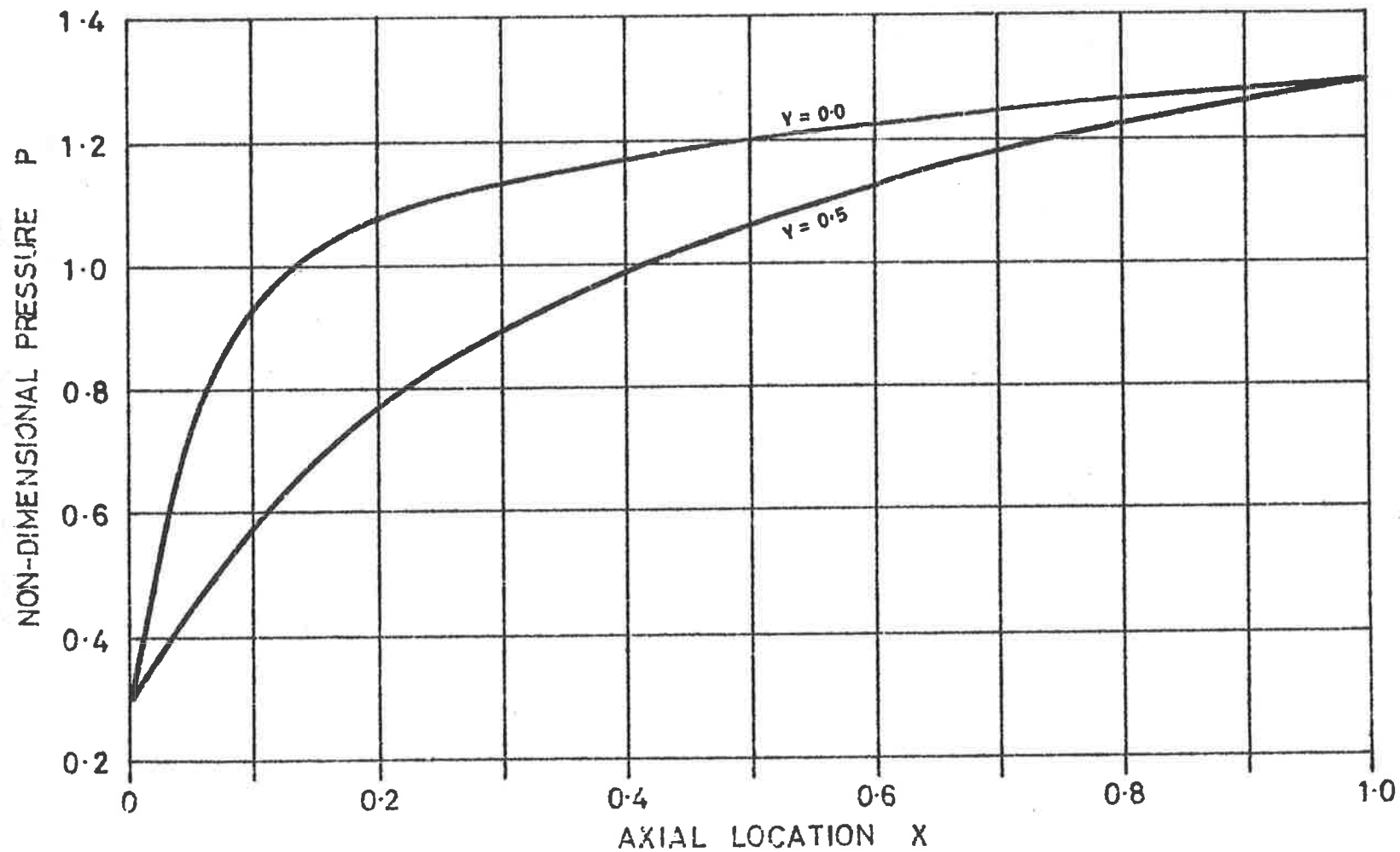
FIGURE 14   Axial pressure distributions in the plane of symmetry
(for L= 2·0, T=1·0, E=1·0)   Compressible   flow (PR=4·4)

indicating greater exit velocities.

Figures 15 and 16 show the effects of the taper ratio and eccentricity ratio on the load coefficient, and Figures 17 and 18 illustrate the effects of these variables on the flow coefficient.

Axial pressure distributions at two circumferential stations for the tilted bearing (Figure II-2, Appendix II) are given in Figure 19. Comparison between these and the curves of Figure 10 show that the effect of compressibility is to decrease the rate of pressure drop along the land - an effect most marked in the region of small clearance ($Y > 0.75$ or $Y < 0.25$). The centre of pressure of the surface is thus moved closer to the exit boundary. The overall effect is an increase in the righting moment above the value obtained for incompressible flow. This can be seen in a comparison of the results of Figures 20 and 11, which present the righting moment coefficient against taper ratio for compressible and incompressible flow respectively. It can also be seen that the effect of compressibility decreases as the taper ratio is increased.

The effect of the pressure ratio on the load, flow and moment coefficients is shown in Figures 21, 22, and 23. It will be observed that the load coefficient (Figure 21) decreases with increasing pressure ratio. If the curves of Figure 21 are extrapolated to a pressure ratio of unity, the values of the load

FIGURE 15   Load coefficient against taper ratio (for L=0·1 and 4·0, E=1·0)
Compressible flow (PR=4·4)
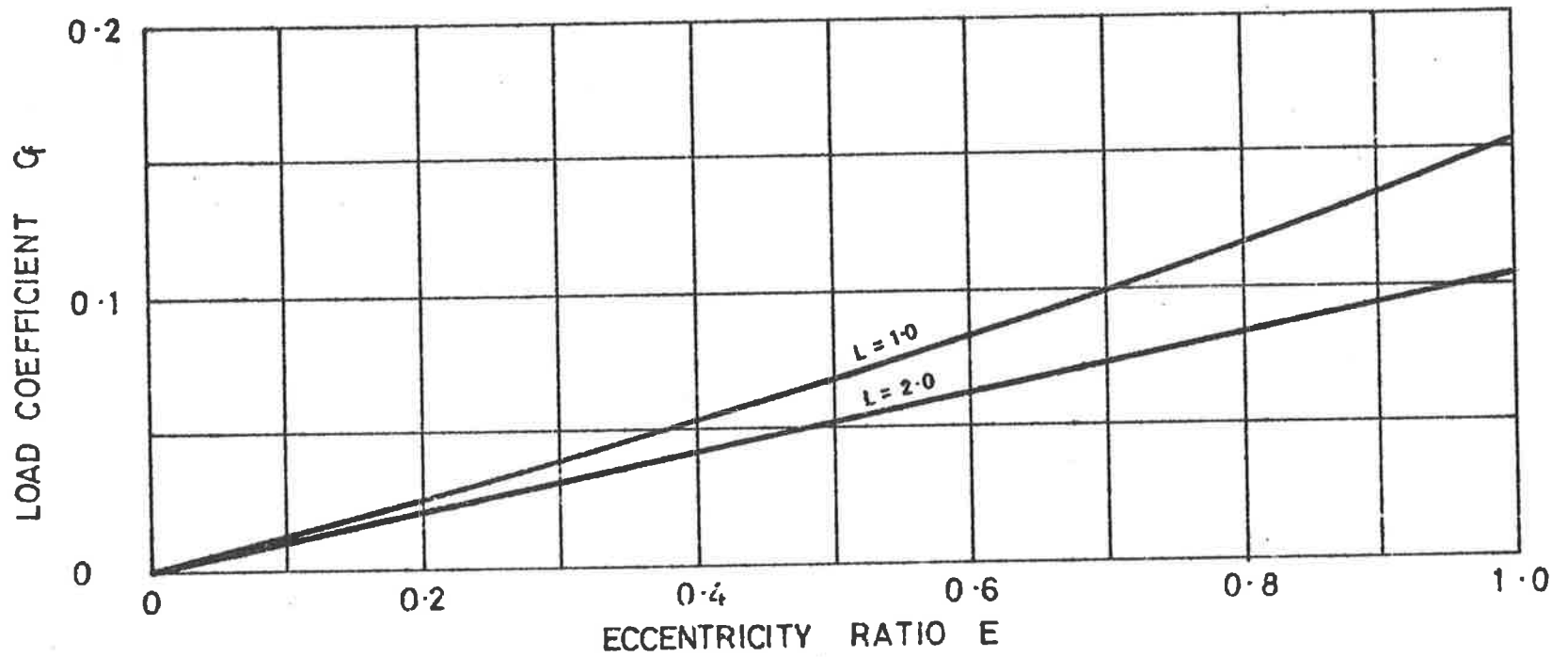
FIGURE 16   Load coefficient against eccentricity ratio (for L= 1·0 and 2·0)
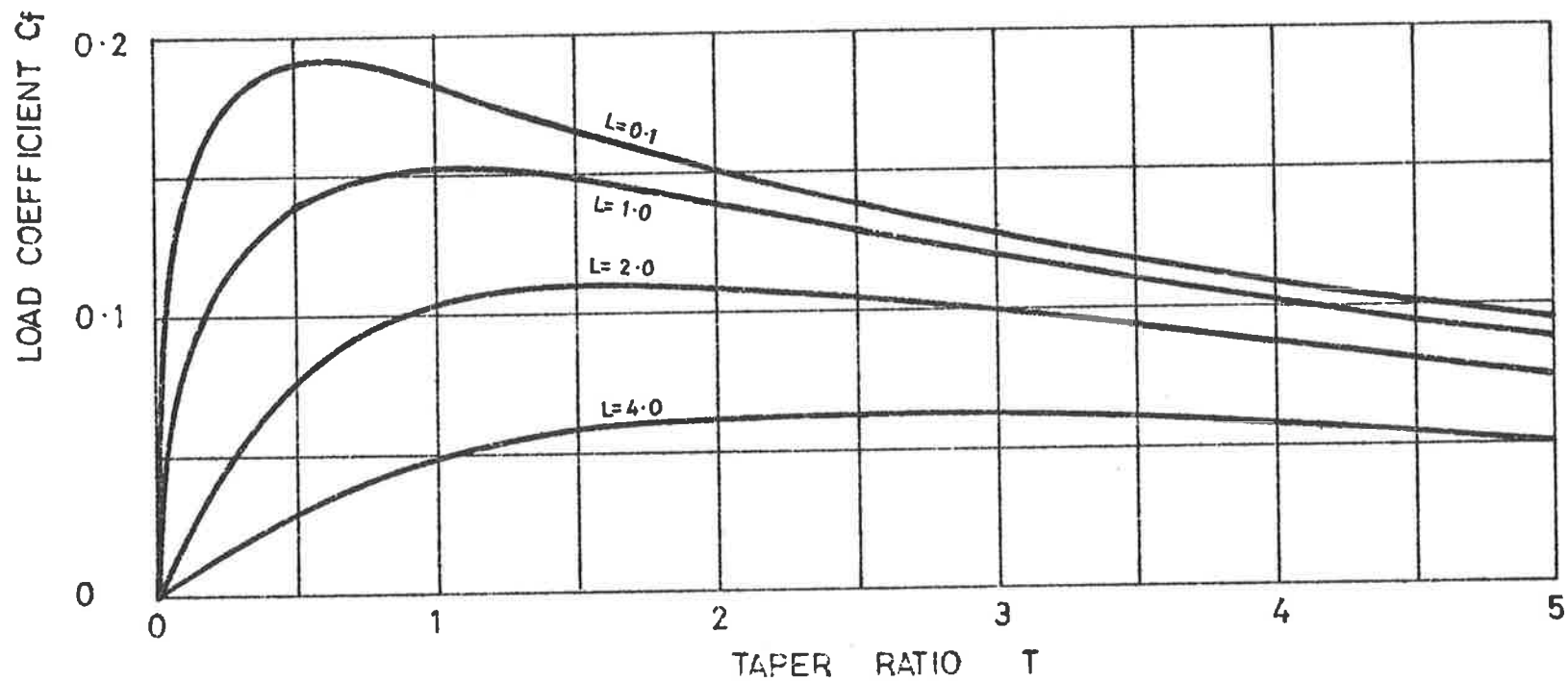Compressible flow (PR = 4·4)
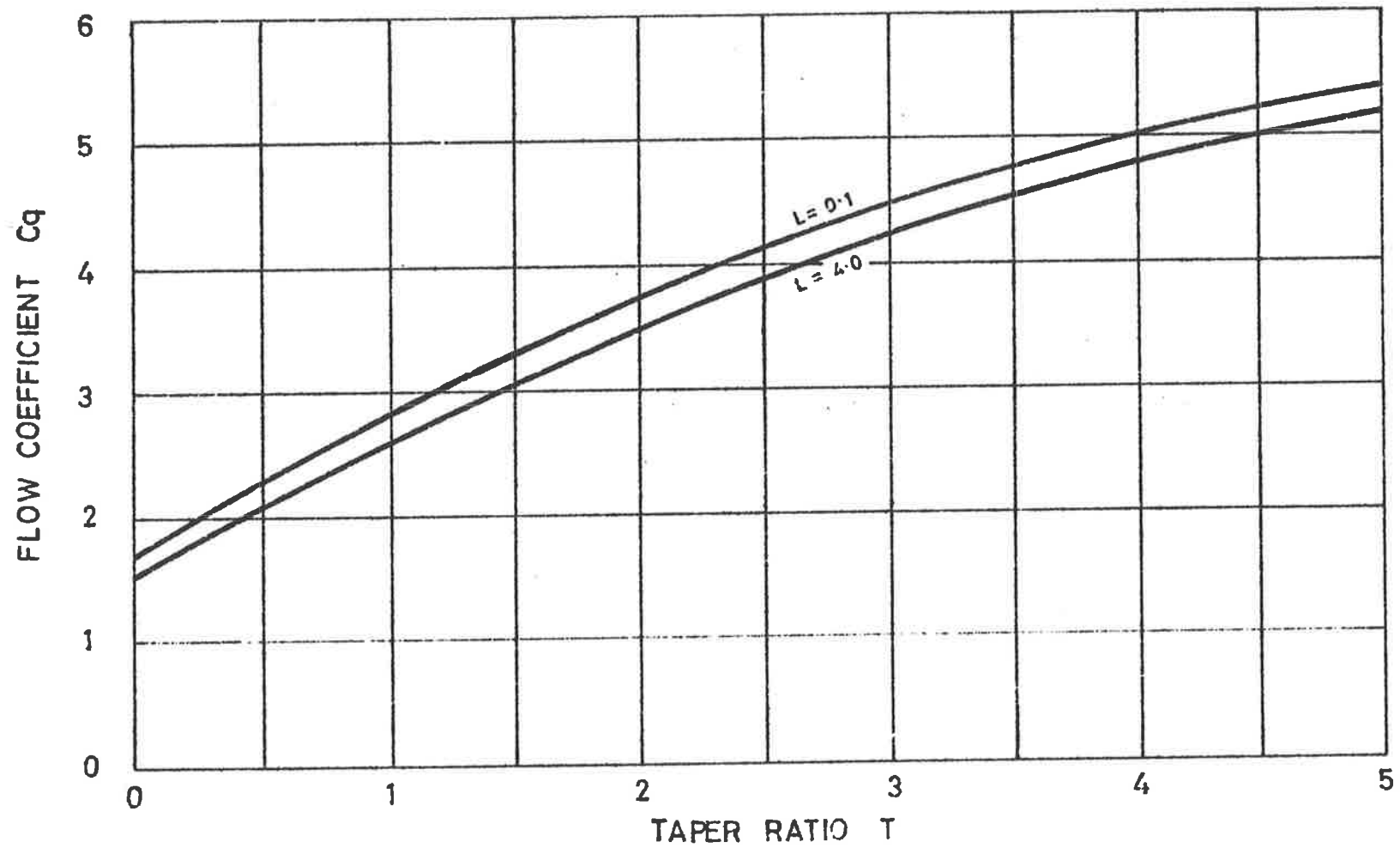
FIGURE 17   Flow coefficient against taper ratio (for L= 0·1 and 4·0 E=1·0)
Compressible flow (PR=4·4)
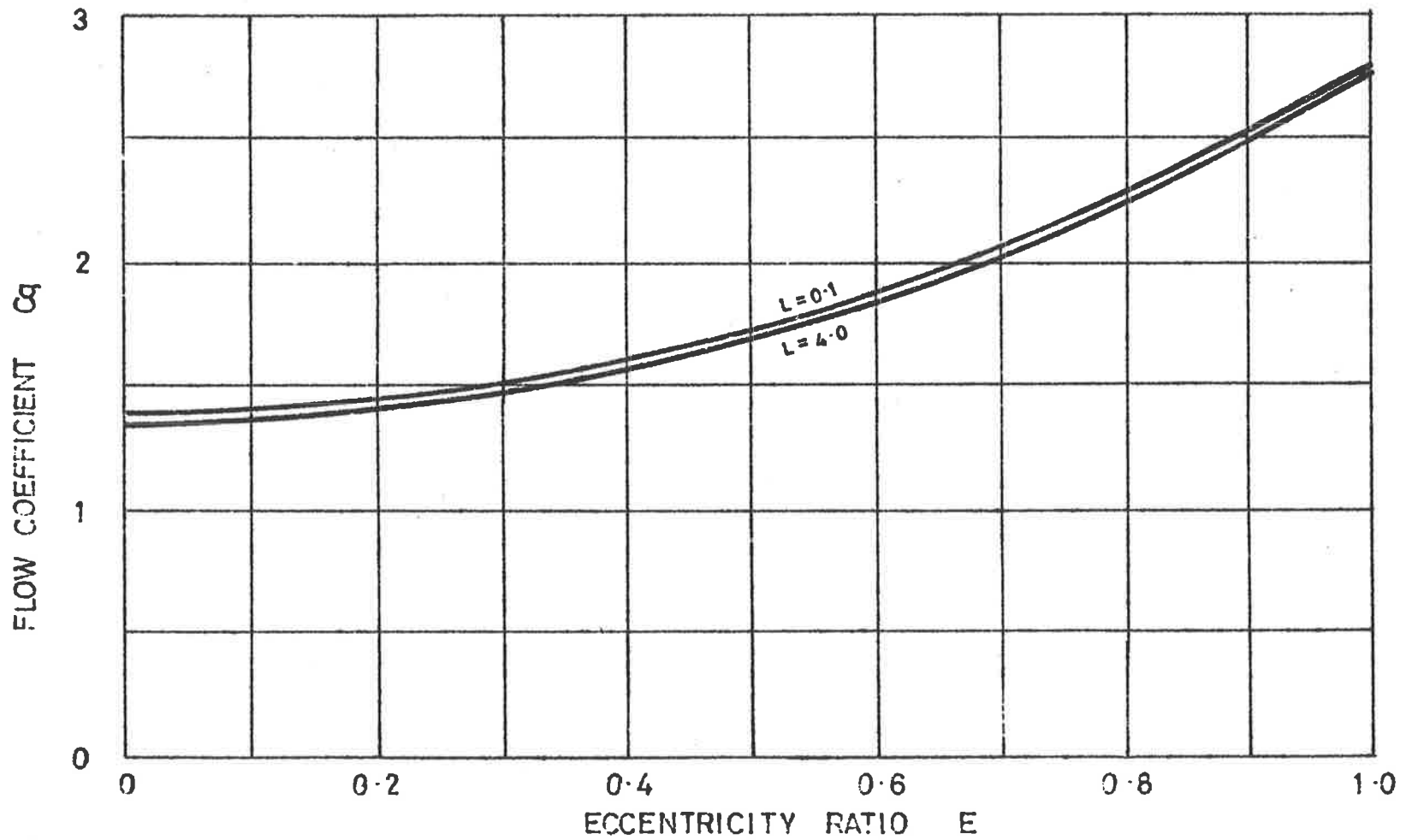
FIGURE 18   Flow coefficient   against   eccentricity   ratio (for L=0·1 and 4·0, T=1·0)   Compressible   flow (PR = 4·4)
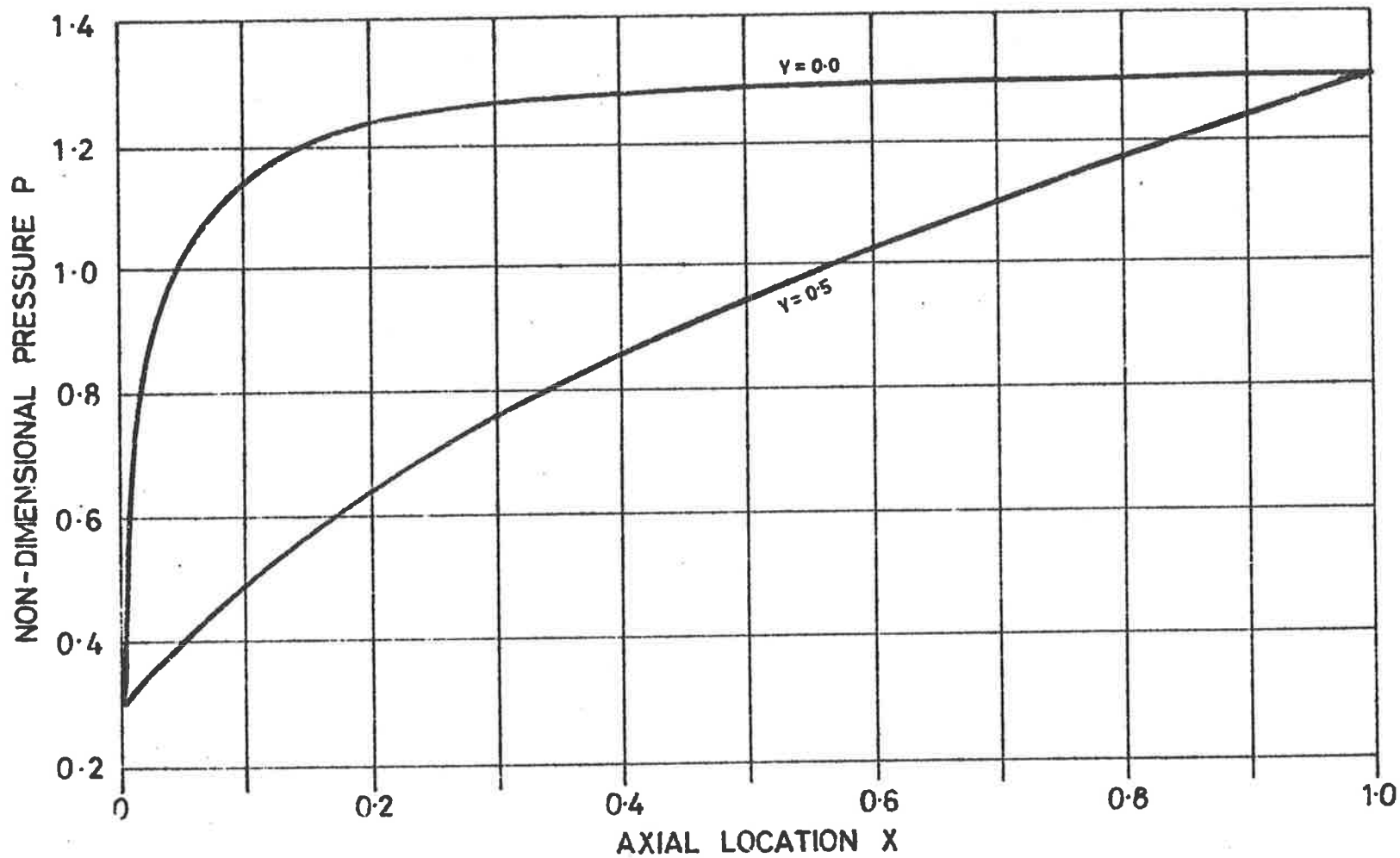
FIGURE 19   Axial pressure distributions in the plane of symmetry – tilted journal (for L = 2·0, T = 1·0, E = 1·0). Compressible flow (PR = 4·4)
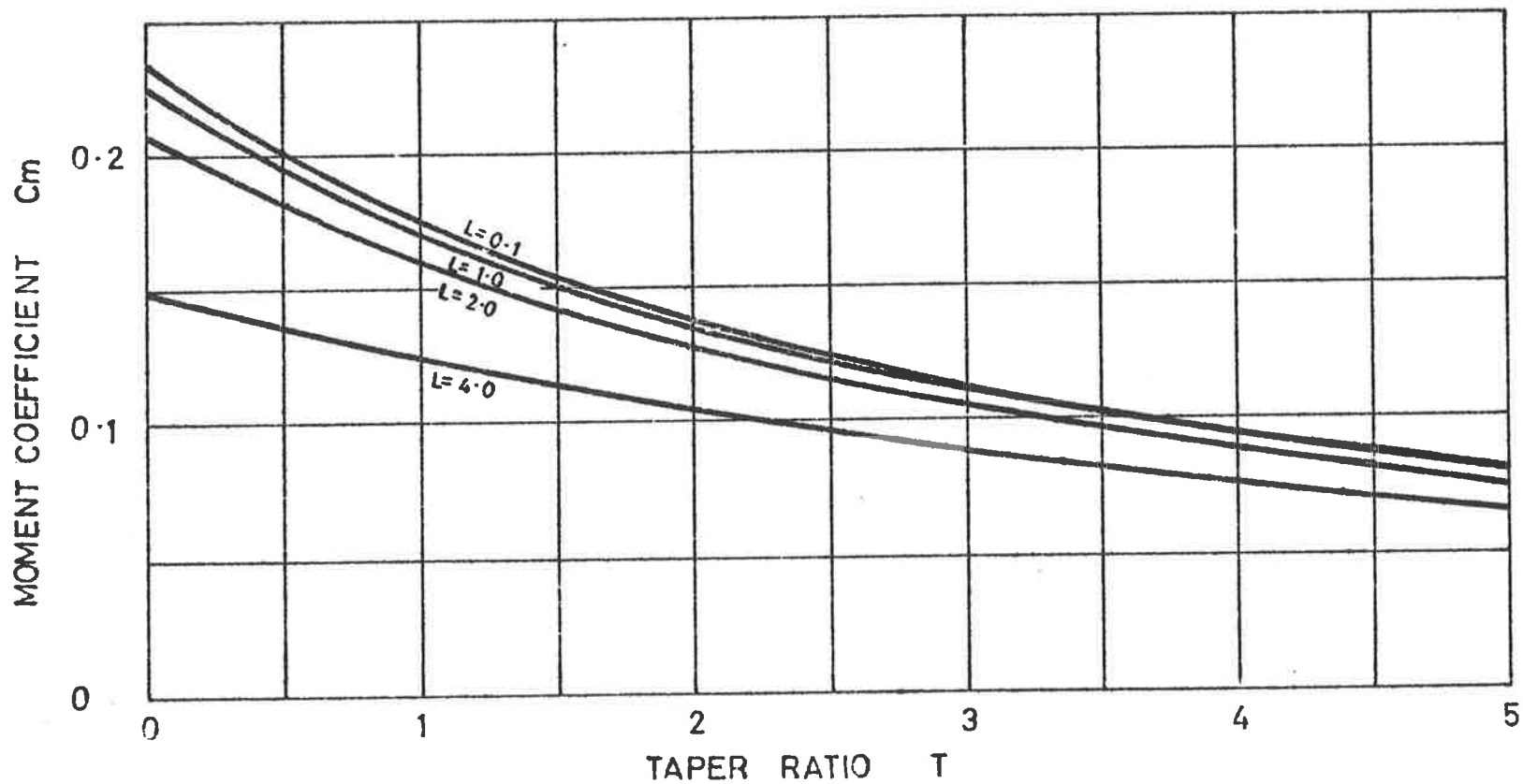
FIGURE 20   Moment   coefficient   against   taper   ratio   (for L=0·1 to 4·0 ,
E=1·0)   Compressible   flow (PR= 4·4)

FIGURE 21   Load coefficient against pressure ratio (for L= 0·1 to 4·0, T= 1·0, E = 1·0)   Compressible flow
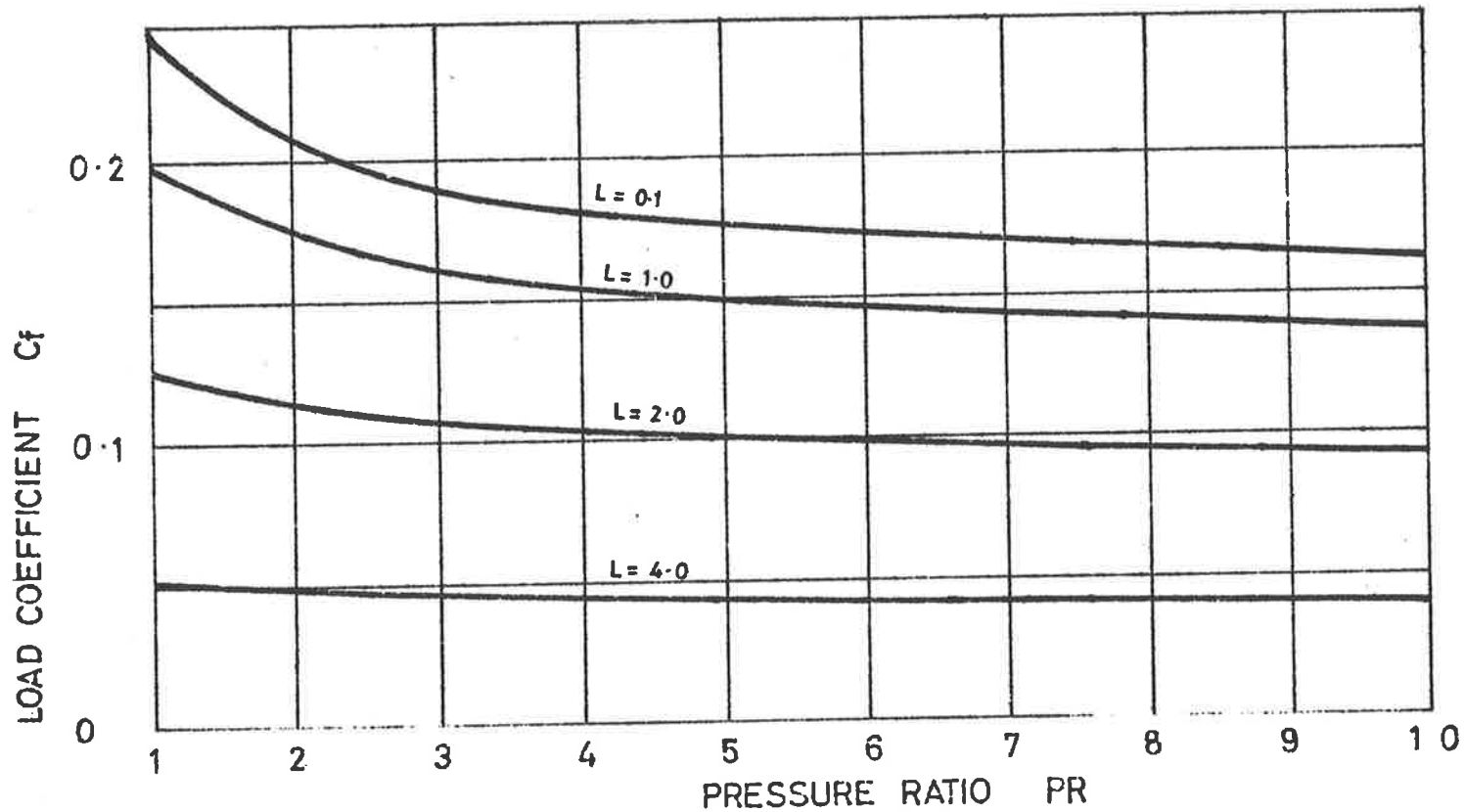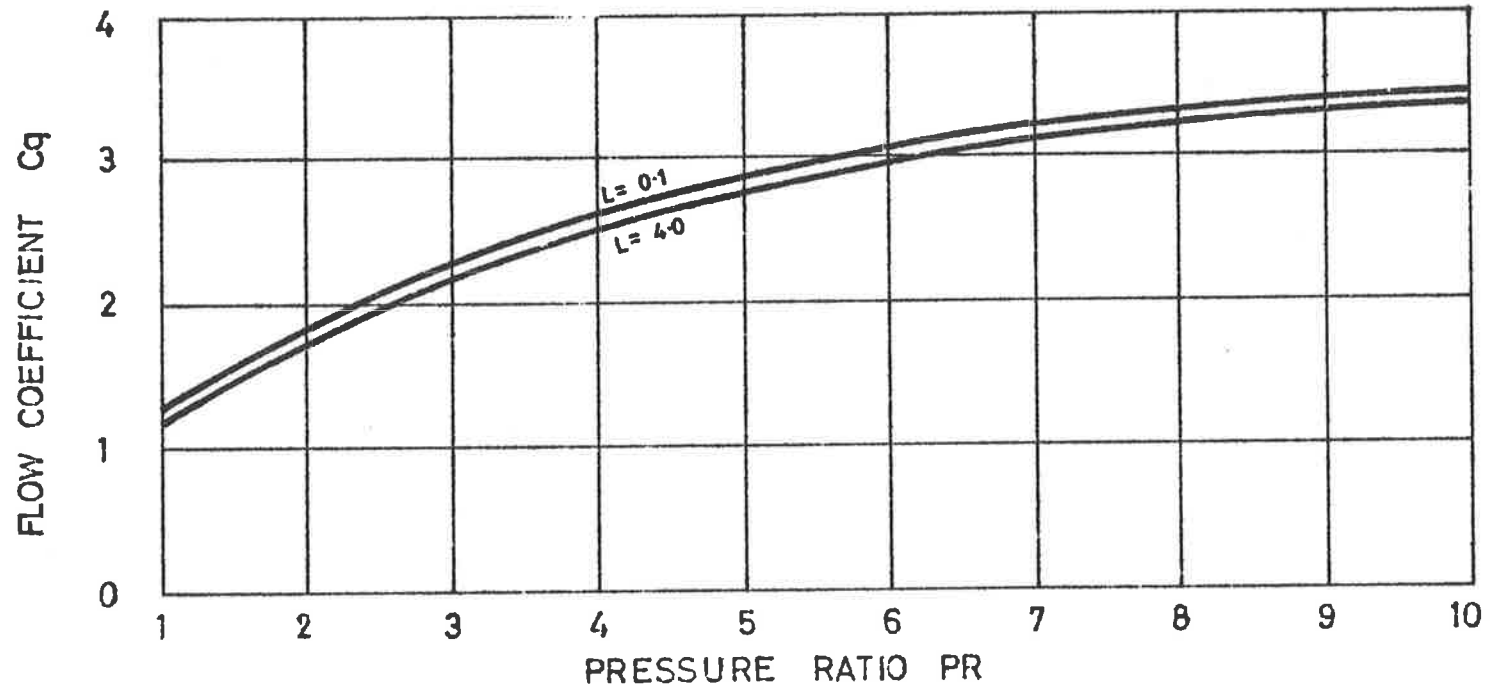
FIGURE 22   Flow   coefficient · against   pressure   ratio (for L=0·1 and 4·0,
T=1·0 , E=1·0)   Compressible   flow
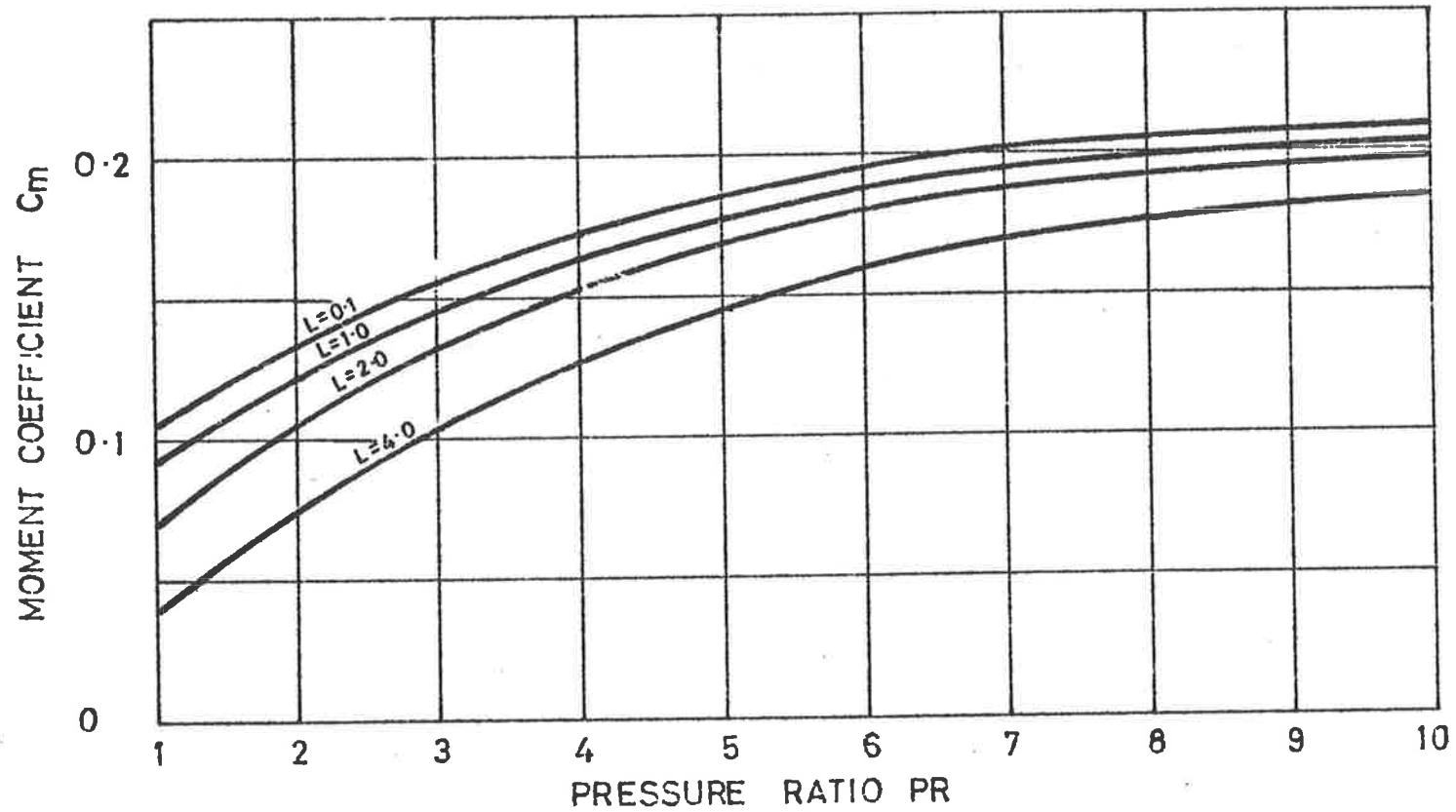
FIGURE 23   Moment coefficient against pressure ratio (for L = 0·1 to 4·0, T = 1·0, E = 1·0)   Compressible   flow

coefficient so obtained are found to be equal to those obtained for the incompressible case (Figure 6, p22). The same effect for the flow and moment coefficients will be apparent in Figures 22 and 23 respectively. This effect was to be expected, since at low pressure ratios the behaviour of a gas approaches that of an incompressible fluid.

3.3.5   The effects of lubricant inertia and choking

During the experimental work, which will be discussed more fully in later sections, it was found that at low pressure ratios good agreement was obtained between theory and experiment. However, the results of the tests at higher pressure ratios deviated substantially from those predicted by theory (Figures 51 and 52, pp 112 and 113). These deviations could not be attributed to experimental error.

It was conjectured that at high pressure ratios the flow conditions in the clearance would be such that inertia effects could no longer be neglected. Moreover, at high pressure ratios, sonic conditions could be reached in some parts of the exit annulus, resulting in partial choking. Therefore it was decided to examine the effects of inertia and choking.

(a)   The effect of inertia.

In the derivation of equation (1), p 8, the total derivatives $\frac{Du}{dt}$, $\frac{Dv}{dt}$, and $\frac{Dw}{dt}$ giving the three components of

acceleration of the fluid were neglected (Appendix I).
However, if the acceleration effects are considered in the
analysis then these derivatives must be included in the
equations. Equation (I-3) and (I-4) of Appendix I then
become

$$\rho \cdot \frac{Du}{dt} = -\frac{\partial p}{\partial x} + \mu \cdot \frac{\partial^2 u}{\partial z^2} \qquad \qquad \ldots(35)$$

$$\rho \cdot \frac{Dv}{dt} = -\frac{\partial p}{\partial y} + \mu \cdot \frac{\partial^2 v}{\partial z^2} \qquad \qquad \ldots(36)$$

The total derivatives are calculated by treating the
velocity as a function of x, y, z and t, where x, y and z
are themselves functions of t, i.e.,

$$\frac{Du}{dt} = \frac{\partial u}{\partial x} \cdot \frac{\partial x}{\partial t} + \frac{\partial u}{\partial y} \cdot \frac{\partial y}{\partial t} + \frac{\partial u}{\partial z} \cdot \frac{\partial z}{\partial t} + \frac{\partial u}{\partial t}$$

$$= u \cdot \frac{\partial u}{\partial x} + v \cdot \frac{\partial u}{\partial y} + w \cdot \frac{\partial u}{\partial z} + \frac{\partial u}{\partial t} \qquad \qquad \ldots(37)$$

With steady state conditions assumed (see Appendix I)

$$\frac{\partial u}{\partial t} = 0$$

and equation (37) reduces to

$$\frac{Du}{dt} = u.\frac{\partial u}{\partial x} + v.\frac{\partial u}{\partial y} + w.\frac{\partial u}{\partial z} \qquad \qquad ...(38)$$

and similarly

$$\frac{Dv}{dt} = u.\frac{\partial v}{\partial x} + v.\frac{\partial v}{\partial y} + w.\frac{\partial v}{\partial z} \qquad \qquad ...(39)$$

Substituting for $\frac{Du}{dt}$ and $\frac{Dv}{dt}$ from equations (38) and (39) in equations (35) and (36) yields

$$\rho(u.\frac{\partial u}{\partial x} + v.\frac{\partial u}{\partial y} + w.\frac{\partial u}{\partial z}) = -\frac{\partial p}{\partial x} + \mu.\frac{\partial^2 u}{\partial z^2} \qquad \qquad ...(40)$$

and

$$\rho(u.\frac{\partial v}{\partial x} + v.\frac{\partial v}{\partial y} + w.\frac{\partial v}{\partial z}) = -\frac{\partial p}{\partial y} + \mu.\frac{\partial^2 v}{\partial z^2} \qquad \qquad ...(41)$$

Since inertia effects are most likely to be significant in short journal bearings, where velocities in the clearance space are high and where there is little circumferential flow, it was decided to introduce the assumption of axial (one dimensional) flow. Equation (41) is then not applicable, and equation (40) reduces to

$$\rho(u.\frac{\partial u}{\partial x} + w.\frac{\partial u}{\partial z}) = -\frac{\partial p}{\partial x} + \mu.\frac{\partial^2 u}{\partial z^2} \qquad \qquad ...(42)$$

The fluid must also satisfy the continuity equation, which may be written in terms of the velocities u and w as

$$\rho \cdot \frac{\partial u}{\partial x} + u \cdot \frac{\partial \rho}{\partial x} + \rho \cdot \frac{\partial w}{\partial z} + w \cdot \frac{\partial \rho}{\partial z} = 0 \qquad \ldots(43)$$

Although isothermal conditions had previously been assumed, it was considered that, with the high velocities experienced at the high pressure ratios, this assumption might become invalid. Therefore a relationship of the form

$$\frac{p}{\rho^n} = K$$

was assumed, and combining this with equation (43) yields

$$p^* \cdot \frac{\partial u}{\partial x} + u \cdot \frac{\partial p^*}{\partial x} + p^* \cdot \frac{\partial w}{\partial z} + w \cdot \frac{\partial p^*}{\partial z} = 0$$

Neglecting the term in $\frac{\partial p}{\partial z}$ and re-arranging gives

$$\frac{\partial u}{\partial x} + \frac{u}{np} \cdot \frac{\partial p}{\partial x} + \frac{\partial w}{\partial z} = 0 \qquad \ldots(44)$$

In addition the following boundary conditions must be satisfied

$$u = 0 \text{ at } z = 0 \qquad \ldots(45a)$$

$$u = 0 \text{ at } z = h \qquad\qquad\qquad \ldots(45b)$$

$$p = p_1 \text{ at } x = 0 \qquad\qquad\qquad \ldots(45c)$$

$$p = p_1 \text{ at } x = 1 \qquad\qquad\qquad \ldots(45d)$$
$$w = 0 \quad \text{at } z = 0 \qquad\qquad\qquad\;\; (45e)$$
$$w = 0 \quad \text{at } z = h \qquad\qquad\qquad\;\; (45f)$$

Equations (42) and (45), together with the boundary conditions
(45a to d) are then solved for the pressure. It has been
shown (3) that, even when the Reynold's number (Re) of the
flow in the clearance space is high $(Re \gg \frac{r}{c})$, the contribution
of the inertia forces to the dynamics of bearings is still
very small.

Since the inertia forces are expected to be small, and
since the fluid film is thin $(\frac{h}{l} < \frac{1}{1000})$, it is considered
reasonable to average out the inertia effects across the
film (3, 5).

Equation (42) may therefore be written as

$$\rho \, \frac{1}{h} \int_0^h \left(u.\frac{\partial u}{\partial x} + w.\frac{\partial u}{\partial z} \right) dz \;=\; -\frac{\partial p}{\partial x} + \mu.\frac{\partial^2 u}{\partial z^2} \qquad \ldots(46)$$

which can be expressed as

$$\frac{\partial^2 u}{\partial z^2} = f(x) \qquad\qquad\qquad \ldots(47)$$

where $f(x)$ is a function of x only, given by

$$f(x) = \frac{1}{\mu}\cdot\frac{\partial p}{\partial x} + \frac{\rho}{\mu h}\int_0^h \left(u\cdot\frac{\partial u}{\partial x} + w\cdot\frac{\partial u}{\partial z}\right)dz \qquad \text{...(48)}$$

Equations (44) and (47) can be solved for the pressure gradient.

Integrating equation (47) twice gives an expression for the velocity u, viz.

$$u = \frac{f(x)}{2}\cdot z^2 + C_1(x)\cdot x + C_2(x) \qquad \text{...(49)}$$

Applying the boundary conditions (45a) and (45b) to equation (58) gives

$$C_2(x) = 0$$

and $C_1(x) = -\frac{f(x)}{2}\cdot h$

Therefore

$$u = \frac{f(x)}{2}\cdot(z^2 - zh) \qquad \text{...(50)}$$

Differentiating equation (50) with respect to x,

$$\frac{\partial u}{\partial x} = \frac{f'(x)}{2}.(z^2 - zh) + \frac{f(x)}{2}.(-zh')$$ ...(51)

Combining equations (50) and (51) yields

$$u.\frac{\partial u}{\partial x} = \frac{f(x)}{2}\left[\frac{f'(x)}{2}.(z^2 - zh)^2 - \frac{f(x)}{2}(z^2 - zh)(zh')\right]$$ ...(52)

Expanding equation (52) and integrating with respect to z results in

$$\int_0^h u.\frac{\partial u}{\partial x}.dz = \frac{f(x)}{4}.h^4.\left[\frac{f'(x).h}{30} + \frac{f(x).h'}{12}\right]$$ ...(53)

Substituting for u and $\frac{\partial u}{\partial x}$ from equations (50) and (51) in the continuity equation (44), p52, yields

$$\frac{f'(x)}{2}.(z^2 - zh) + \frac{f(x)}{2}.(-zh') + \frac{f(x)}{2}.(z^2 - zh).\frac{1}{np}.\frac{\partial p}{\partial x} + \frac{\partial w}{\partial z} = 0$$

...(54)

Integrating equation (54) with respect to z,

$$\frac{f'(x)}{2}.(\frac{z^3}{3} - \frac{z^2 h}{2}) + \frac{f(x)}{2}.(-\frac{z^2 h'}{2}) + \frac{f(x)}{2}.(\frac{z^3}{3} - \frac{z^2 h}{2}).\frac{1}{np}.\frac{\partial p}{\partial x} \ldots$$

$$\ldots + w = C_1(x)$$ ...(55)

and applying the boundary conditions (54e)   yields

$$C_1(x) = 0$$

Equation (55) may then be written as

$$w = \frac{f(x)}{2}.\left(\frac{z^2 h'}{2}\right) - \left(\frac{z^3}{3} - \frac{z^2 h}{2}\right)\left(\frac{f'(x)}{2} + \frac{1}{np}.\frac{\partial p}{\partial x}.\frac{f(x)}{2}\right) \quad ...(56)$$

Differentiating the velocity u (equation (50), p54) with respect to z gives

$$\frac{\partial u}{\partial z} = \frac{f(x)}{2}(2z - h) \qquad\qquad ...(57)$$

Combining equations (56) and (57) yields

$$w.\frac{\partial u}{\partial z} = \frac{f(x)}{2}.\frac{f(x)}{4}.(2z^3 h' - z^2 hh') - \left(\frac{2z^4}{3} - \frac{4z^3 h}{3} + \frac{z^2 h^2}{2}\right) \quad ...$$

$$... \quad \left(\frac{f'(x)}{2} + \frac{1}{np}.\frac{\partial p}{\partial x}.\frac{f(x)}{2}\right).\frac{f(x)}{2} \qquad ...(58)$$

Integrating equation (58) from 0 to h,

$$\int_0^h w.\frac{\partial u}{\partial z}.dz = \frac{f(x).h^4}{4}.\left(\frac{f(x).h'}{12} + \frac{h}{30}(f'(x) + \frac{1}{np}.\frac{\partial p}{\partial x}.f(x))\right) \qquad\qquad ...(59)$$

Substituting for $\int_0^h u.\frac{\partial u}{\partial x}.dz$ and $\int_0^h v.\frac{\partial u}{\partial z}.dz$ from equations (53), p55, and (59) in equation (48), p54, results in an expression for $f(x)$, viz.

$$f(x) = \frac{1}{\mu}.\frac{\partial p}{\partial x} + \frac{\rho h'}{4\mu}.f(x)\left[\frac{f(x).h'}{6} + \frac{h}{30}.(2f'(x) + \frac{1}{np}.\frac{\partial p}{\partial x}.f(x))\right]$$
$$\qquad\qquad ...(60)$$

Applying the remaining boundary conditions (45f) to equation (56) yields

$$f'(x) = -\frac{3f(x)}{h^3}.(h^2h' + \frac{h'}{3}.\frac{1}{np}.\frac{\partial p}{\partial x}) \qquad ...(61)$$

Substituting for $f'(x)$ from equation (61), equation (60) becomes

$$f(x) = \frac{1}{\mu}.\frac{\partial p}{\partial x} + \frac{\rho h'}{4\mu}.f^2(x)\left[\frac{h'}{6} - \frac{h}{30}.(\frac{6h'}{h} + \frac{1}{np}.\frac{\partial p}{\partial x})\right] \quad ...(62)$$

The mass flow/unit circumference is given by

$$m = \rho \int_0^h u.dz$$

Substituting for u from equation (50), p54, and evaluating the integral yields

$$m = - \frac{\rho \cdot f(x) \cdot h^3}{12} \qquad \qquad \ldots (63)$$

Re-arranging equation (63) results in a further expression
for $f(x)$, viz.

$$f(x) = - \frac{12m}{\rho h^3} \qquad \qquad \ldots (64)$$

Substituting for $f(x)$ from equation (64) in equation (62)
gives

$$-\frac{12m}{\rho h^3} = \frac{1}{\mu} \cdot \frac{\partial p}{\partial x} - \frac{6m^2}{5\mu\rho h^3} \left[h' + \frac{h}{mp} \cdot \frac{\partial p}{\partial x} \right] \qquad \ldots (65)$$

Re-arranging equation (65),

$$\frac{\partial p}{\partial x} = \frac{p}{h} \cdot \frac{6m(mh' - 10\mu)}{5\rho h' p - \frac{6m^2}{m}} \qquad \qquad \ldots (66)$$

From equation (50), p54,

$$\rho = \rho_0 \cdot \left(\frac{p}{p_0} \right)^{\frac{1}{4}}$$

and substituting for ρ in equation (66) gives

$$\frac{\partial p}{\partial x} = \frac{p}{h} \cdot \frac{6m(mh' - 10\mu)}{5\rho_0 \cdot \left(\frac{p}{p_0}\right)^{\frac{1}{2}} \cdot ph^2 - \frac{6m^2}{n}} \qquad \ldots(67)$$

Replacing the terms in x and h by their non-dimensional

equivalents, viz.

$$x = X.l$$

$$h = H.c$$

$$h' = H'.c = T.c$$

yields

$$\frac{\partial p}{\partial X} = \frac{p}{H.c} \cdot \frac{6ml(mTc - 10\mu)}{5\rho_0 \cdot \left(\frac{p}{p_0}\right)^{\frac{1}{2}} \cdot pH^2 c^2 - \frac{6m^2}{n}} \qquad \ldots(68)$$

To ascertain the effect of including the inertia term in the

analysis it is necessary to compare inertia-neglected and

inertia-corrected theories. However, the original analysis

that neglected the inertia effects used a relaxation method

of solution, whereas the inertia-corrected theory employs

the predictor-corrector method (6) to evaluate the pressure

field. As these two finite difference methods have different

degrees of inherent error associated with them, it was
decided that, for accurate comparison, the two theories
should be evaluated by the same method.

An expression for the pressure gradient in the axial
direction (inertia effects neglected) is given in Appendix
III viz.

$$\frac{\partial p}{\partial x} = -\frac{12 \mu m}{\rho h^3} \qquad \qquad ...(69)$$

The expression for the pressure gradient with inertia effects
taken into account is given by equation (66), p58. Re-writing
equation (66) as

$$\frac{\partial p}{\partial x} = \frac{p}{h} \cdot \frac{6m(m^* h' - 10\mu)}{5\rho h^2 p - \frac{6(m^*)^2}{n}} \qquad \qquad ...(70)$$

It can be seen that, by putting $m^* = 0$, equation (70) reduces
to

$$\frac{\partial p}{\partial x} = -\frac{12 \mu m}{\rho h^3} \qquad \qquad ...(71)$$

which is the same as equation (69). The inertia-neglected
solution can therefore be obtained by putting $m^* = 0$ in

equation (70), while the inertia-corrected solution is obtained by putting $m^* = m$.

Equation (70) was programmed for solution by the Runge-Kutta method (6), as described in Appendix V. The computation was carried out on the CDC 6400 computer and the results are presented in Figures 24 and 25. It can be seen that the effect of inertia is negligible - of the order of one percent, even at the highest pressure ratio used (PR = 10). These results are consistent with those obtained by OSTERLE (5) who found that for self-acting bearings the effect of inertia was very small, even at high rotational speeds.

The effect of varying the polytropic index (n) is clearly illustrated. With the larger value (n = 1.4) the load capacity is higher, and the leakage flow lower, than that for the isothermal case (n = 1.0).

(b)   The effect of choking.

Choking was considered to be another contributing factor that could have caused the deviations of the experimental results from those obtained from the theoretical analysis. Therefore, it was considered worthwhile to make a closer examination of this phenomenon.

If the journal is concentric with the bearing shell then both the axial pressure gradient and the film thickness will be constant around the circumference. The axial velocity at

FIGURE 24 Load against pressure ratio. One-dimensional flow, showing the effect of inertia and the polytropic index (n). Journal land length l=1·5in , diameter d=3·0in. Compressible flow.
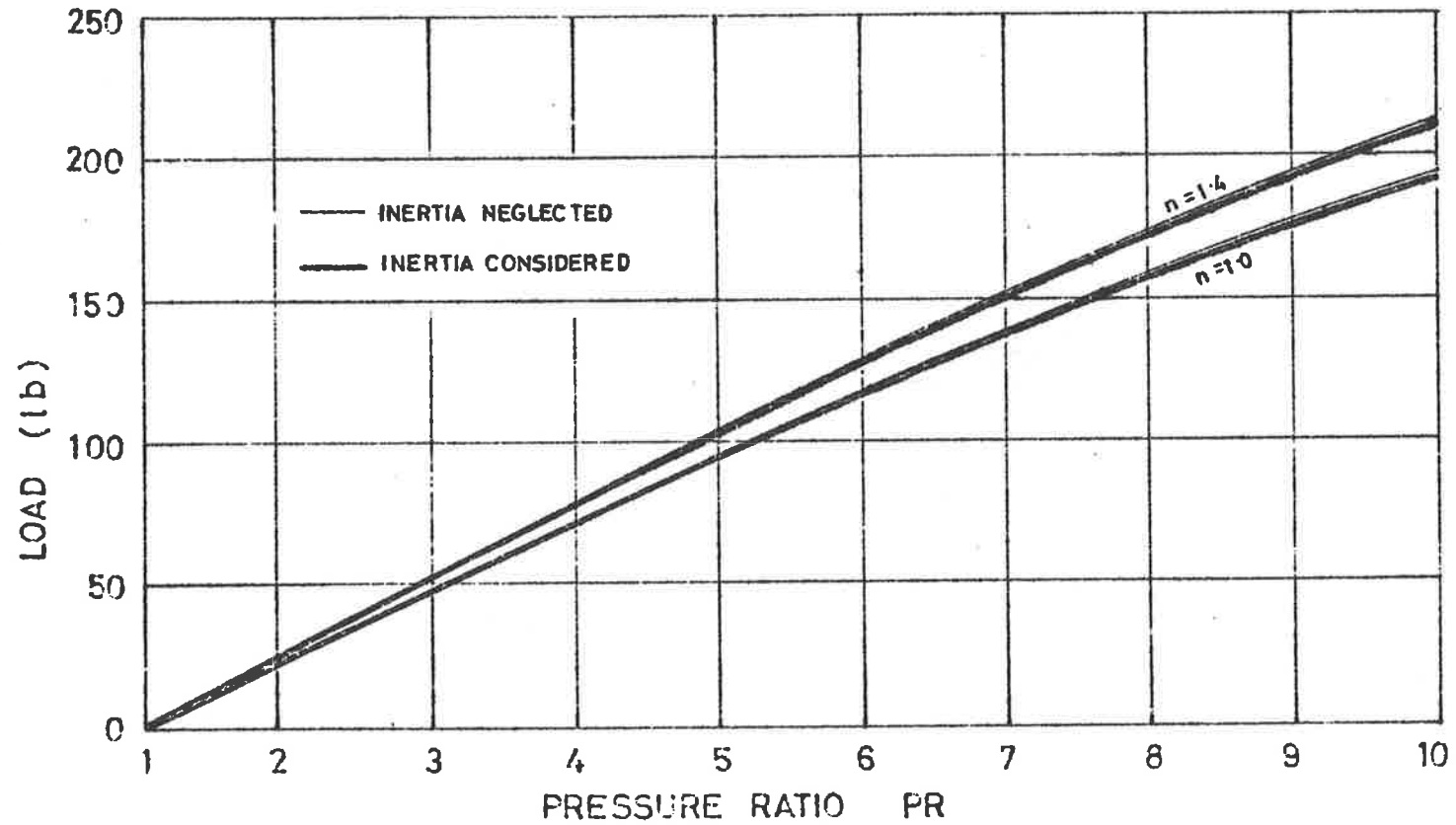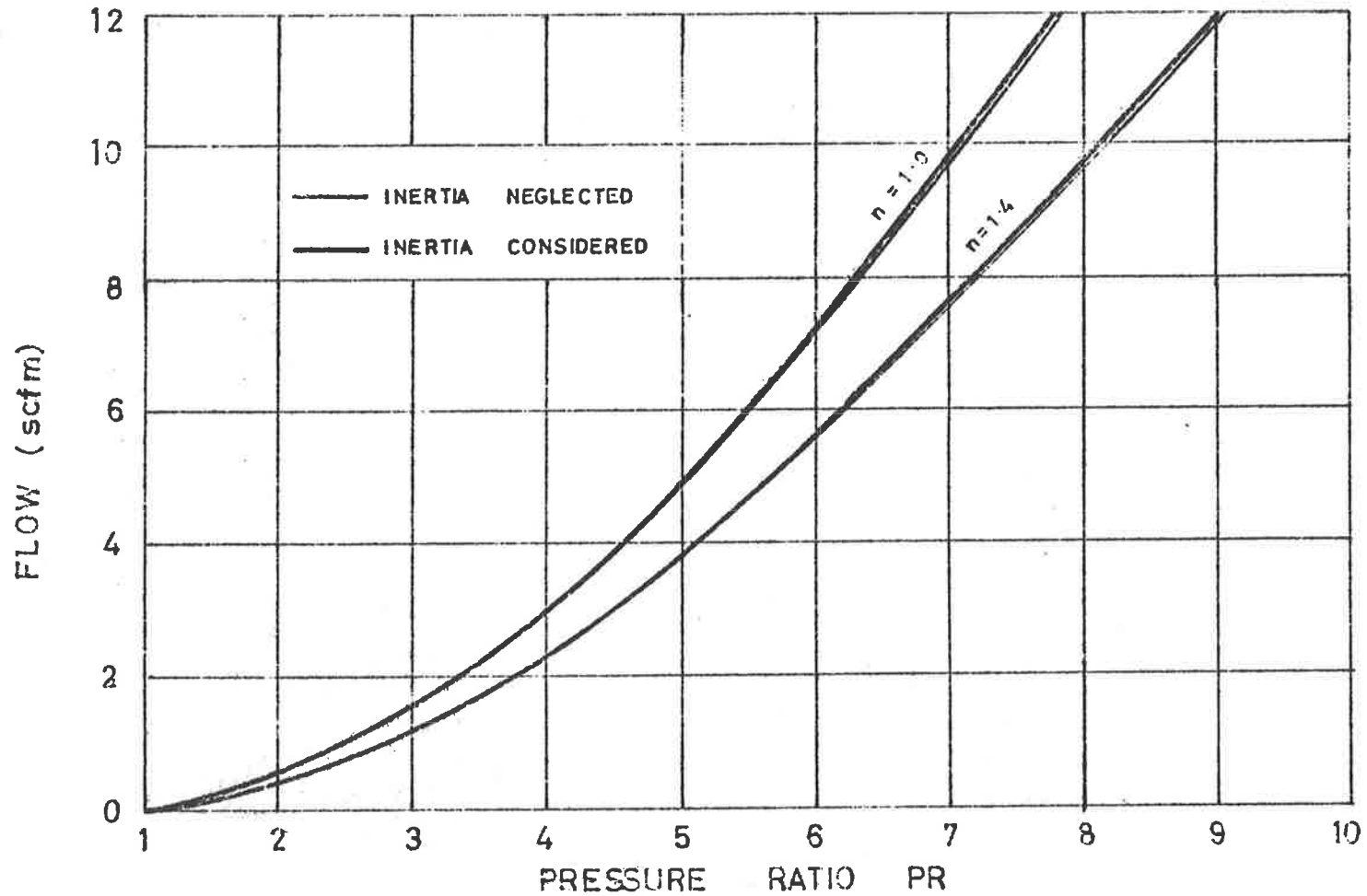
FIGURE 25   Flow against pressure ratio. One-dimensional flow, showing the effect of inertia and the polytropic index (n). Journal land length $l=1.5$ in, diameter $d=3.0$ in, clearance $c=0.001$ in. Compressible flow

exit, which is dependent on these two parameters, will therefore also be constant around the circumference. For this reason, when sonic conditions are reached (at a pressure ratio $PR \geqslant PR_{crit}$) the whole clearance at exit will be choked.

However, if the journal is displaced, then neither the pressure gradient nor the film thickness will be constant, and for a given pressure ratio (above PR_{crit}) choking will only occur in part of the clearance. For a given eccentricity the degree of choking will depend on the pressure ratio.

Figure 26 shows the velocity distributions around the exit annulus at pressure ratios of 2,4 and 8 as predicted by the previous theory, with the sonic velocity level at exit conditions superimposed. It can be seen that, at the high pressure ratio $(PR = 8)$, the predicted velocity in a considerable part of the annulus exceeds the sonic level. Such a velocity distribution could not exist in practice.

An exact analytical representation of this phenomenon was found to be intractible. However, an approximate analysis was carried out to allow for this effect. The actual procedure adopted was as follows.

The computation was arranged so that the maximum velocity at exit was limited to the sonic velocity at prevailing exit conditions. When the theory predicted a velocity greater than sonic, then the exit pressure was raised by some related
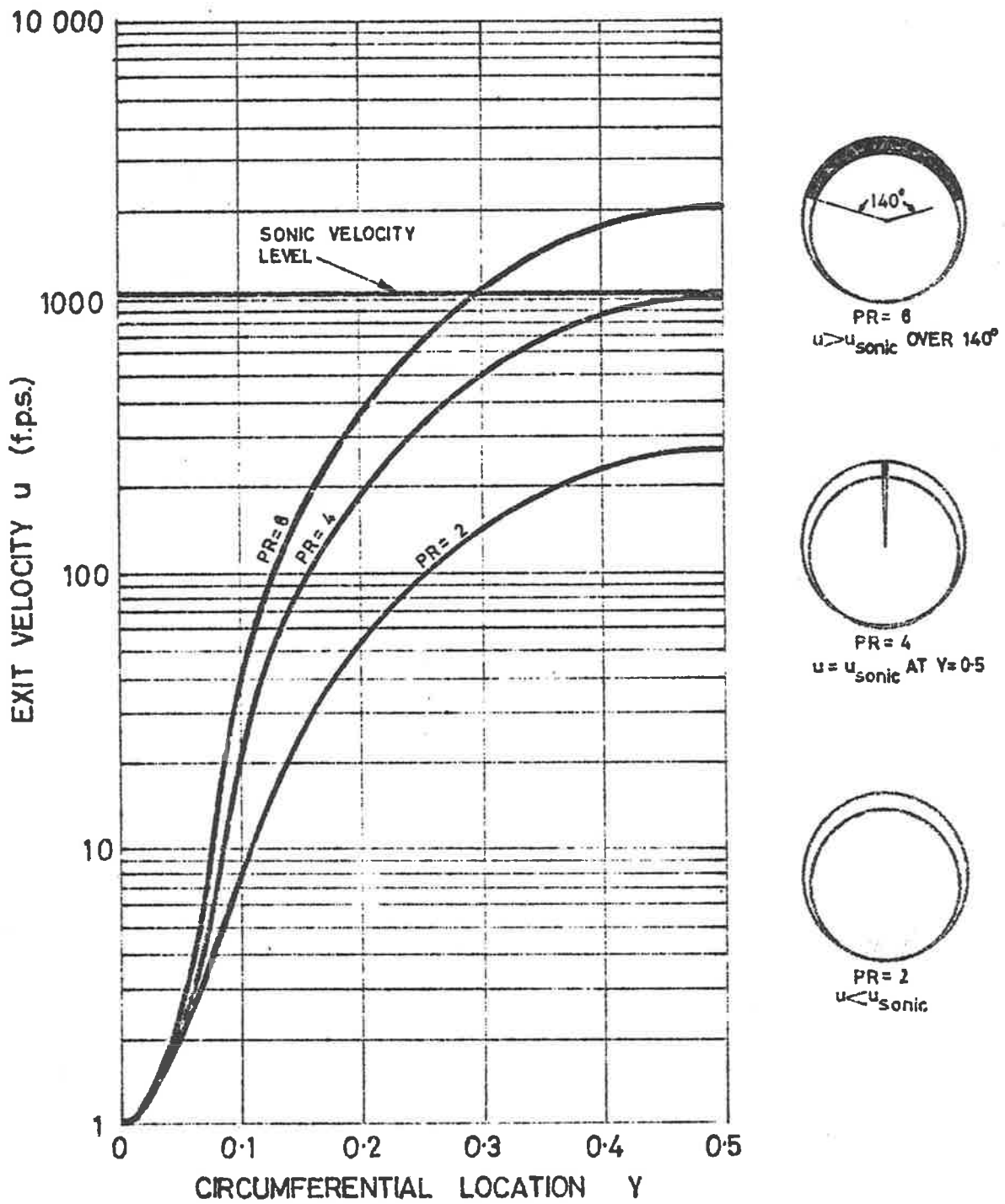
FIGURE 26   Circumferential velocity distributions at exit
            (for E=1·0). One-dimensional, compressible
            flow (PR = 2,4 and 8)

amount, and the pressure distribution along the streamline was re-calculated on the basis of the new boundary pressure. This process was repeated until an exit velocity equal to the sonic condition was obtained.

A test program was evolved to determine the degree of change required in the exit pressure for any predicted excess of exit velocity. This process was then incorporated into the inertia-corrected program described in the previous section.

Circumferential velocity distributions as predicted by the modified theory are presented in Figure 27 for pressure ratios between 1 and 10. It will be seen that the degree of choking in the exit annulus increases with increasing pressure ratio.

Load and flow results were obtained for a given bearing configuration (L = 1.0, T = 1.0) and are compared with the original theory, and with experiment, in Figures 28 and 29. It can be seen that the shapes of the fully corrected curves closely approach those of the experimental relationships. It should be noted that the actual values of the theoretical and experimental curves were not expected to agree, since in the theoretical analysis only one-dimensional flow was considered, whereas in the experimental work the flow was two-dimensional.

3.4   Stepped Land Bearings

Since the commercial production of journals with tapered lands
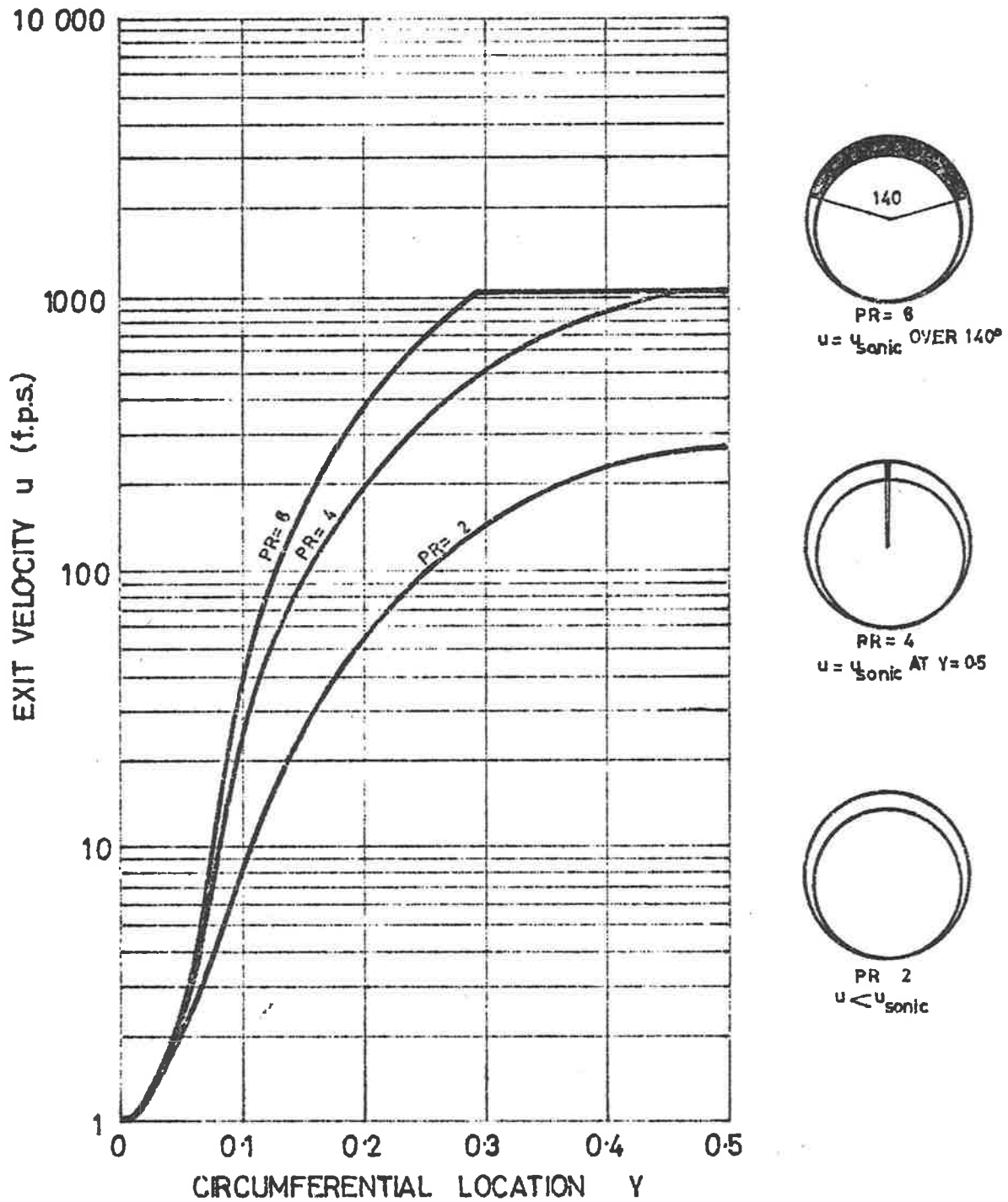
FIGURE 27 Circumferential velocity distributions at exit (for E=1·0) corrected for inertia and choking. One-dimensional, compressible flow (PR = 2, 4 and 8)
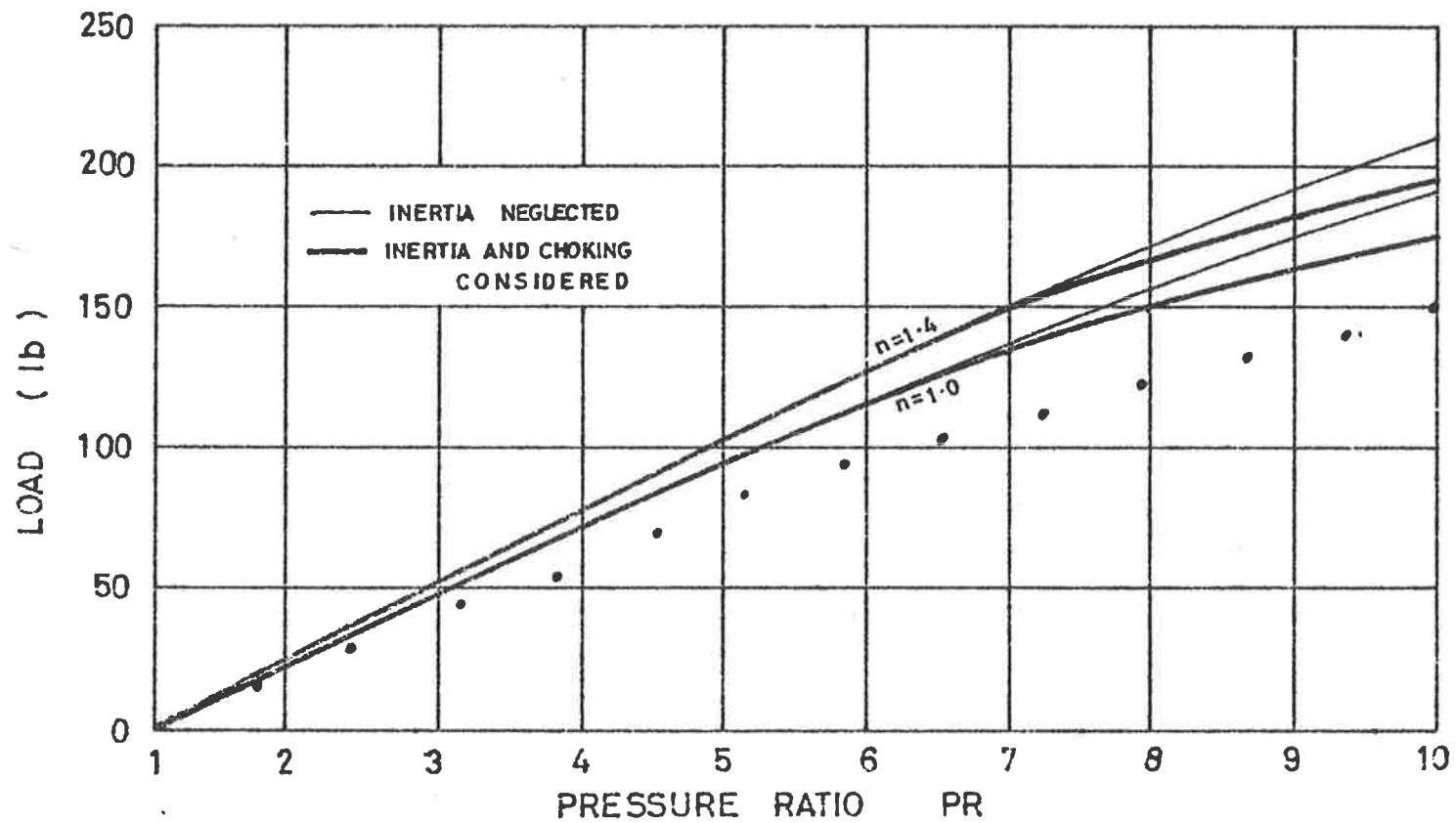
FIGURE 28 Load against pressure ratio. One-dimensional flow, showing the effect of inertia, choking, and the polytropic index (n). Journal land length l=1·5 in, diameter d=3·0 in. Compressible flow.
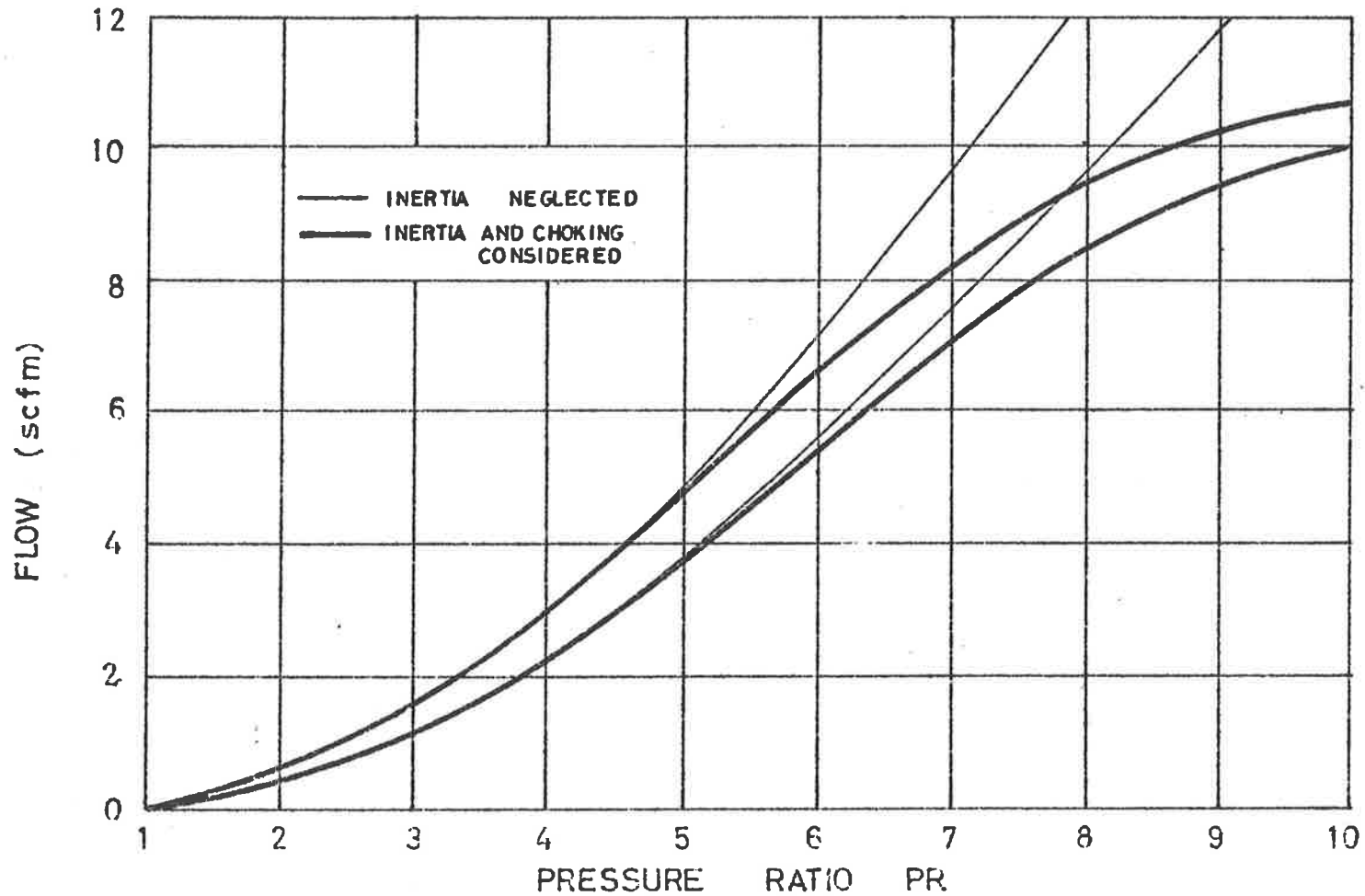
FIGURE 29 Flow against pressure ratio. One-dimensional flow, showing the effect of inertia, choking, and the polytropic index (n) Journal land length l=1·5in, diameter d=3·0in.

can introduce some manufacturing difficulties, it was decided to examine the behaviour of stepped land journals, as being the closest approximation to the tapered land form. For purposes of the analysis the case of one step was considered for both incompressible and compressible flow. The configuration examined is shown in Figure 30.

3.4.1 Incompressible flow

To obtain the pressure distribution in the clearance space, equation (2), p8 , must be solved for the new configuration. As stated previously, equation (2) can only be solved by approximate methods. However, by neglecting the circumferential pressure gradient (a close approximation for short bearings) the second term of equation (2) is eliminated, and an analytical (axial flow) solution may be obtained.

(1)   Short bearing analysis

Making this simplification, equation (2) reduces to

$$\frac{\partial}{\partial x} \cdot \left(h^3 \frac{\partial p}{\partial x} \right) = 0$$

which in expanded form becomes

$$h^3 \frac{\partial^2 p}{\partial x^2} + \frac{\partial p}{\partial x} \cdot 3 h^2 \frac{\partial h}{\partial x} = 0 \qquad \qquad \ldots(72)$$
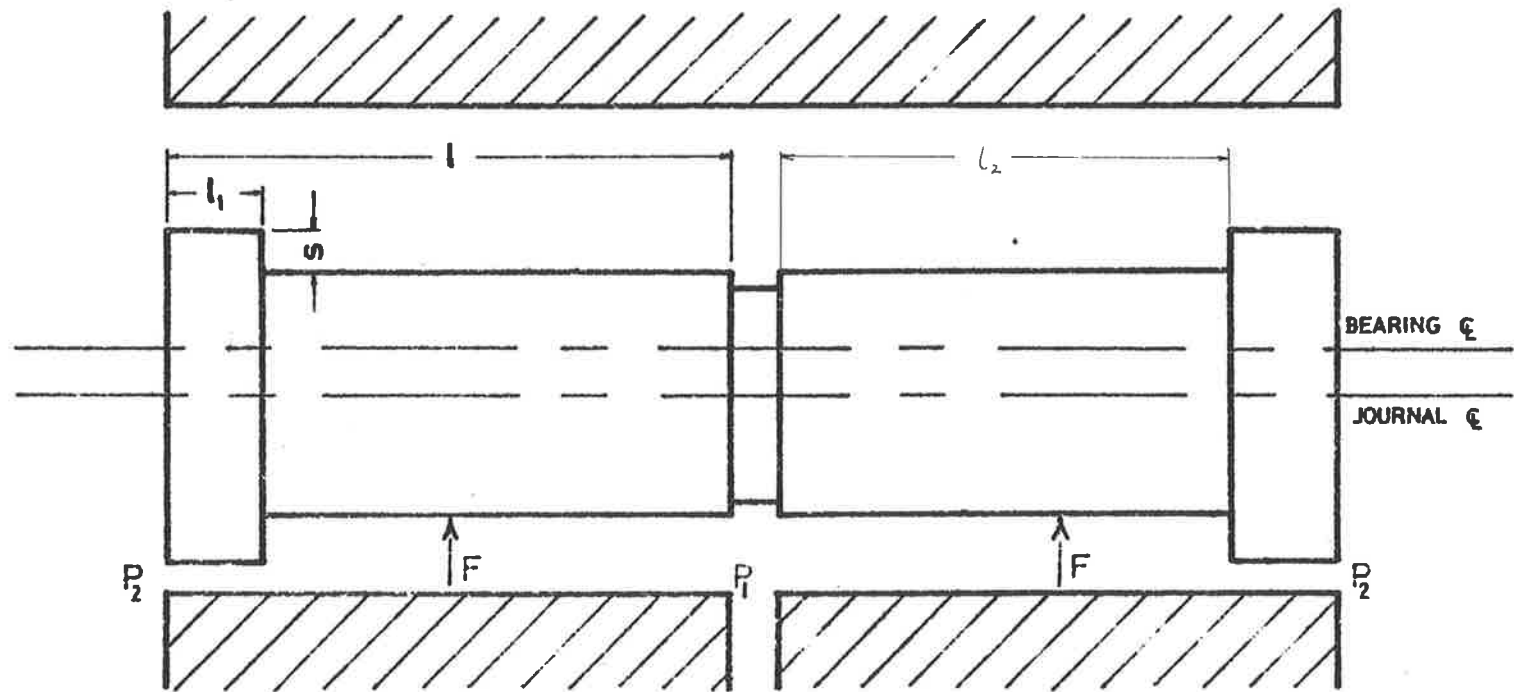
FIGURE 30 Stepped land journal bearing (parallel alignment)

For the parallel lands (l_1 and l_2 Figure 30) of the stepped bearing

$$\frac{\partial h}{\partial x} = 0$$

and equation (72) reduces to

$$h_2^3 \frac{\partial^2 p}{\partial x^2} = 0 \qquad\qquad ...(73)$$

Integrating equation (73) twice gives the pressure distributions along the two sections of the land, viz.

$$p = A_1 \cdot x + B_1 \qquad \text{for land } l_1 \qquad ...(74)$$

and

$$p = A_2 \cdot (x - l_1) + B_2 \quad \text{for land } l_2 \qquad ...(75)$$

where A_1, A_2, B_1, and B_2 are constants to be evaluated by the application of the appropriate boundary conditions, being

$$p = P_2 \text{ at } x = 0 \ (\text{land } l_1) \qquad\qquad ...(76a)$$

$$p = P_1 \text{ at } x = 1 \ (\text{land } l_2) \qquad\qquad ...(76b)$$

$$p_{l_1} = p_{l_2} \quad \text{at the step} \qquad \ldots(76c)$$

$$Q_{l_1} = Q_{l_2} \quad \text{at the step} \qquad \ldots(76d)$$

Applying the boundary condition (76a) to equation (74) gives

$$B_1 = p_2$$

and hence equation (74) becomes

$$p = p_2 + A_1 x \quad \text{for land 1,} \qquad \ldots(77)$$

Applying the boundary condition (76b) to equation (75) yields

$$B_2 = p_1 - A_2 (1 - l_1)$$

and hence equation (75) can be written as

$$p = p_1 - A_2 (1 - x) \qquad \ldots(78)$$

The pressures for both lands will be equal at the step (boundary condition (76c)) and hence, from equations (77) and (78),

$$p_2 + A_1 l_1 = p_1 - A_2 (1 - l_1) \qquad \ldots(79)$$

Making the substitution $l_2 = (1 - l_1)$ in equation (79) and re-arranging, gives

$$p_1 - p_2 = A_1 \cdot l_1 + A_2 \cdot l_2 \qquad \qquad \ldots(80)$$

Using the boundary condition for flow at the step (76d),

$$\int_0^{2\pi r} \frac{h_1^3}{12\mu} \cdot \left(\frac{\partial p}{\partial x}\right)_{l_1} \cdot dy = \int_0^{2\pi r} \frac{h_2^3}{12\mu} \cdot \left(\frac{\partial p}{\partial x}\right)_{l_2} \cdot dy$$

and hence

$$\frac{h_1^3}{h_2^3} = \frac{\left(\frac{\partial p}{\partial x}\right)_{l_2}}{\left(\frac{\partial p}{\partial x}\right)_{l_1}} \qquad \qquad \ldots(81)$$

It follows from equations (77) and (78) that

$$\frac{\left(\frac{\partial p}{\partial x}\right)_{l_1}}{\left(\frac{\partial p}{\partial x}\right)_{l_2}} = \frac{A_1}{A_2}$$

and substituting in equation (81) results in

$$\left(\frac{h_1}{h_2}\right)^3 = \frac{A_2}{A_1} \qquad \qquad \ldots(82)$$

Solving equations (80) and (82) gives the constants A_1 and A_2 as

$$A_1 = \frac{(p_1 - p_2) \cdot \left(\frac{h_2}{h_1}\right)^3}{\left(\frac{h_2}{h_1}\right)^3 l_1 + l_2}$$

and

$$A_2 = \frac{(p_1 - p_2)}{\left(\frac{h_2}{h_1}\right)^3 \cdot l_1 + l_2}$$

and substituting for these constants in equations (77) and (78) results in expressions for the pressure distributions along the two lands, viz.,

$$p = p_2 + \frac{(p_1 - p_2) \cdot \left(\frac{h_2}{h_1}\right)^3}{\left(\frac{h_2}{h_1}\right)^3 \cdot l_1 + l_2} \cdot x \quad \text{for the land } l_1 \qquad \ldots(83)$$

and

$$p = p_1 - \frac{(p_1 - p_2)}{\left(\frac{h_2}{h_1}\right)^3 \cdot l_1 + l_2} \cdot (1 - x) \text{ for the land } l_2 \qquad \ldots(84)$$

Using equations (83) and (84), the pressure distributions over the bearing surface were obtained for a number of different journal configurations. The load capacity of each was then obtained numerically as described in Appendix III. The results are presented in non-dimensional form in Figure 31 where the load coefficient (C_f) is plotted against the step length ratio (SLR) for several values of the step depth ratio (SDR). It can be seen that for a given step depth ratio there is an optimum value of step length ratio where the load coefficient reaches a maximum. Also, it will be seen that this peak value of the load coefficient increases with increasing step depth ratio and decreasing step length ratio.

(2)   Finite bearing analysis

Prior to the solution of the two dimensional case certain approximations had to be made. It was not possible to apply the relaxation technique directly to the step bearing configuration because of the discontinuity in the pressure gradient at the step. Therefore the step was replaced by a short ramp (Figure 32). This enabled a solution to be obtained by the relaxation method. It was found that, as long as the ramp length did not exceed 20% of the length of the land l_1, this modification did not introduce significant errors.

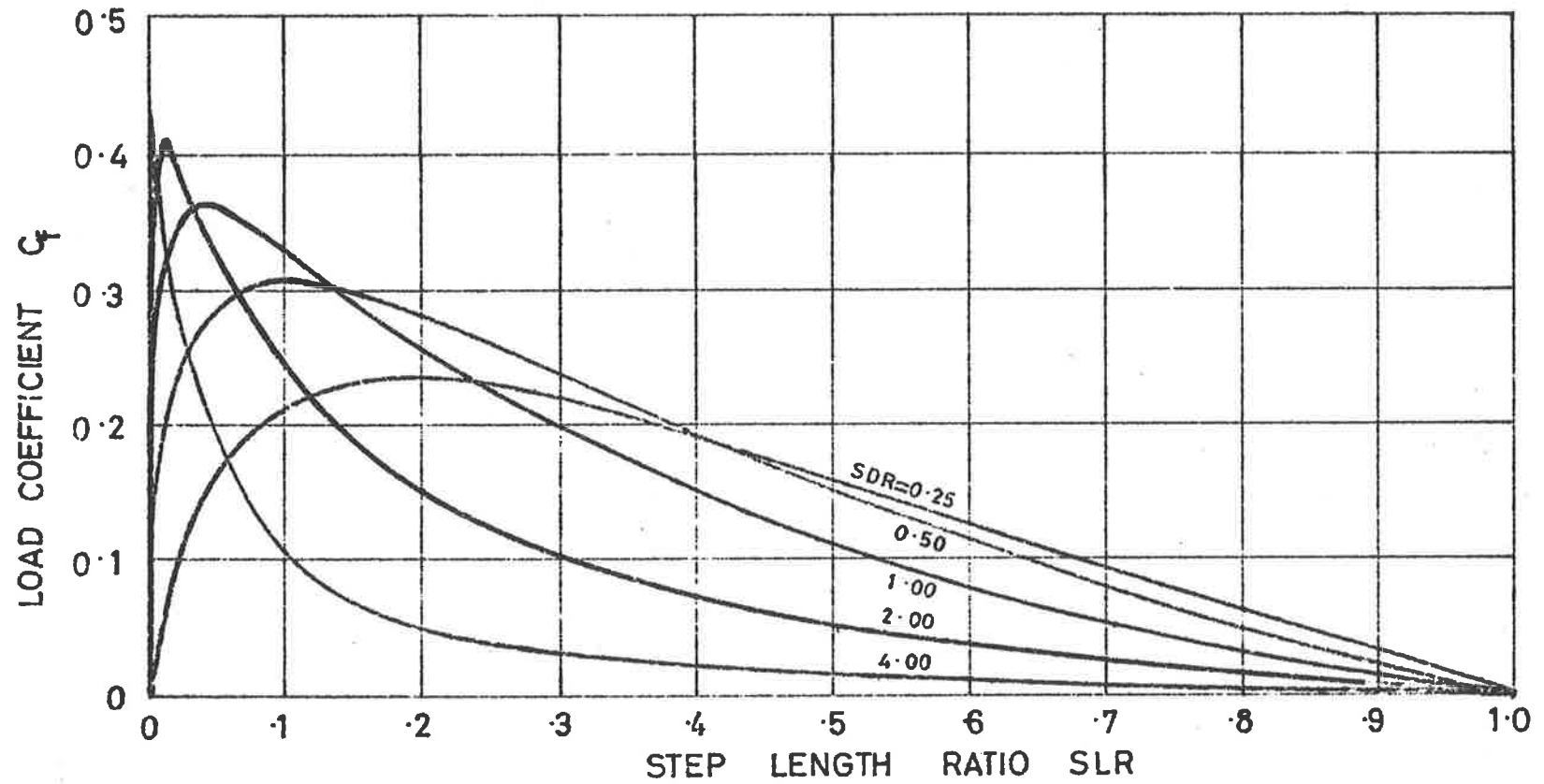It was decided to analyse a number of configurations that were

FIGURE 31 Load coefficient against step length ratio (for SDR = 0·25 to 4·0, E = 1·0) One-dimensional, incompressible flow.
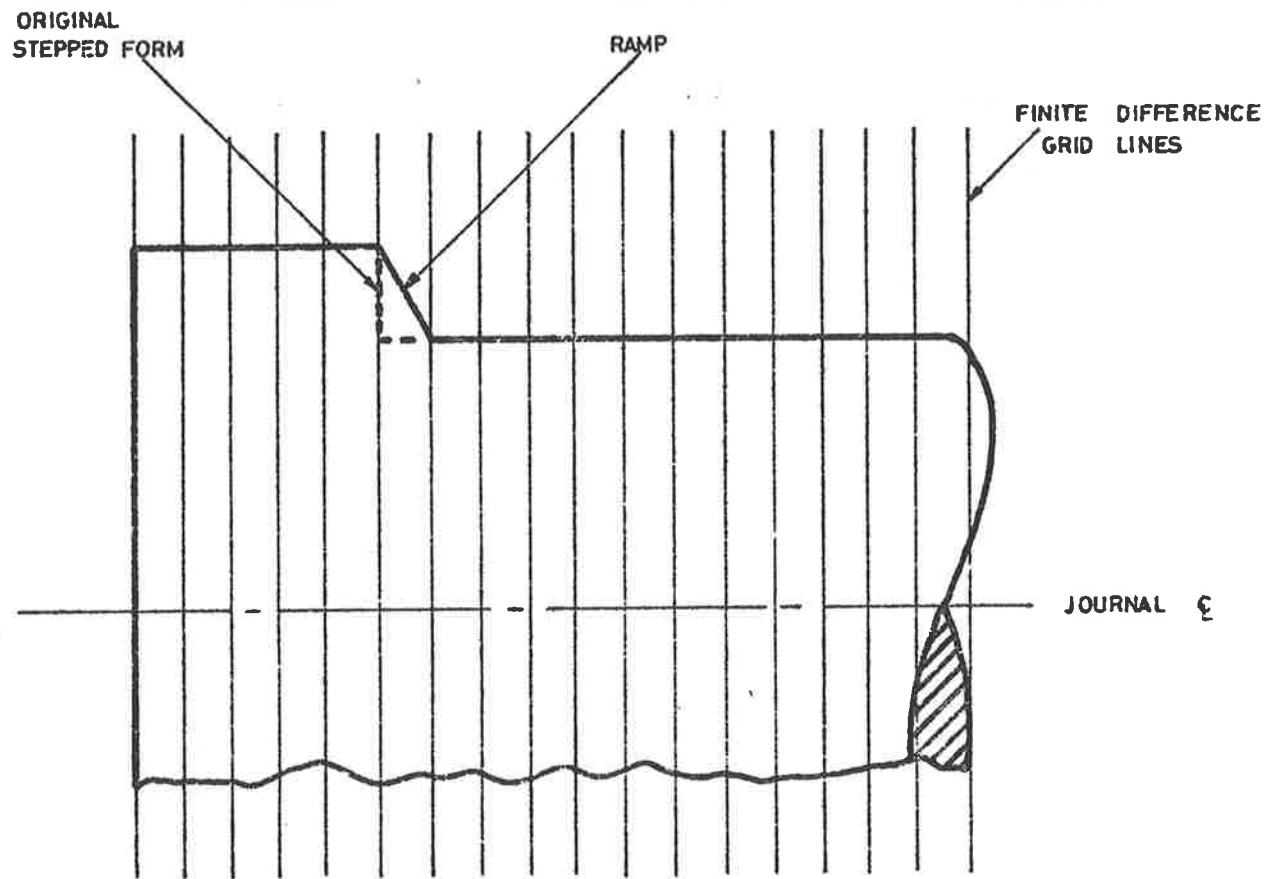
FIGURE 32   Ramp   modification   to   stepped   land   journal.

considered to cover the range likely to be used in practice.
The values chosen for analysis were

$$L = 1.0, \; 2.0$$

$$SLR = 0.1, \; 0.25$$

$$SDR = 0,1,2,3,4$$

The results of this analysis are presented in Figure 33. The
similarity between these curves and those obtained for the
tapered land bearing, Figure 6, p22, can be observed. It can
also be seen that the stepped land bearing can carry approx-
imately the same loads as can its tapered land counterpart.

3.4.2   Compressible flow

The pressure distribution in the clearance space is obtained
by solving equation (30), p31, and making the transformation from
ϕ to p as before.

(1)   Short bearing analysis

Making the axial flow assumption, equation (30) reduces to

$$\frac{\partial}{\partial x}(h^3 \frac{\partial \phi}{\partial x}) = 0 \qquad \qquad ...(85)$$

FIGURE 33   Load coefficient against step depth ratio (for L=1·0 and 2·0, SLR=0·1 and 0·25, E=1·0)   Two-dimensional, Incompressible flow.

which is identical in form to equation (73), p72.

The solutions to equation (85) will therefore be given by equations (83) and (84). The pressure distributions for the two lands (l_1 and l_2) are then obtained by the application of the transformation

$$\phi = p^2$$

which yields

$$p = \sqrt{p_2^2 + \frac{(p_1^2 - p_2^2).\left(\frac{h_2}{h_1}\right)^3}{\left(\frac{h_2}{h_1}\right)^3.l_1 + l_2}.x} \quad \text{for the land } l_1 \qquad ...(86)$$

and

$$p = \sqrt{p_1^2 - \frac{(p_1^2 - p_2^2)}{\left(\frac{h_2}{h_1}\right)^3.l_1 + l_2}.(1 - x)} \quad \text{for the land } l_2 \qquad ...(87)$$

As before (p79) load coefficients were obtained for a range of bearing geometries, and the results are presented in Figure 34. The similarity between the incompressible (Figure 31) and compressible flow results is immediately obvious. It will be
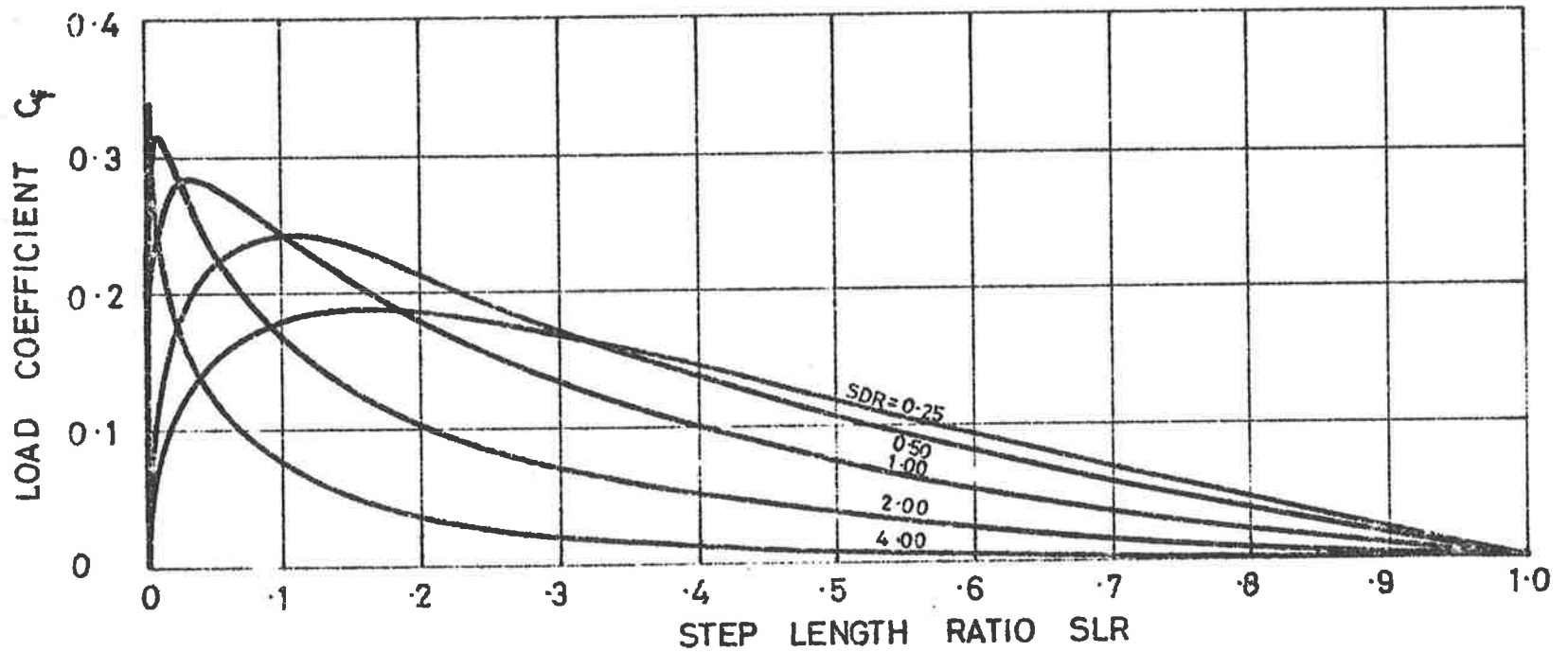
FIGURE 34   Load coefficient against step length ratio (for SDR = 0·25
to 4·0, E = 1·0)   One-dimensional, compressible flow.

noted that the trends in the two figures are the same, and that the load coefficients for compressible flow are lower than those obtained for incompressible flow.

(2) Finite bearing analysis

The two-dimensional solution was obtained by the same method as described on p76, using the p to p' transformation as before. The results obtained are presented in Figure 35.

(3) The effect of Pressure Ratio

The effect of pressure ratio, established for the tapered land bearing (Figure 21, p46) was also investigated for the stepped land configuration. It was decided, to examine the effect of pressure ratio on one length ratio ($L = 1.0$) and a number of SLR-SDR combinations, chosen to correspond to the peaks of the curves of Figure 34. The values chosen for analysis were

$L = 1.0$	$SDR = 0.25$	$SLR = 0.150$
	0.50	0.075
	1.00	0.025
	2.00	0.0125

The results of this analysis are presented in Figure 36. As was observed for the tapered land bearings (p39) the effect of increasing the pressure ratio is to decrease the load

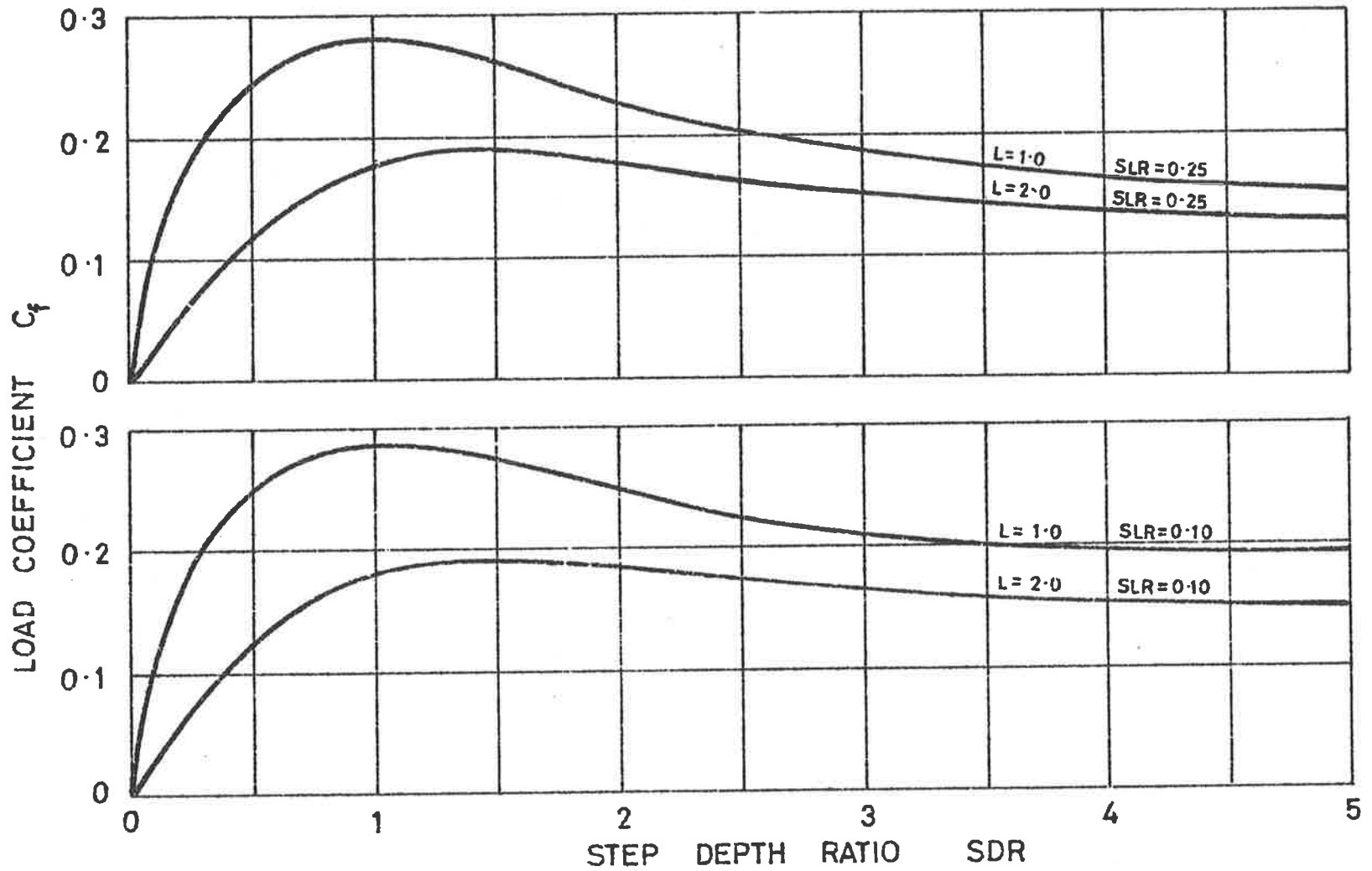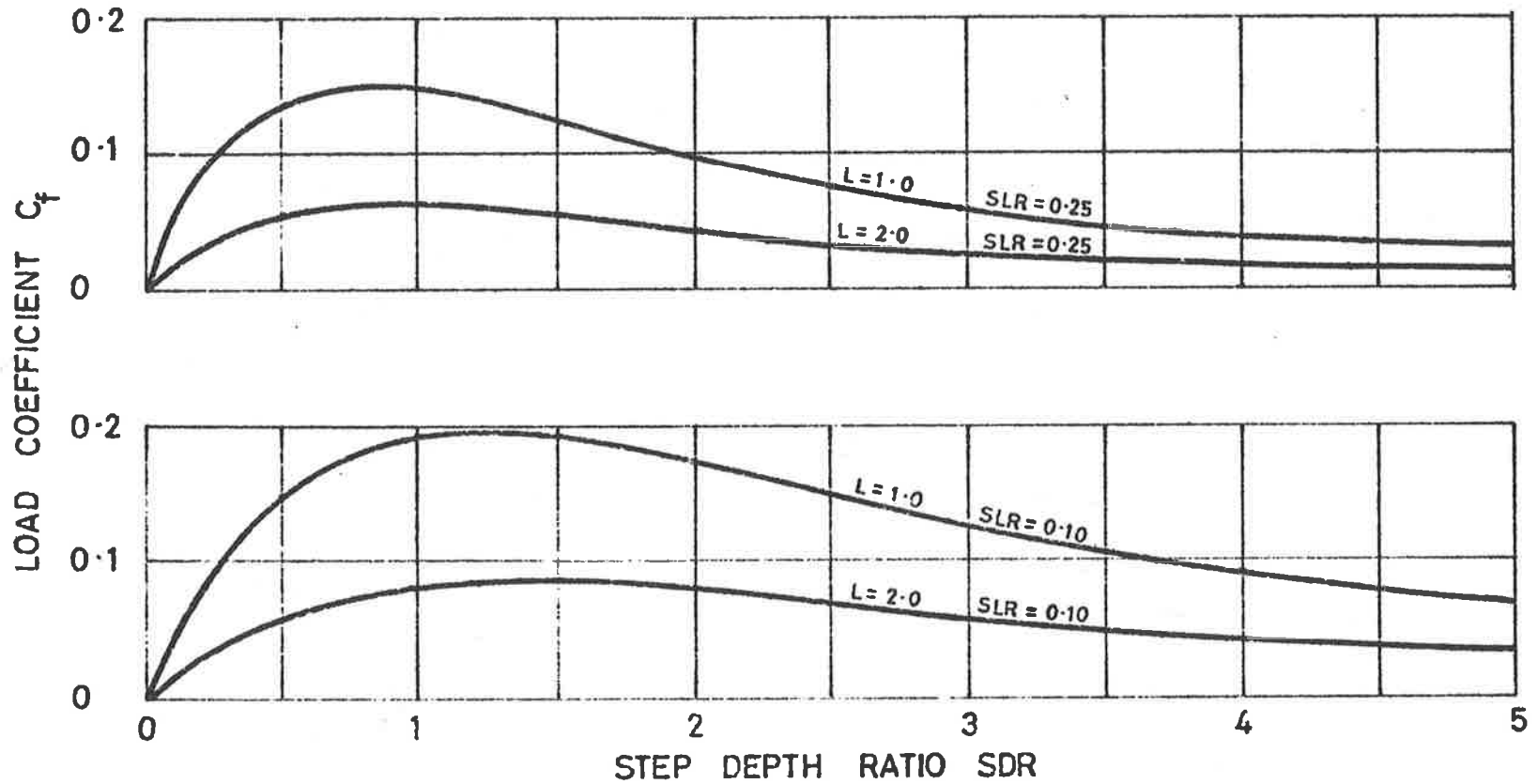FIGURE 35   Load   coefficient   against   step depth ratio (for L=1·0 and 2·0,
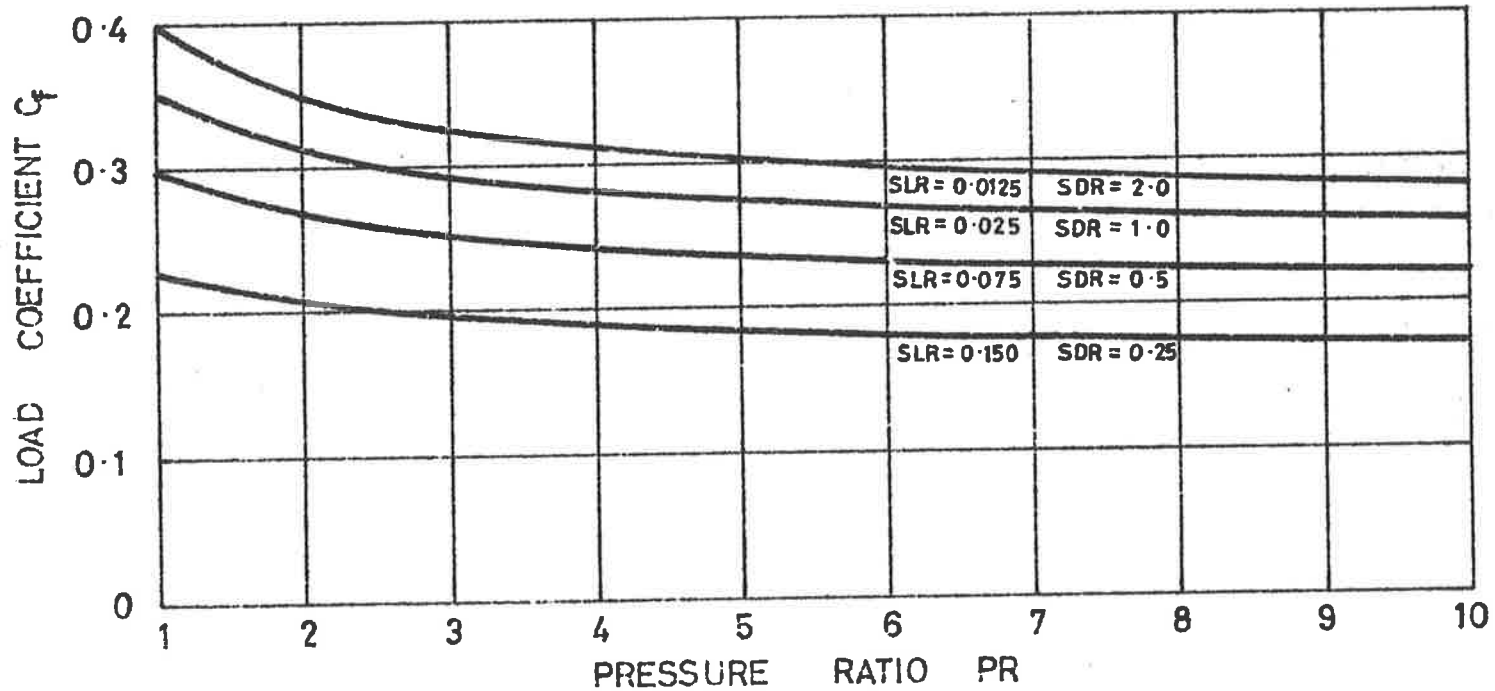SLR=0·1 and 0·25,   E=1·0)   Two-dimensional Compressible flow.

FIGURE 36   Load coefficient against pressure ratio (for selected values of SLR and SDR, E 1·0)   One-dimensional, Compressible flow.

coefficient. It is again noted that the values of the load coefficient at low pressure ratios ($PR \rightarrow 1.0$) approach those for the incompressible flow case.

4 EXPERIMENTAL WORK

4.1 Incompressible flow

4.1.1 Test Apparatus

The apparatus (Figure 37) consisted of the bearing (1) rigidly fixed in a cradle (2) and containing the journal (3). The journal was suspended by stirrups from one end of a counter-balanced lever (4). A spring balance (5) attached to the other end of the lever measured the load which was applied by means of a screw-capstan (6). Oil was supplied to the central annulus of the journal under high pressure from a vane pump (7). The main quantity of oil was by-passed and a branch was taken to the test assembly, the flow being regulated by a needle valve. A surge tank (8) in the oil circuit damped out the fluctuations caused by the pump. A set of pressure tappings (9) arranged around the bearing surface and connected through a selector unit (10) to a 6 in. Bourden tube pressure gauge (11) enabled the pressure distribution in the clearance space to be determined. The leakage through the annulus was either run into a graduated cylinder (12) for measuring the flow or returned to the oil reservoirs. Capacitance type transducers (13) fixed to the bearing were used to measure the relative movement between the bearing and journal. The bearing and journals were made from dimensionally stable oil hardening steel, and the surfaces were
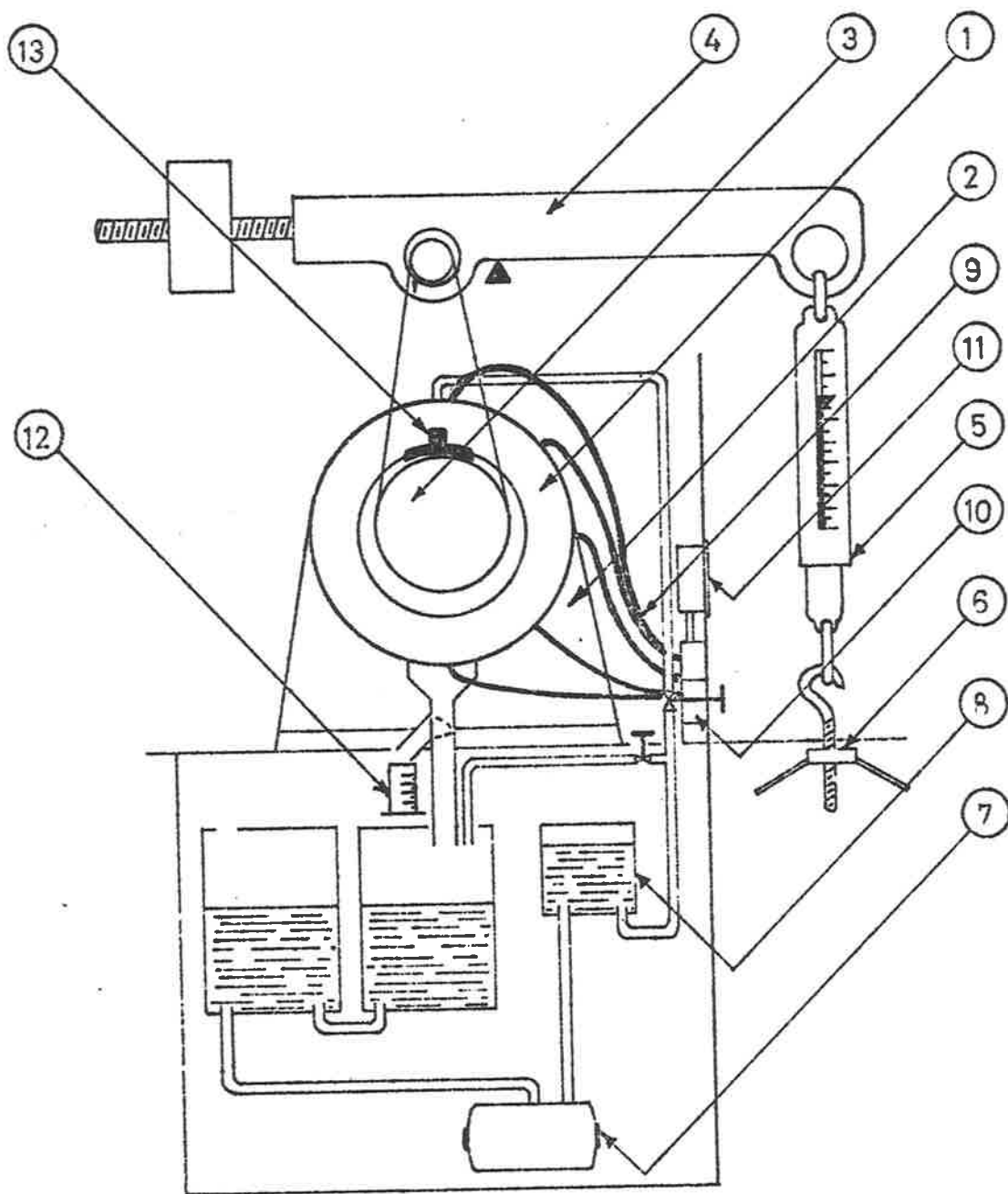
FIGURE 37   Incompressible flow test apparatus.

finish ground. Journals having length ratios L = 1.0 and 2.0, and taper ratios T = 1.2 and 1.85 respectively (the 'optimum' values, obtained from figure 6, p22) were used. Figure 38 shows the salient dimensions of the test pieces.

4.1.2   Test Procedure

The displacement transducers were calibrated with the journal in position, so that full scale deflection corresponded to the journal being moved from one side of the clearance to the other. Thus the transducer was adjusted to read eccentricity ratio (E), positive or negative, directly.

Oil was then circulated, and the supply pressure adjusted to the required value at the central annulus. The load on the spring balance was then adjusted until the journal just made contact with the bore, and the load (registered by the spring balance) and the leakage flow rate (measured by timing the flow into a graduated cylinder) were recorded. The temperature of the out-flowing oil was measured with a 0-100°F mercury-in-glass thermometer.

The load was reduced in equal decrements, and at each value the eccentricity and leakage flow were noted. Several test runs were made at each supply pressure to check the scatter of the results, and the mean values were recorded. The procedure was repeated at a number of values of the supply pressure.
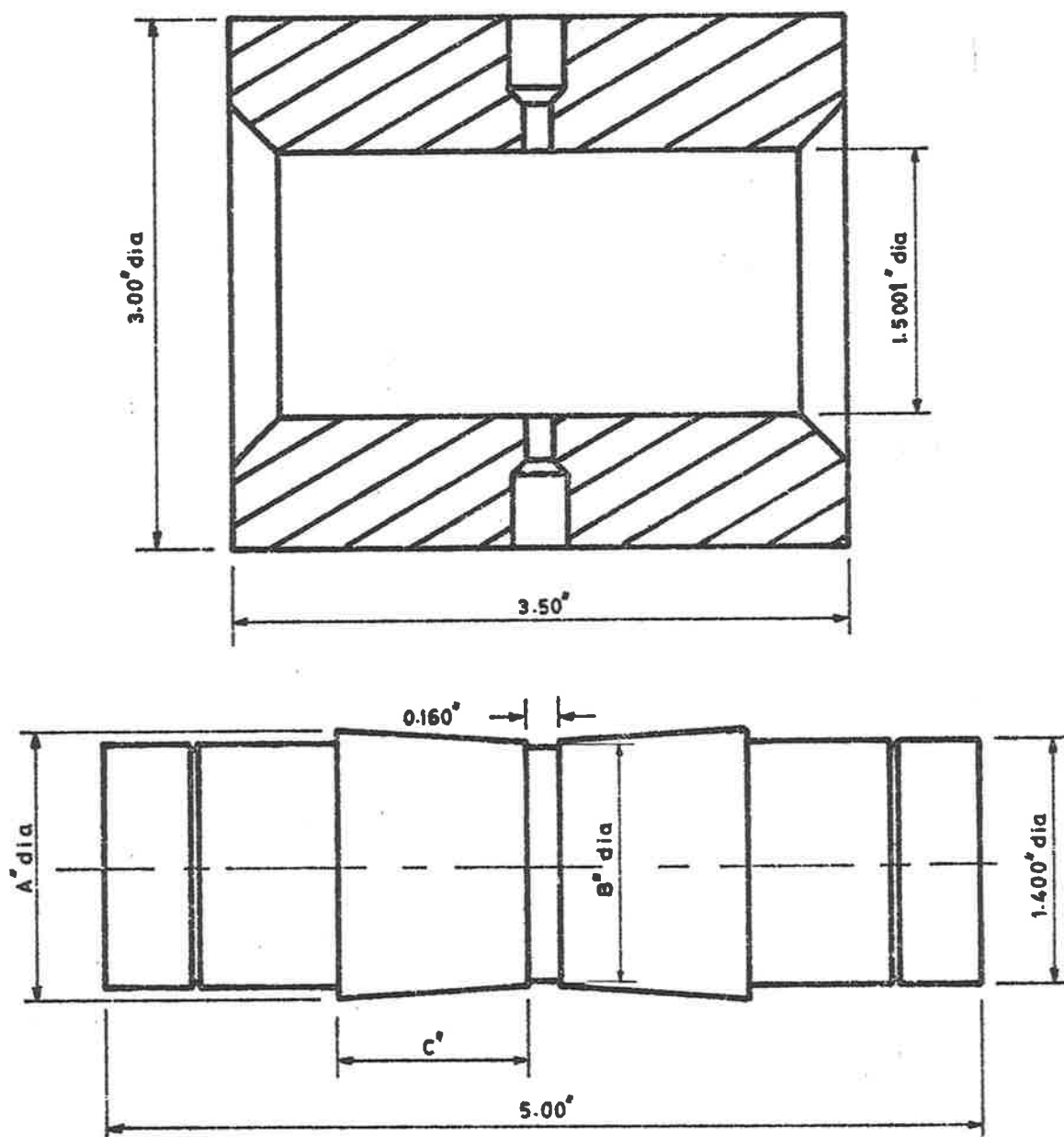
| JOURNAL | SALIENT DIMENSIONS | | | TAPER RATIO, T |
	A	B	C	(average of readings taken on both lands)
1	1.4982	1.4946	1.502	1.89
2	1.4980	1.4953	0.749	1.24

FIGURE 38   Incompressible flow test bearing and journal.

The accuracy of determination of the parameters measured
(obtained from the specifications of the instruments used) was

(a) Eccentricity $\pm$ 5% (positive indication at full eccentricity)

(b) Pressure $\pm$ 2%

(c) Load $\pm$ 2%

(d) Flow $\pm$ 2%

(e) Temperature $\pm$ 2%

4.1.3 Test results

(1) Pressure distribution

Figure 39 compares the experimental and theoretical
pressure distributions for the bearing with length ratio (L)
= 2.0 and taper ratio (T) = 1.8. It will be observed that
good agreement was obtained between theory and practice.

(2) Load carrying capacity

Figure 40 indicates the good agreement between the
experimental and theoretical load-eccentricity relationships.

(3) Leakage flow

Figure 41 shows the experimental variations of flow with
eccentricity ratio for the two journals. The value of the
viscosity used in the calculations of the predicted leakage
flow was obtained from Figure VIII-1, Appendix VIII. The
temperature at which the viscosity was determined was that
measured in the tests - 70° F.

FIGURE 39   Circumferential pressure distributions at several transverse stations (for L=2·0, T=1·8, E=1·0) Incompressible flow. (S.A.E 10W oil at 70°F)
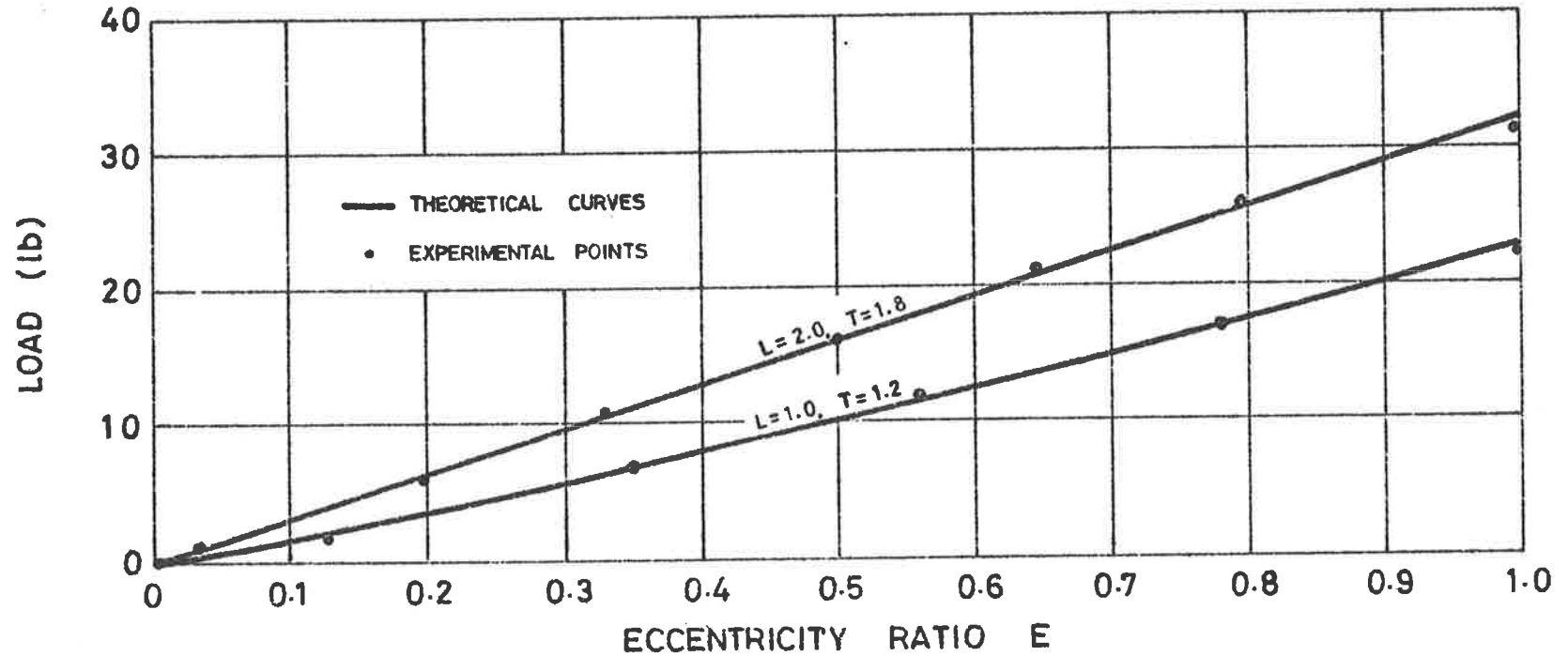
FIGURE 40   Load against eccentricity ratio (for L=1·0 and 2·0, T=1·2 and 1·8). Journal land length l = 1·5 and 3·0 in., diameter d = 3·0 in. Compressible flow.
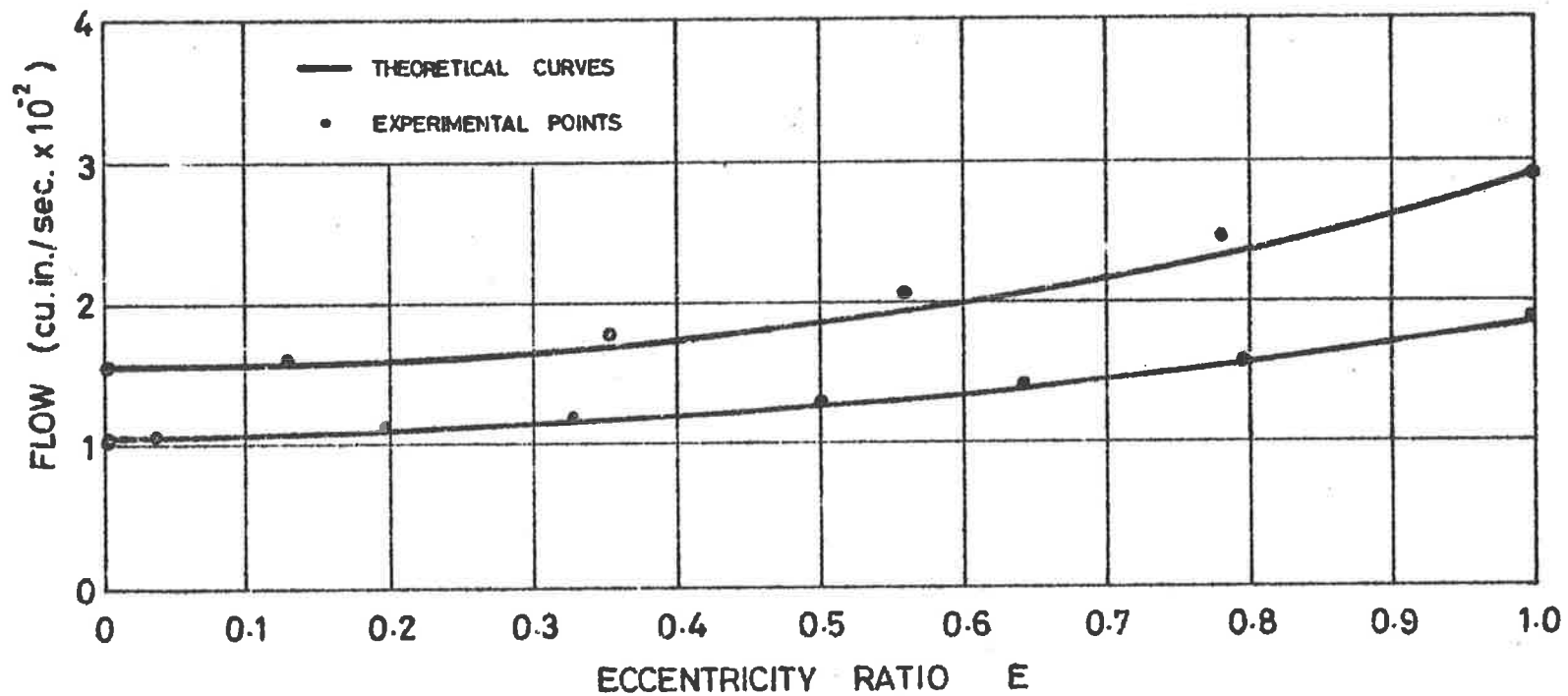
FIGURE 41 Flow against eccentricity ratio (for L = 1·0 and 2·0, T = 1·2 and 1·85, E = 1·0). Journal land length l = 0·75 in. and 1·50 in., diameter d = 1·5 in., clearance c = 0·001 in. Incompressible flow. (SAE 10W oil).

(4) Angular stiffness

The design of the apparatus was such that it could not easily be modified to enable measurements of the righting torque to be obtained. However, it was decided that a measure of the accuracy of the theory could be obtained from a comparison of the theoretical and experimental pressure distributions. This is given in Figure 42, where the close agreement suggests that the theoretical righting torque (derived from the pressure distribution) would closely approach the practical value.

4.2 Compressible flow

4.2.1 Test Apparatus

The apparatus used for the incompressible flow tests was not suitable for use with a gas without considerable modification. Therefore it was decided to retain the apparatus intact for possible further tests, and to construct a set-up suitable for use with a gas. The bearing was made larger to enable a greater number of pressure tappings to be positioned around the surface. In most other respects the two test rigs were identical. In this case (Figure 43) the bearing (1) contained the journal (2) which was rigidly fixed to the base plate (3). The bearing was supported by stirrups (4) from one end of a counterbalanced lever (5). A spring balance (6) attached to the other end of the lever
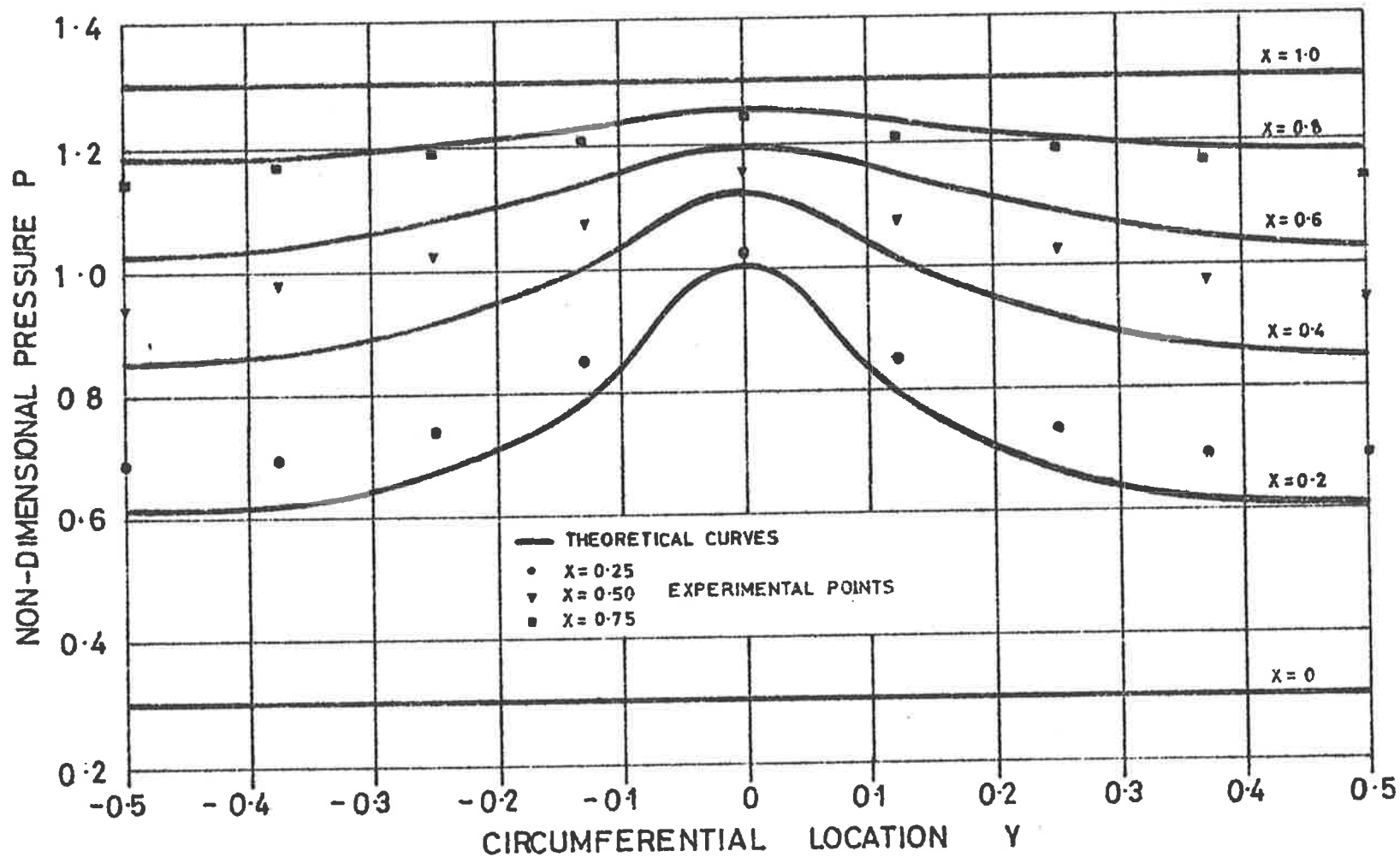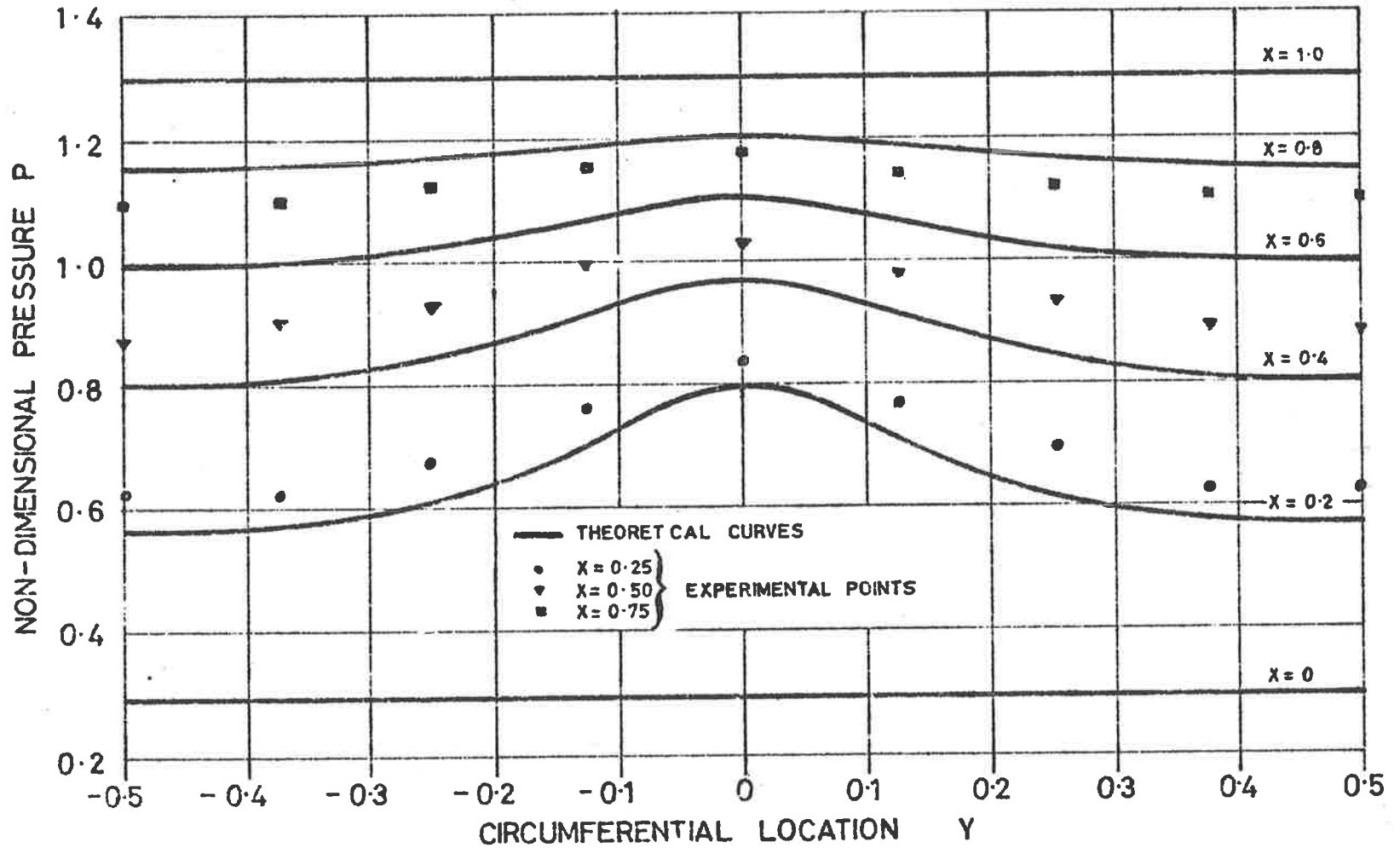
FIGURE 42   Circumferential pressure distributions at several transverse stations (for L=2·0, T=1·8; tilted journal). Incompressible flow (S.A.E. 10W oil at 70° F).
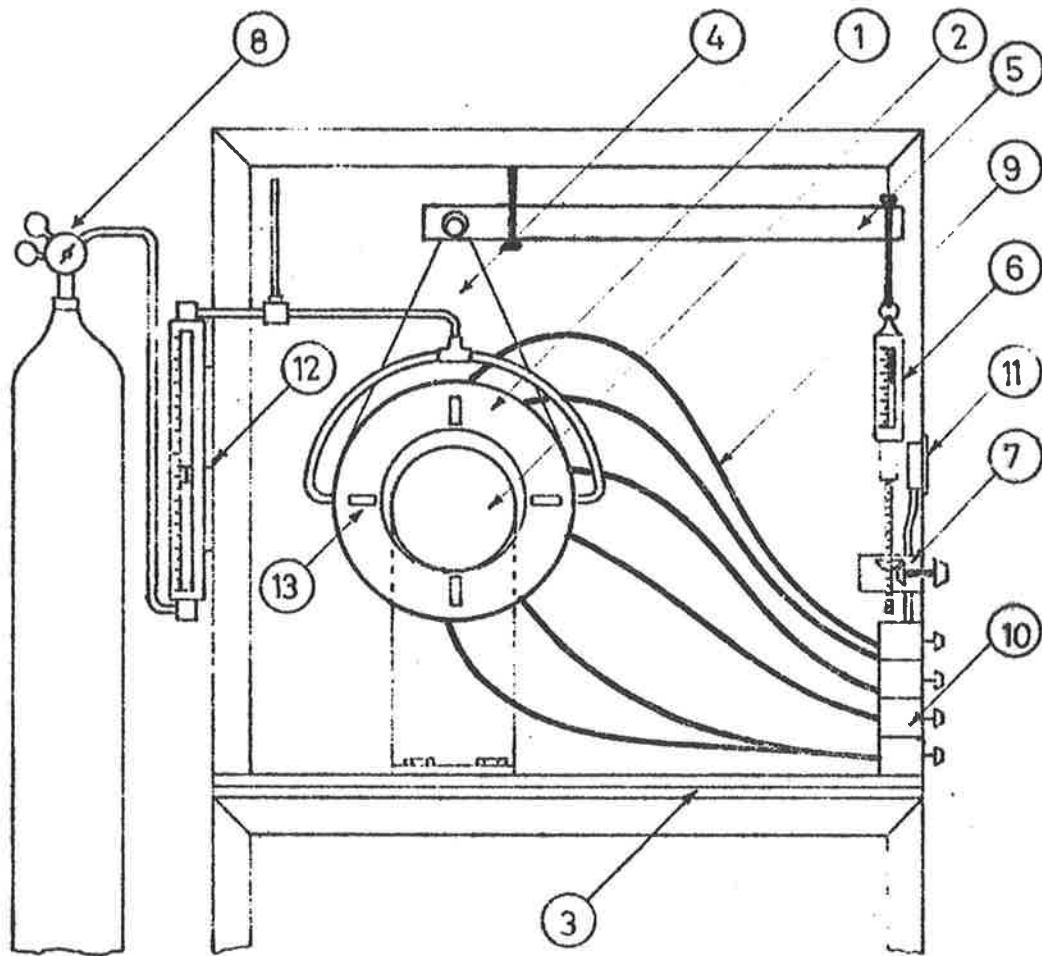
FIGURE 43   Compressible   flow   test   apparatus.

measured the load which was applied by means of a geared capstan (7). Air under pressure was supplied to the central annulus from an air bottle (8). A set of pressure tappings (9) arranged around the bearing and connected through a selector unit (10) to a 6" Bourdon tube pressure gauge (11) enabled the pressure distribution in the clearance space to be determined. The leak-age through the clearance was measured with a flowrator (12). Induction type displacement transducers (13) – found to be more suitable than the capacitance type previously used (see Appendix IX) – were positioned at each end of the bearing assembly and gave a continuous and accurate indication of the relative position of the bearing and journal during the tests. The whole apparatus was enclosed within a rigid framework mounted on a vibration isolated section of the laboratory floor.

Journals having length ratios L = 1.0 and 2.0 and taper ratios T = 1.0, 2.0, 3.0 and 4.0 were prepared for the tests. The salient dimensions of these test pieces are given in Figure 44.

4.2.2 Test Procedures

The displacement transducers were calibrated on the apparatus as for the incompressible flow tests. Air was then supplied to the central annulus at the required pressure. The bearing was then loaded until it just made contact with the journal – the fully eccentric position – and the load and flow were recorded.
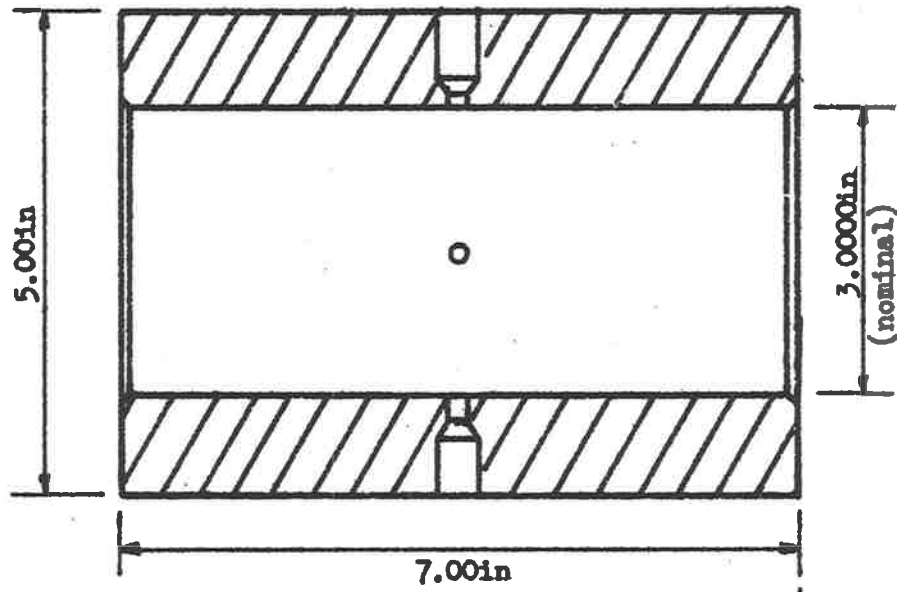
A metrology report on the bearing gave:-

(1) The maximum and minimum bore diameters as

    (a) Max. 2.99949 inches.

    (b) Min. 2.99934 inches.

(2) The maximum ovality as 0.00015 inches.

(3) The surface finish as varying between 23 and 27
    micro-inches CLA.

For detailed bore dimensions refer to Figure 44(b)

* Metrology and Standards Section, W.R.E. Salisbury, Ref.1765/65/5

FIGURE 44(a) Compressible flow test pieces — Bearing.
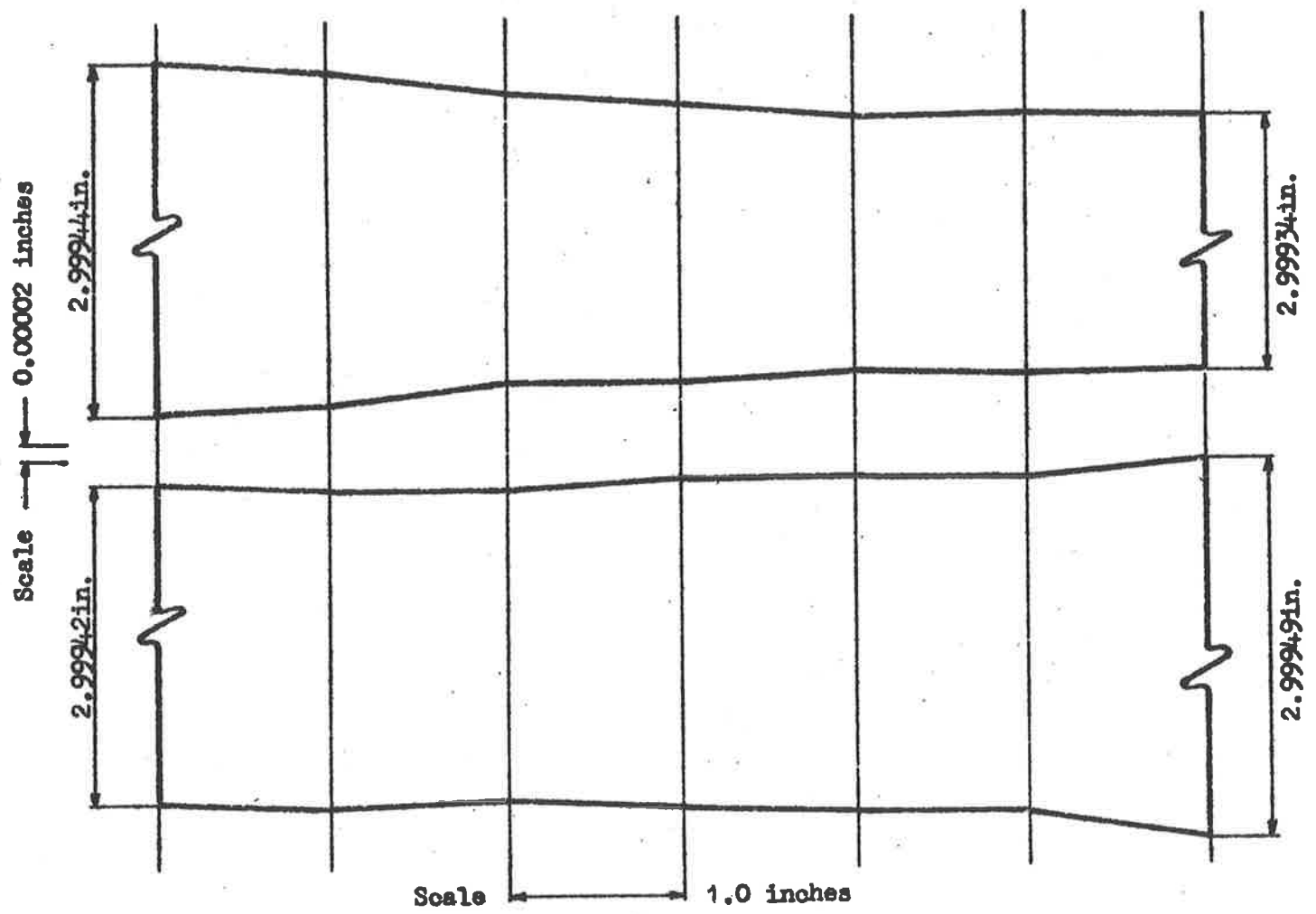
FIGURE 44(b) Compressible flow test pieces — Bearing bore profiles.
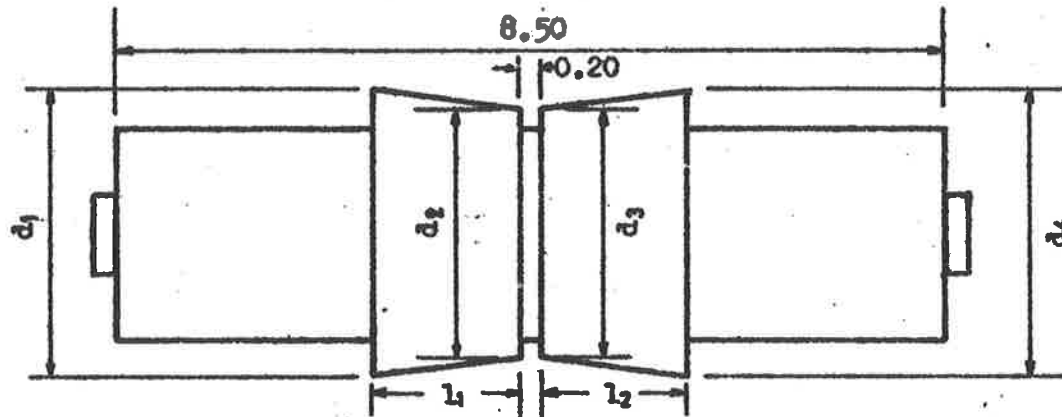
Nominal Taper Ratio	Nominal Length Ratio L = 1.0						Derived Values			
	Measured Values									
	d_1	d_2	d_3	d_4	l_1	l_2	c*	t**	T	L
T = 1.0	2.9977	2.9955	2.9956	2.9976	1.503	1.505	0.0009	0.0010	1.11	1.00
T = 2.0	2.9977	2.9935	2.9934	2.9976	1.503	1.505	0.0009	0.0021	2.33	1.00
T = 3.0	2.9977	2.9918	2.9919	2.9976	1.503	1.505	0.0009	0.0029	3.22	1.00
T = 4.0	2.9977	2.9899	2.9898	2.9976	1.503	1.505	0.0009	0.0039	4.33	1.00

* Average reading, measured in conjunction with the bearing of Figure 44(a).

** Average reading from the two journal lands.   All dimensions in inches.

FIGURE 44(c)   Compressible flow test pieces — short journals.

Nominal Taper Ratio	Nominal Length Ratio L = 2.0 Measured Values						Derived Values			
	d_1	d_2	d_3	d_4	l_1	l_2	c*	t**	T	L
T = 1.0	2.9976	2.9958	2.9959	2.9978	3.002	3.004	0.0009	0.0008	0.89	2.00
T = 2.0	2.9976	2.9937	2.9936	2.9978	3.002	3.004	0.0009	0.0020	2.22	2.00
T = 3.0	2.9976	2.9916	2.9917	2.9978	3.002	3.004	0.0009	0.0030	3.34	2.00
T = 4.0	2.9976	2.9898	2.9898	2.9978	3.002	3.004	0.0009	0.0039	4.33	2.00

* Average reading, measured in conjunction with the bearing of Figure 44(a).

** Average reading from the two journal lands.   All dimensions in inches.

FIGURE 44(d)   Compressible flow test pieces — long journals.

The load was then reduced, and at eccentricity ratios of 0.8, 0.6, 0.4, 0.2 and zero the load and flow were noted. Several test runs were made at each supply pressure to check the scatter of the results and mean values were recorded. The procedure was repeated for each journal at supply pressures ranging from 5 to 150 p.s.i.g. Pressure distributions tests were carried out for the long journal (L = 2.0, T = 1.0) at full and half eccentricity, and in the fully tilted position.

The accuracy of determination of the parameters measured was obtained from the specifications of the instruments used as

(1) Eccentricity $\pm$ 1%   (Positive indication at full eccentricity)

(2) Pressure $\pm$ 2%

(3) Load $\pm$ 2%

(4) Flow $\pm$ 2%

(5) Temperature $\pm$ 2%

4.2.3   Test Results

(1) Pressure distribution

Figure 45 compares the experimental and theoretical pressure distribution in the clearance space for the bearing with length ratio L = 2.0 and taper ratio T = 1.0 at eccentricity ratio E = 1.0, with supply pressure P = 50 p.s.i.g., and exit pressure P = 0 p.s.i.g. It will be noticed that good agreement between theory and experiment

FIGURE 45   Circumferential pressure distributions at several transverse stations (for L = 2·0, T = 1·0, E = 1·0). Compressible flow. (PR = 4·4).

was obtained, except in the region of contact. Figure 46
presents a similar comparison for the same journal at
eccentricity ratio $E = 0.5$. The discrepancy between theory
and experiment in the minimum clearance region can be observed
to be significantly less than that shown in Figure 45. This
can be explained as follows.

It has been shown (2) that even a small degree of journal
or bearing ovality can considerably affect the pressure
distribution in the clearance space. Although the ovality of
the test pieces is slight (Figure 44), it becomes significant
in regions where the clearance is small. Hence, in the region
of contact it is reasonable to expect experimentally determined
pressures to vary from the theoretical results (Figure 45).
However, when the journal is moved away from the bearing shell
(eccentricity ratio decreased), the ovality becomes less
significant compared with the increased film thickness, and
the effect on the pressure distribution is considerably reduced
(Figure 46).

However, it will be observed that, even in the worst case
(Figure 45), the region effected by ovality is small. The
resultant effect on the load capacity will therefore be slight.

(2)   Load carrying capacity

Figure 47 presents the experimental variations of the load
coefficient with taper ratio for the journals having length
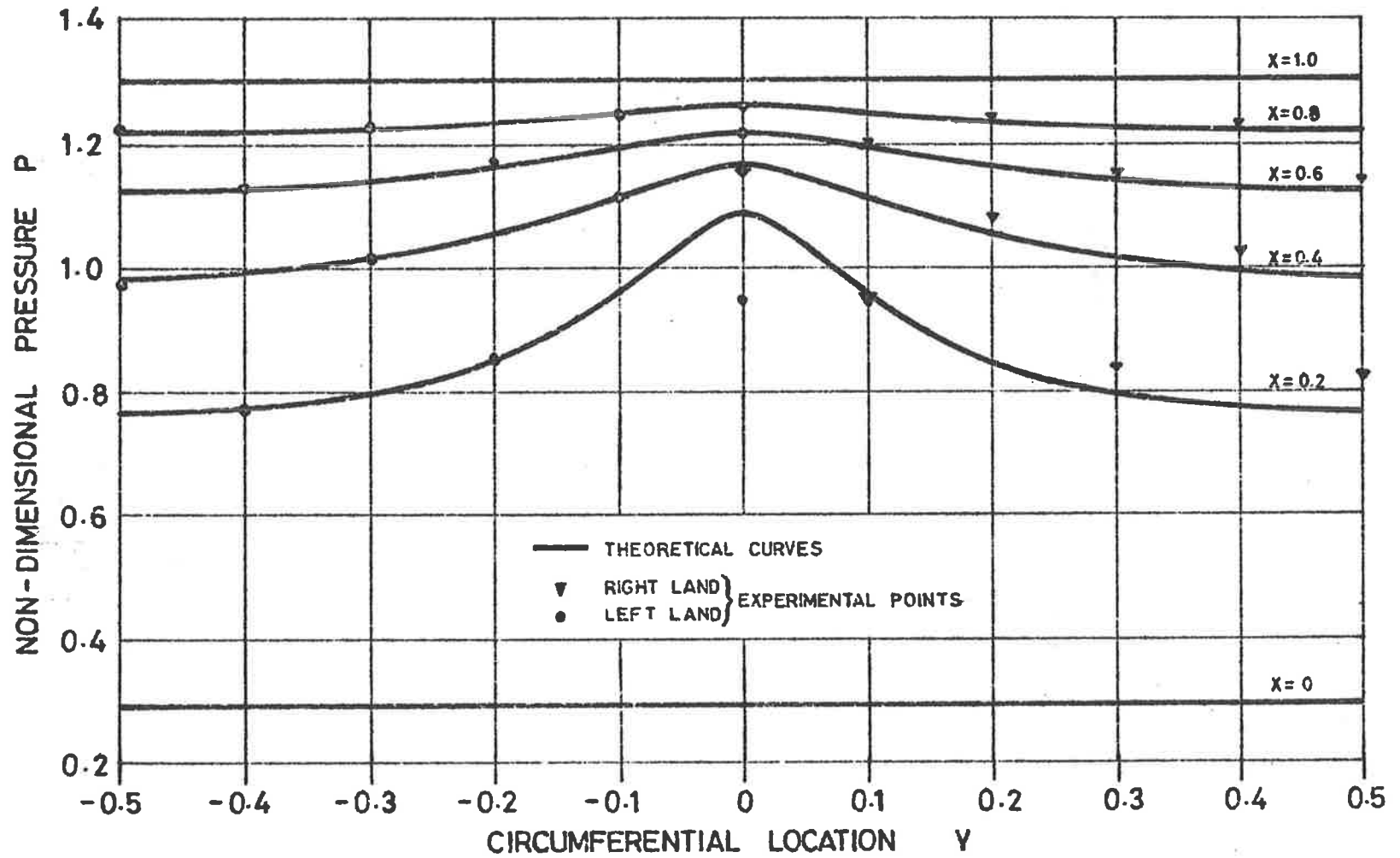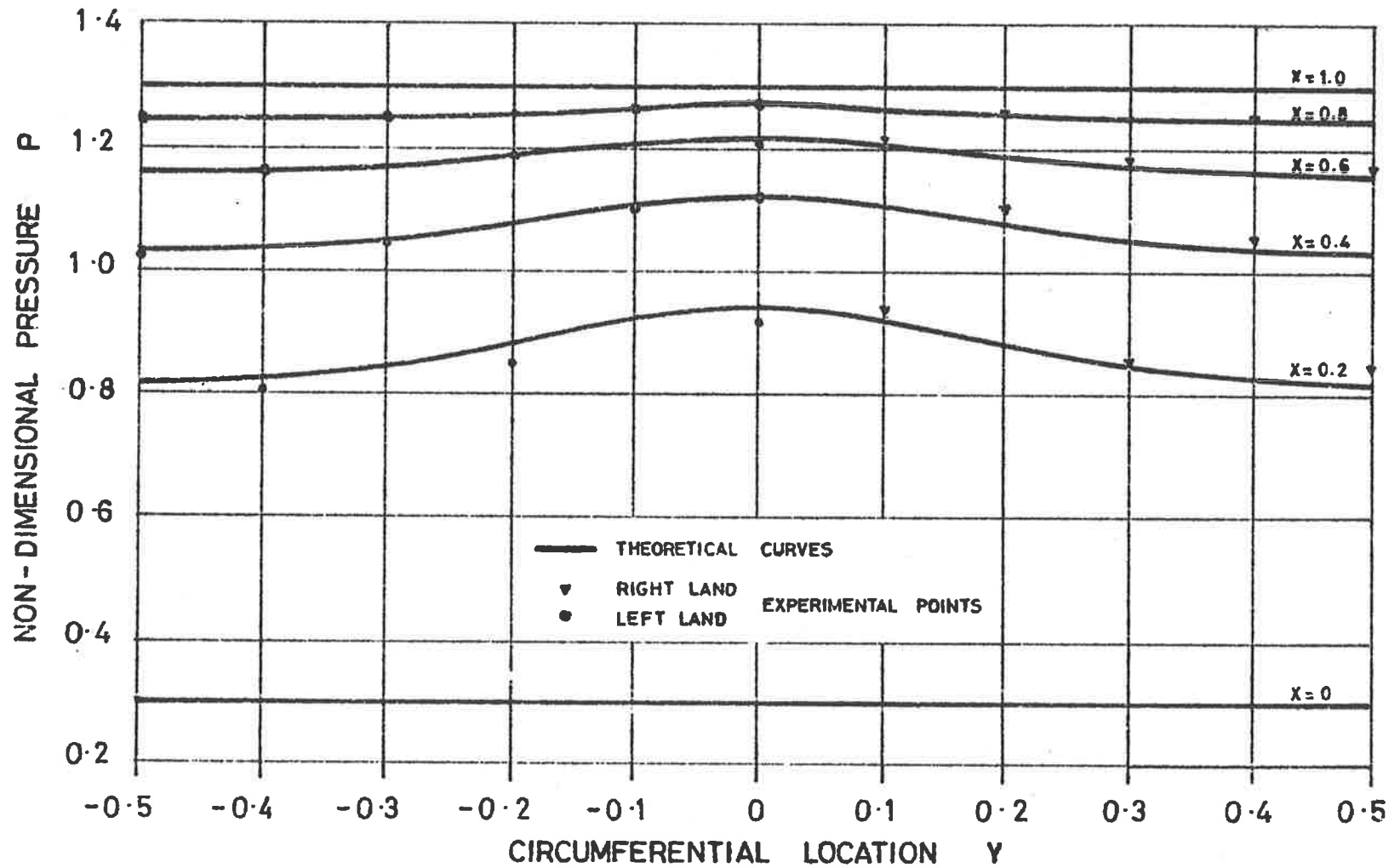
FIGURE 46 Circumferential pressure distributions at several transverse stations (for L = 2·0, T = 1·0, E = 0·5). Compressible flow. (PR = 4·4).
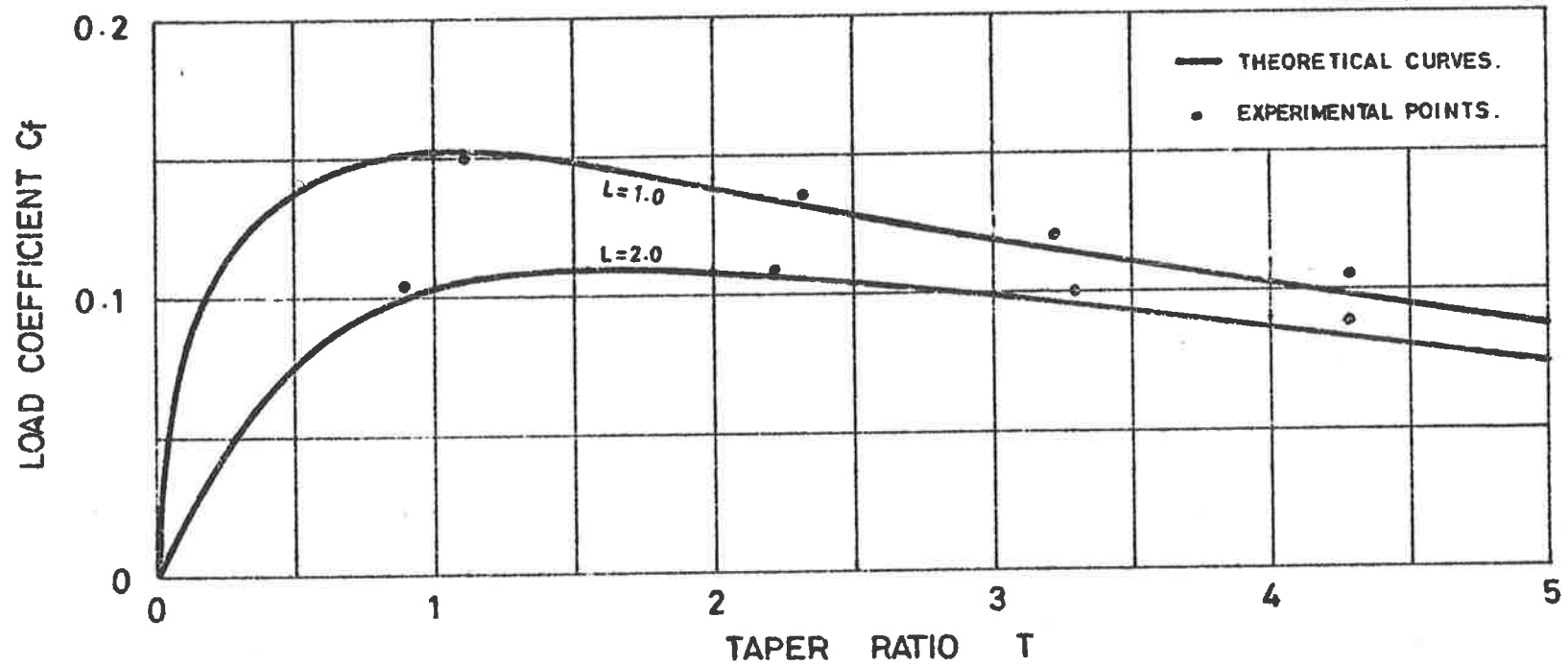
FIGURE 47   Load coefficient against taper ratio (for L=1·0 and 2·0, E=1·0). Compressible flow. (PR=4·4).

ratios L = 1.0 and 2.0, in the fully eccentric position
(E = 1.0). Supply pressure P_1 = 50 p.s.i.g., and exit
pressure P_2 = 0 p.s.i.g.

Figure 48 shows the comparison between the experimental
and theoretical variations of the load with eccentricity ratio.
In both these figures, good agreement between theory and
experiment is apparent.

(3)   Leakage flow

Figure 49 compares the experimental and theoretical
variation of the flow coefficient with taper ratio. The
viscosity of the air was obtained (for the measured ambient
temperature - 70 F) from Figure VIII-2, Appendix VIII, for
the calculation of the predicted leakage flow.
Figure 50 presents the experimental and theoretical variations
of the leakage flow with eccentricity ratio. In both figures
good agreement can be observed between the experimental values
and those obtained from the theoretical analysis.

(4)   The effect of Pressure Ratio

Figures 51 and 52 show the effect of pressure ratio $(\frac{P_1}{P_2})$
on the load and flow respectively for the two journals. It
will be observed that agreement between theory and experiment
is good for pressure ratios up to PR = 5, but that beyond this
both the load and flow fall below the predicted values. As
already discussed in Section 3.3.5, p49, these deviations were
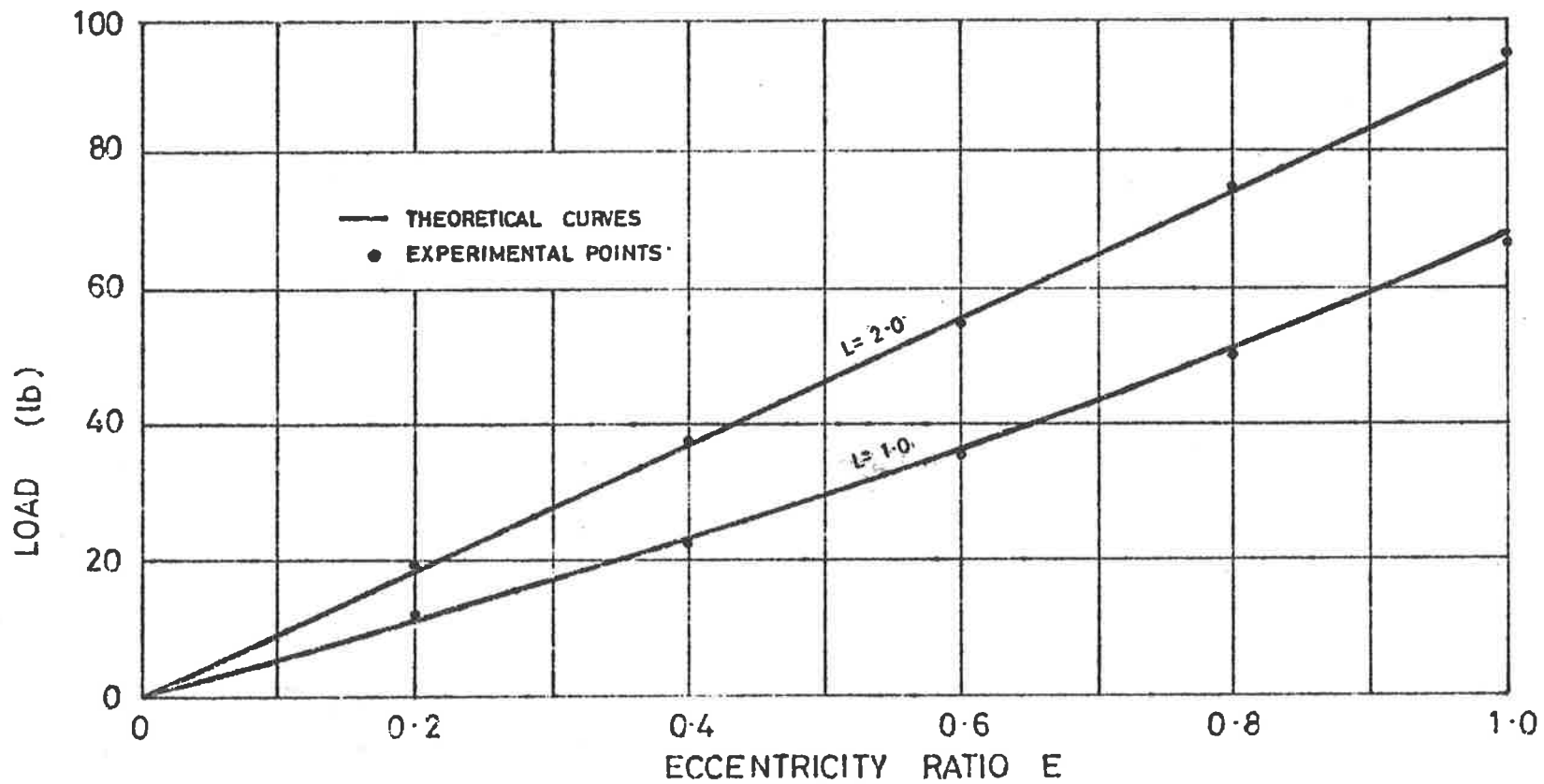
FIGURE 48   Load against eccentricity ratio (for L=1·0 and 2·0, T=1·0)
Compressible flow (p_1 = 50, p_2 = 0 psig)
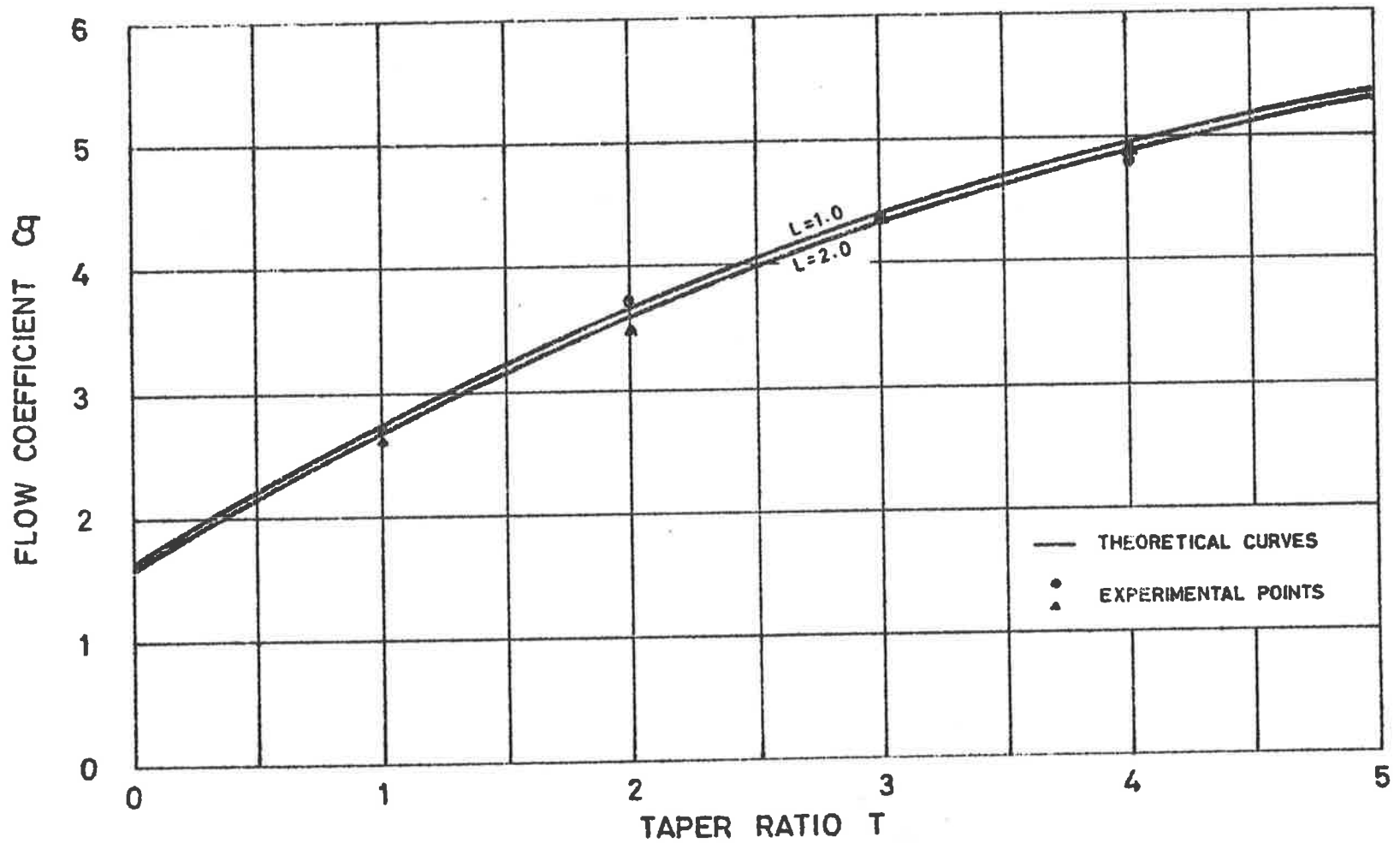
FIGURE 49   Flow coefficient against taper ratio (for L=1·0 and 2·0, E=1·0)
Compressible flow (PR= 4·4).
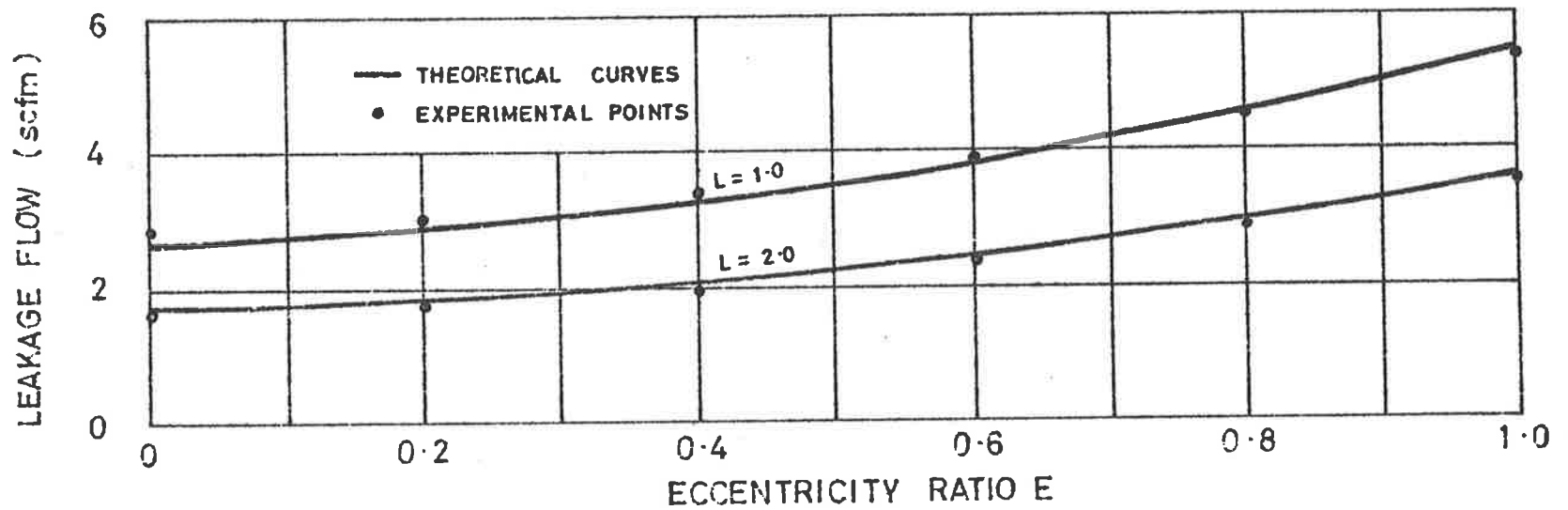
FIGURE 50   Leakage flow against eccentricity ratio (for L=1·0 and 2·0, T=1·0)   Compressible flow (p_1=50 , p_2= 0psig)
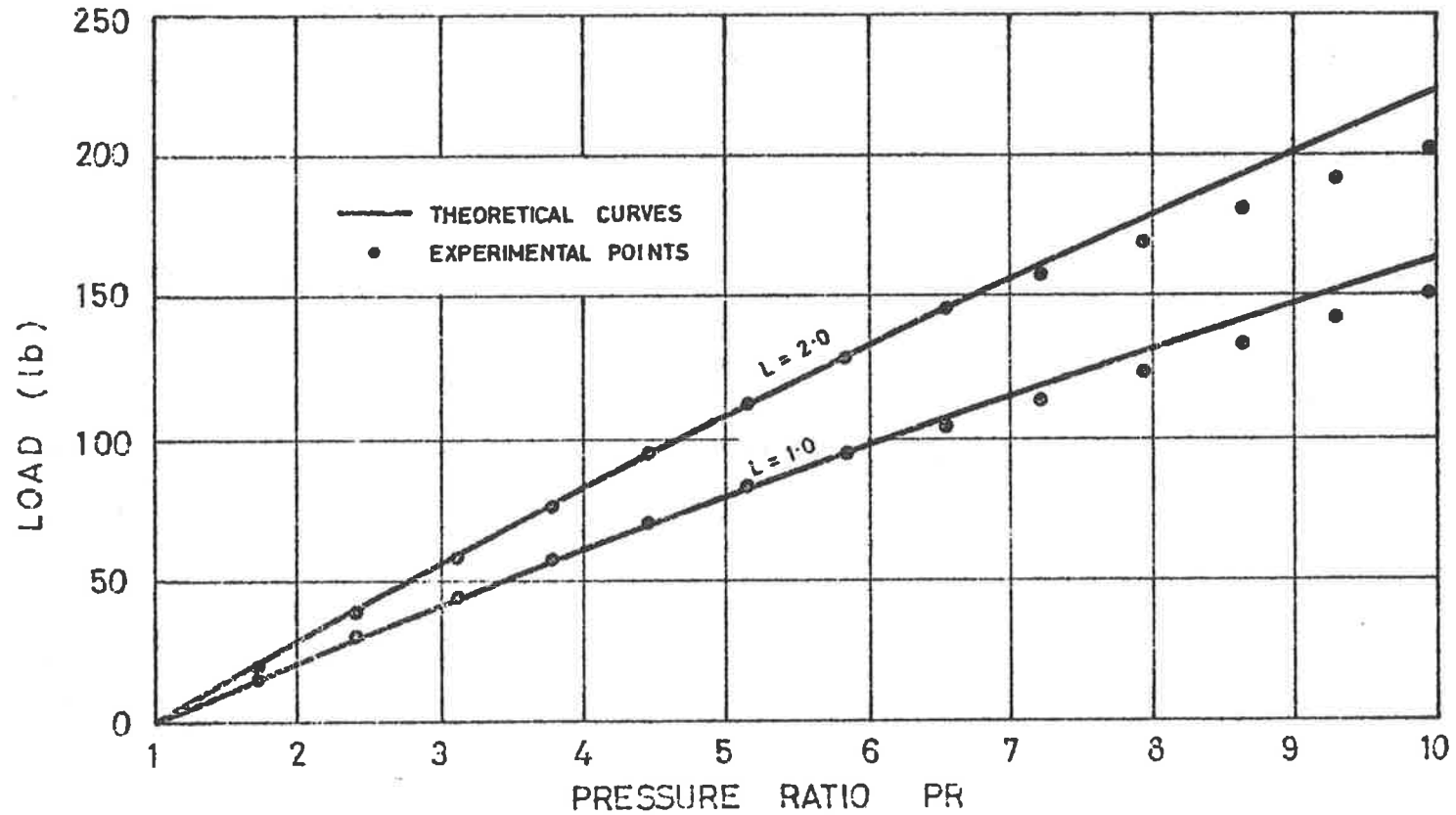
FIGURE 51 Load against pressure ratio (for L=1·0 and 2·0, T=1·0, E=1·0). Journal land lengths l = 1·5 and 3·0 in, diameter d = 3·0 in. Compressible flow.
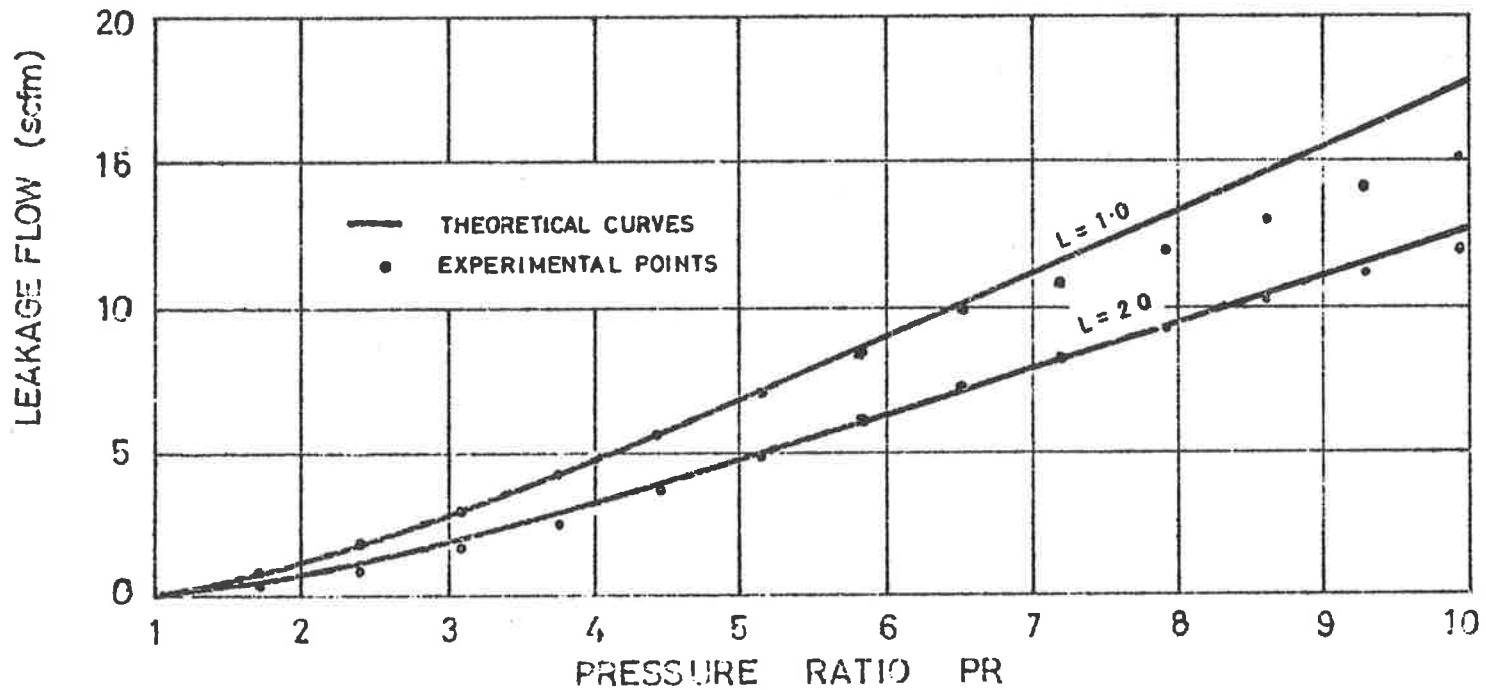
FIGURE 52   Leakage flow against pressure ratio (for L=1·0 and 2·0, T=1·0, E=1·0). Journal land lengths l=1·5 and 3·0 in, diameter d = 3·0 in, clearance c=0·001 in. Compressible flow.

mainly due to choking of the flow in the clearance space. Evidence to support this is found in Figure 53. Here axial pressure distributions near the exit at several circumferential stations are presented for pressure ratios in the 'unchoked' and 'choked' regions. These curves were obtained using a micrometer screw head to adjust the axial position of the end of the journal relative to a pressure tapping in the bearing shell. Readings were taken at 0.012in. intervals. It can be seen that at the lower pressure ratio the pressure rises steadily away from the exit at all points around the circumference. However, at the high pressure ratio those distributions in the large clearance region (where velocities are highest) show a sudden rise in pressure at the exit, and close to the exit actually lie above the curves for the small clearance (normally higher pressure) region. Such a condition could only arise if the flow had become choked in the large clearance region.

(5)   Angular stiffness

As for the incompressible flow tests (Section 3.2.3) no measurement of the righting torque was undertaken. However, the good agreement between the theoretical and experimental pressure distributions for the tilted journal suggests that the moment coefficient (obtained from the theoretical distribution) would not be significantly in error.
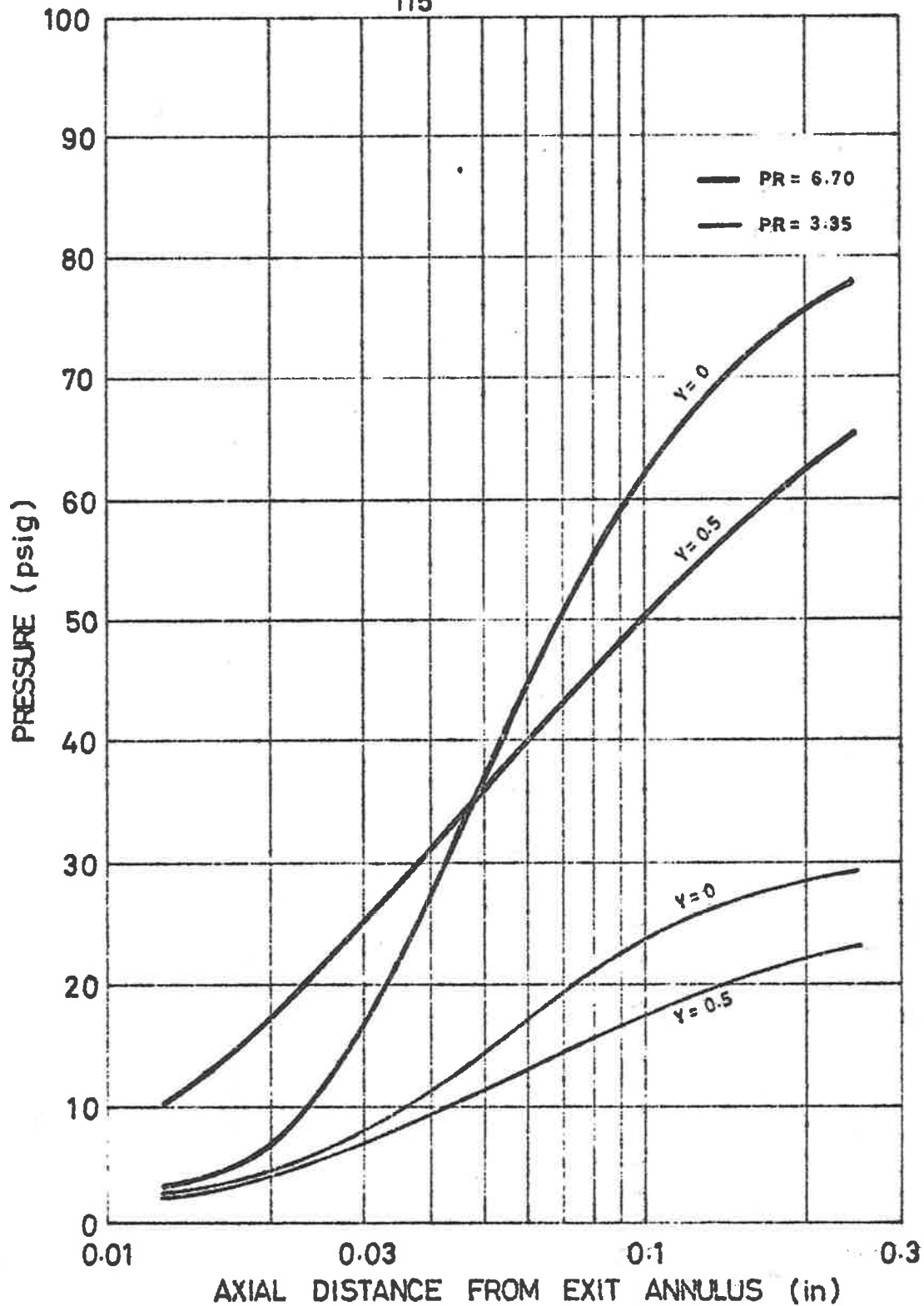
FIGURE 53 Axial pressure distributions in the plane of symmetry (for L=1·0, T=1·0, E=1·0) at high and low pressure ratios.

4.2.4 Stepped land bearings

(1) Test pieces

For the tests on the stepped land bearings, the following journal configurations were used.

L = 1.0, 2.0

SDR = 1.0, 2.0, 4.0

SLR = 0.05, 0.10, 0.25, 0.50

To ensure uniformity of the step depth ratio (SDR) for each series of the step length ratio (SLR), the manufacturing method adopted was to first make a journal having the step length ratio SLR = 0.50, and then to grind the land length l (Figure 30, p71) back to the next required value without altering the step depth. Adoption of this method also meant that only six journals had to be prepared.

The actual dimensions of the test pieces are given in Figure 54.

The results of the tests are presented in Figures 55 to 58, where the load and load coefficient are plotted against the step length ratio and step depth ratio respectively, and in Figure 58a tl experimental values are compared with the theory.
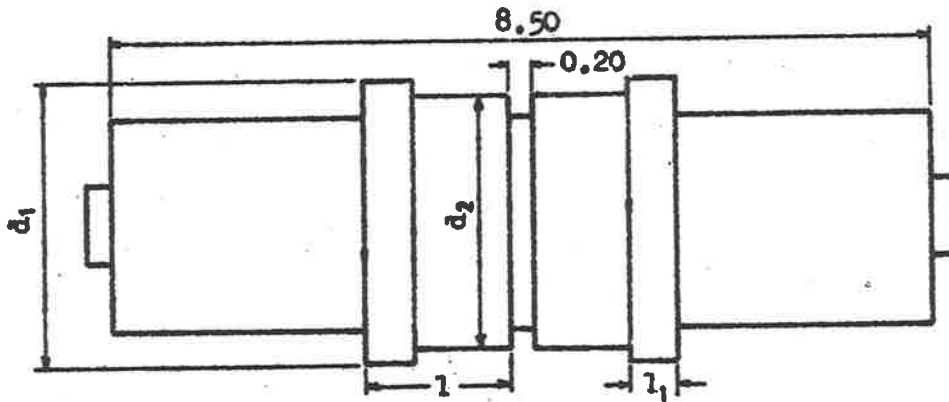
Nominal Ratios		Nominal Length Ratio L = 1.0 Measured Values				Derived Values				
SLR	SDR	d_1	d_2	l	l_1	o^*	s	L	SLR	SDR
0.50	1.0	2.9975	2.9953	1.502	0.755	0.0010	0.0011	1.00	0.50	1.10
0.50	2.0	2.9975	2.9933	1.502	0.755	0.0010	0.0021	1.00	0.50	2.10
0.50	4.0	2.9975	2.9895	1.502	0.755	0.0010	0.0040	1.00	0.50	4.00
0.25	1.0	2.9974	2.9955	1.504	0.376	0.0010	0.0010	1.00	0.25	1.00
0.25	2.0	2.9974	2.9932	1.504	0.376	0.0010	0.0021	1.00	0.25	2.10
0.25	4.0	2.9974	2.9894	1.504	0.376	0.0010	0.0040	1.00	0.25	4.00
0.10	1.0	2.9975	2.9854	1.500	0.156	0.0010	0.0011	1.00	0.10	1.10
0.10	2.0	2.9975	2.9835	1.500	0.156	0.0010	0.0020	1.00	0.10	2.00
0.10	4.0	2.9975	2.9892	1.500	0.156	0.0010	0.0042	1.00	0.10	4.20
0.05	1.0	2.9973	2.9956	1.498	0.074	0.0011	0.0009	1.00	0.49	0.82
0.05	2.0	2.9973	2.9932	1.498	0.074	0.0011	0.0021	1.00	0.49	1.91
0.05	4.0	2.9973	2.9890	1.498	0.074	0.0011	0.0042	1.00	0.49	3.92

* Average reading, measured in conjunction with the bearing of Figure 44(a)

FIGURE 54(a)   Stepped land test pieces — short journals.
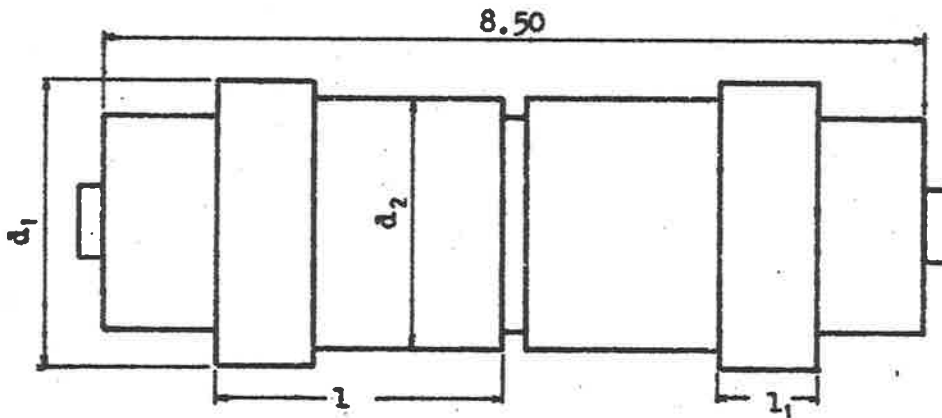
Nominal Ratios		Nominal Length Ratio L = 2.0 Measured Values				Derived Values				
SLR	SDR	d_1	d_2	l	l_1	c^*	s	L	SLR	SDR
0.50	1.0	2.9974	2.9955	3.004	1.501	0.0010	0.0010	2.00	0.50	1.00
0.50	2.0	2.9974	2.9936	3.004	1.501	0.0010	0.0019	2.00	0.50	1.90
0.50	4.0	2.9974	2.9894	3.004	1.501	0.0010	0.0040	2.00	0.50	4.00
0.25	1.0	2.9973	2.9955	3.004	0.753	0.0011	0.0009	2.00	0.25	0.82
0.25	2.0	2.9973	2.9932	3.004	0.753	0.0011	0.0021	2.00	0.25	1.91
0.25	4.0	2.9973	2.9890	3.004	0.753	0.0011	0.0042	2.00	0.25	3.82
0.10	1.0	2.9975	2.9954	3.002	0.303	0.0010	0.0011	2.00	0.10	1.10
0.10	2.0	2.9975	2.9933	3.002	0.303	0.0010	0.0021	2.00	0.10	2.10
0.10	4.0	2.9975	2.9892	3.002	0.303	0.0010	0.0042	2.00	0.10	4.20
0.05	1.0	2.9974	2.9955	3.000	0.149	0.0010	0.0010	2.00	0.05	1.00
0.05	1.0	2.9974	2.9932	3.000	0.149	0.0010	0.0021	2.00	0.05	2.10
0.05	1.0	2.9974	2.9894	3.000	0.149	0.0010	0.0040	2.00	0.05	4.00

* Average reading, measured in conjunction with the bearing of Figure 44(a)

FIGURE 54(b) Stepped land test pieces — long journals.
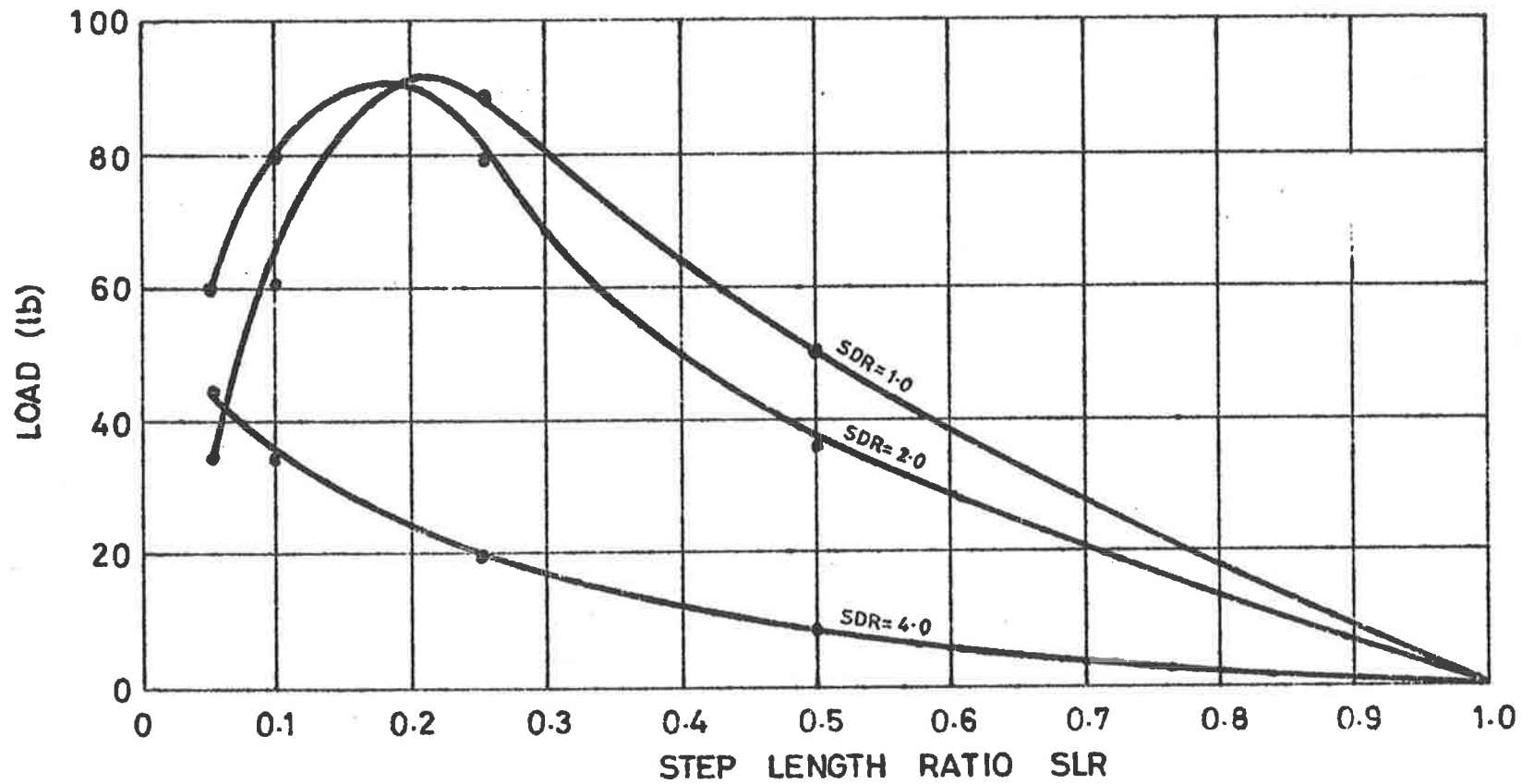
FIGURE 55   Load against step length ratio (for L= 1.0, SDR$\overset{*}{=}$1.0, 2.0 and 4.0, E=1.0). Experimental points with fitted curves. Journal land length l = 1.5 in., diameter d = 3.0 in. Compressible flow. * Nominal values.
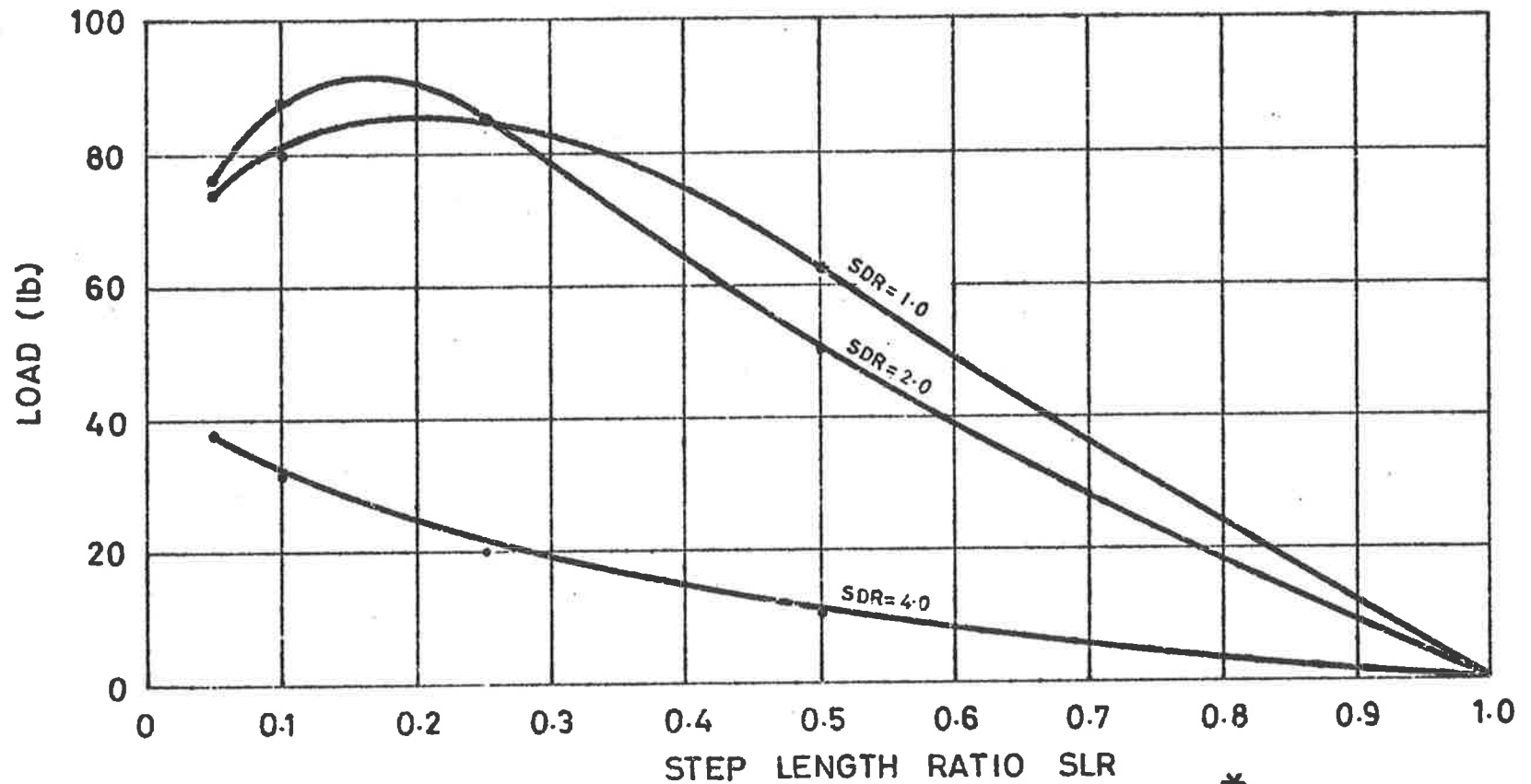
FIGURE 56   Load against step length ratio (for L=2·0, SDR*=1·0, 2·0 and 4·0, E=1·0). Experimental points with fitted curves. Journal land length l=3·0 in., diameter d=3·0 in. Compressible flow.
* Nominal values
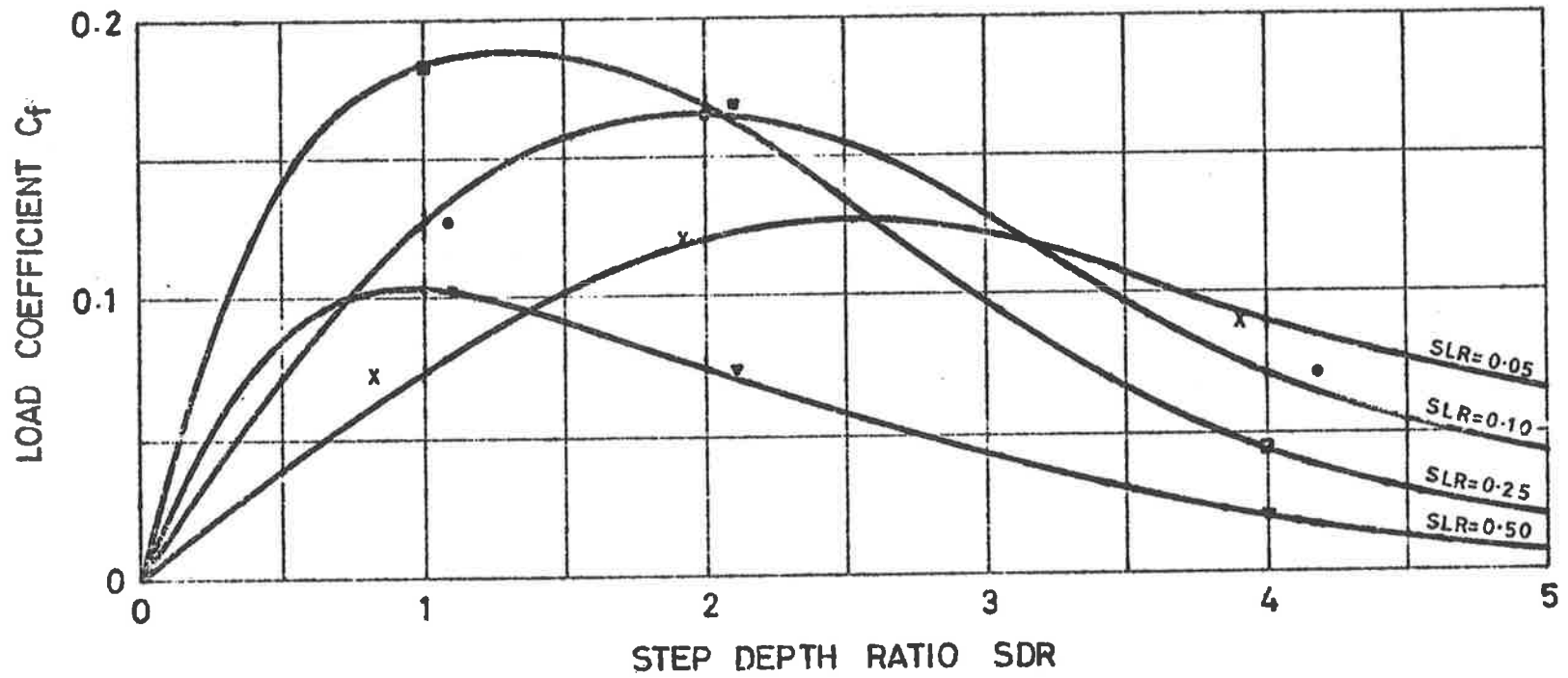
FIGURE 57   Load coefficient against step depth ratio (for SLR=0.05, 0.10, 0.25, 0.50, L=1.0, E=1.0). Experimental points with fitted curves* Journal land length l=1.5 in., diameter d=3.0 in. Compressible flow.   * From Figure 55
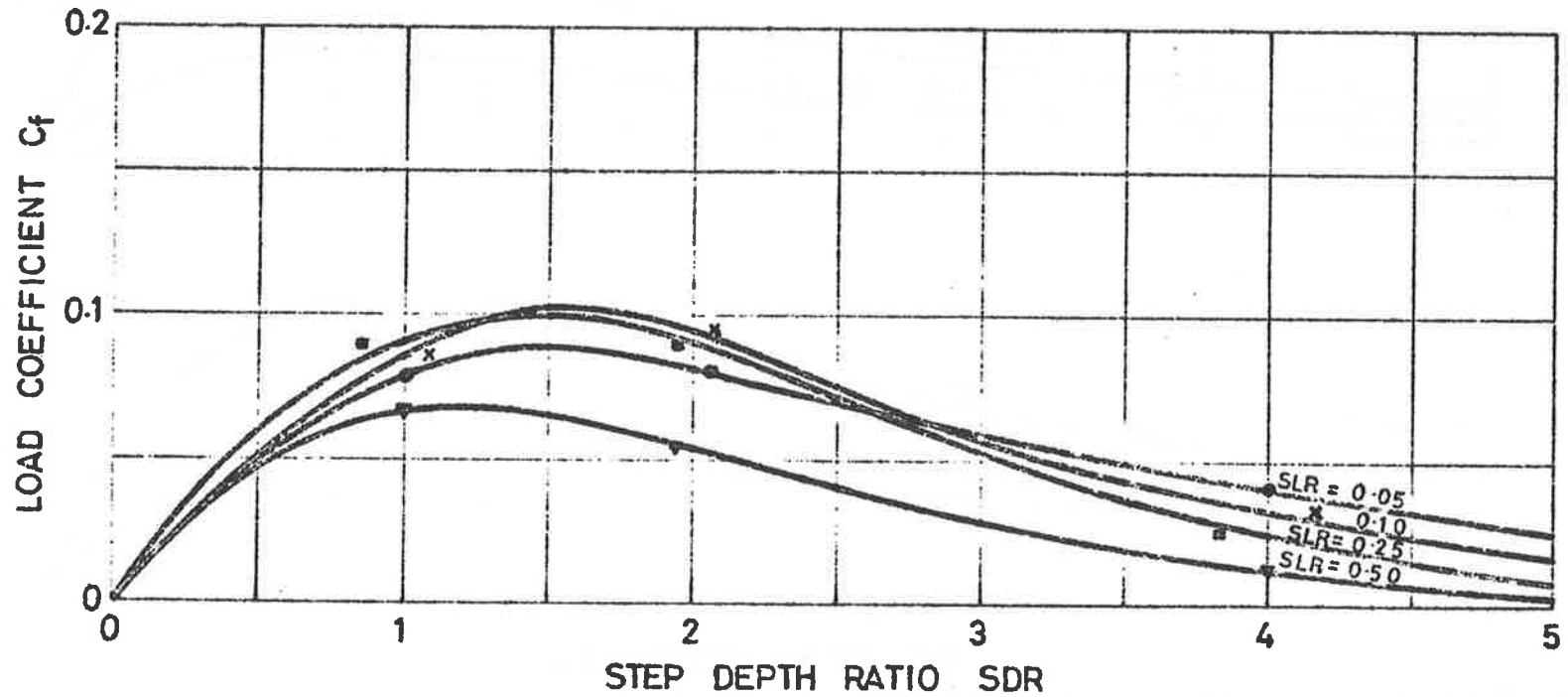
FIGURE 58 Load coefficient against step depth ratio (for L=2·0, E=1·0, SLR= 0·05, 0·10, 0·25, 0·50). Experimental points with fitted curves* Journal land length l=3·0 in., diameter d=3·0 in. Compressible flow. * From Figure 56

It will be noticed that, with the exception of the curve for
L = 1, SLR = 0.1, the divergence between theory and experiment
is greater than could normally be attributed to experimental
error.

In order that this discrepancy be adequately explained, it
was considered that further work should be done both on the
theory and on the experiment. However, some suggestions as to
the reasons for the discrepancies can be made.

It is possible that inertia effects become significant as the
gas accelerates over the step. Also, in the case of the bearing
with L = 1, SLR = 0.1 (a short bearing with a short step) it is
possible that choking could be present, which has already been
shown to have the effect of reducing the load capacity.

4.2.5 Modifications to improve the load carrying capacity

Comparison of the peak values of the curves of Figures 47 and
54 with those of the corresponding theoretical curves of Figures
15 and 35 shows that, for each bearing type, the load coefficient
obtainable in practice (two dimensional flow) falls short of that
predicted for axial (one dimensional) flow. As explained pre-
viously, this is due to the existance of short circuiting
(circumferential) flow. It was decided, therefore, to investigate
the possibility of improving the load capacity of those bearings
by modifying the geometry to limit short circuiting flow.
The axial grooved bearing proposed by Hirs (8) achieves a degree

of flow straightening by the 'dams' left between successive
grooves. A journal of this type was produced, having a con-
figuration recommended by its designer (9), but its load
carrying capacity (measured experimentally) was much less than
Hirs' theory predicted.

It was decided to use the principle of straightening 'dams' or
'vanes' to improve the load carrying capacity of the tapered and
stepped land configurations. A modified tapered land journal
was produced by electroplating 16 vanes onto the tapered lands,
and subsequently grinding them back to obtain the form shown in
Figure 59. This journal developed a load coefficient C = 0.14,
compared with a previous value for the basic tapered form of 0.11.

A stepped land bearing also having 16 vanes was produced by a
photo-electro-etch method developed by the author for this
purpose. A parallel land journal was produced by conventional
workshop methods (the starting point for a tapered land journal
also). The surface glaze was removed with grit abrasive powder,
and the journal was then chemically cleaned in a trichloroethylene
vapour degreaser.

A film of photosensitive resist was sprayed onto the journal
under safelight conditions and allowed to dry. A mask (the
negative of the form required) was wrapped around the land
surfaces, and the journal was then exposed to ultra-violet
radiation for a specified time (9).
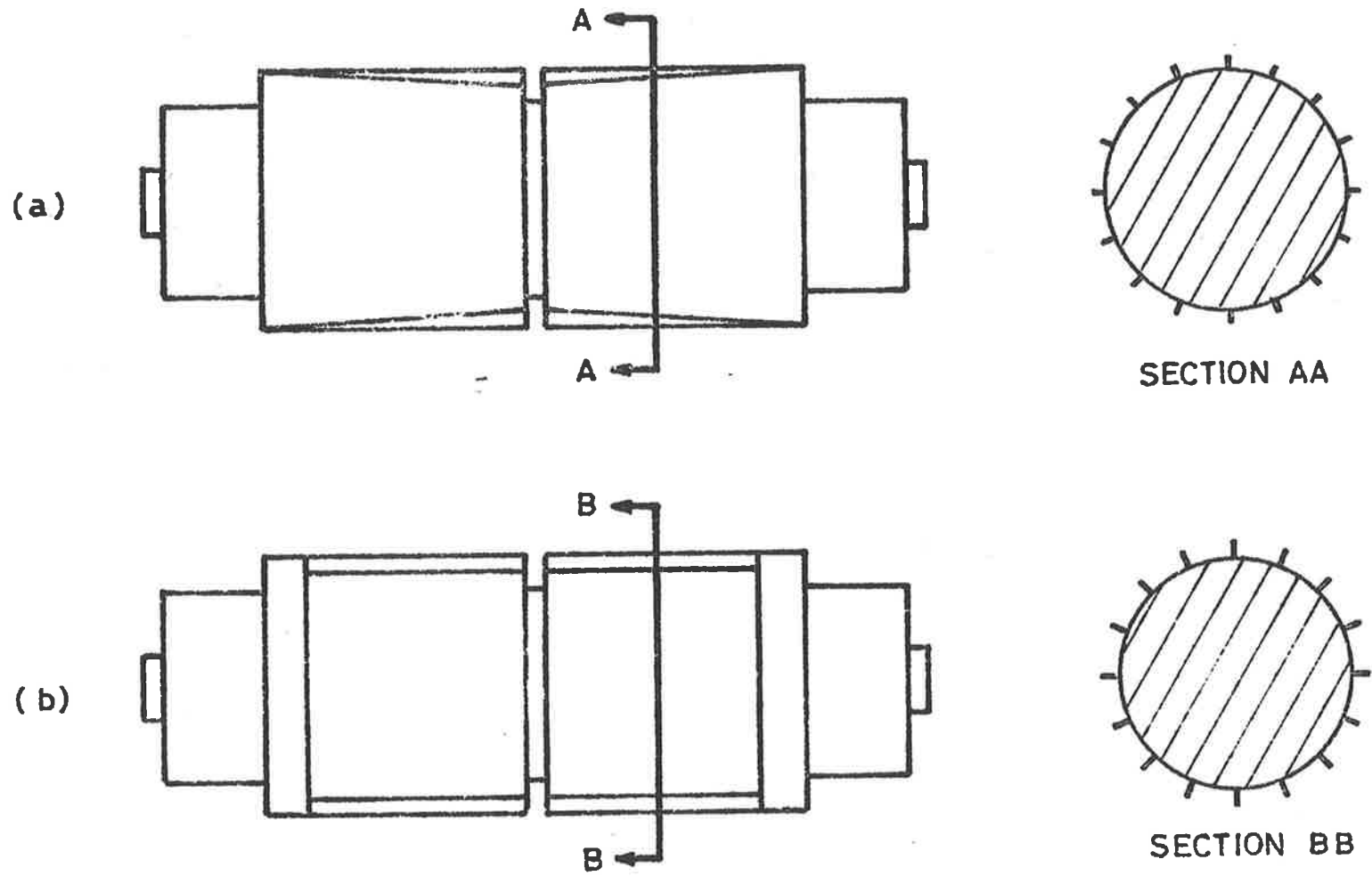
FIGURE 59   Modified tapered (a) and stepped (b) land journals.

Subsequent development in the trichloroethylene bath resulted in an impervious mask of hardened photo-resist firmly attached to the journal surface.

The journal was then rotated in an electro-etching bath for a predetermined time, during which the land surfaces were etched away between thin vanes protected by the mask of resist.

The rate of etching was dependent on the current density used, and was adjusted to 0.0005 in.per hour to allow adequate control over the depth of etch. This slow rate of etching also gave a degree of electro-polishing, resulting in an improvement in the surface finish of the journal. The test piece was then cleaned in the degreaser and the mask removed with a wire brush. The resulting form is shown in Figure 60.

This journal developed a load coefficient $C_l = 0.15$ compared with 0.08 for the stepped land form without vanes.

It was considered that there would be an optimum number of vanes at which the maximum load coefficient would be developed. Consequently it was decided to test the effect of varying the number of vanes. As the stepped land bearing had shown the greater degree of improvement in the load coefficient due to the addition of vanes, it was decided to restrict this test to the stepped land configuration.

Journals having 64, 32, 16, 8, 4 and 2 vanes were prepared, on a journal with a basic configuration given by

FIGURE 60(a)   Modified   tapered-land   journal.
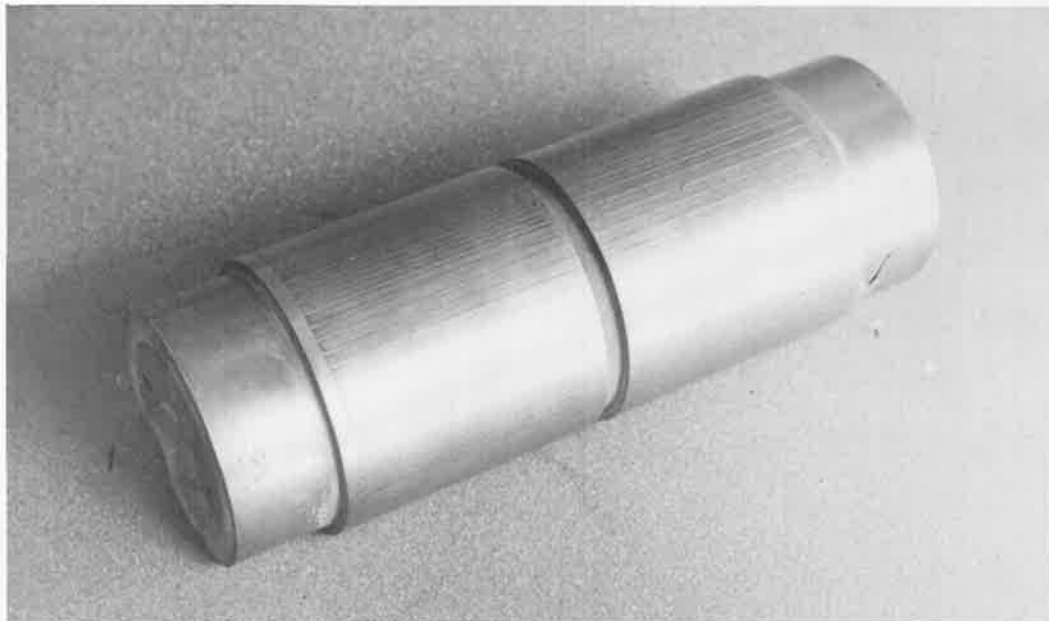
FIGURE 60(b)   Modified   stepped-land   journal.

$L = 2.0$

$SLR = 0.05$

$SDR = 1.0$

and vane width $= 0.020$ in.

Only one test piece was used. The 64 vane journal was prepared first, and then every alternate vane was ground off to give the 32 vane specimen. This procedure was repeated until all vanes were removed, and the simple stepped form was tested to check the load capacity against the results of the earlier tests.

The results of the tests are shown in Figure 61, where the load capacity is plotted against the number of vanes. It can be seen that the maximum load occurs with 32 vanes, and that the load falls off sharply when this number is increased. In terms of the land area, the maximum load occurs when approximately 10% of the land was occupied by the straightening vanes.

Comparison of the curves of Figure 61 shows that, for the bearing tested, the maximum gain in the load coefficient was equal to approximately two thirds of the difference between the one and two dimensional results. Although these results are not a sufficient foundation upon which to base a general theory of the 'vane type' journal bearing, it is considered that they are
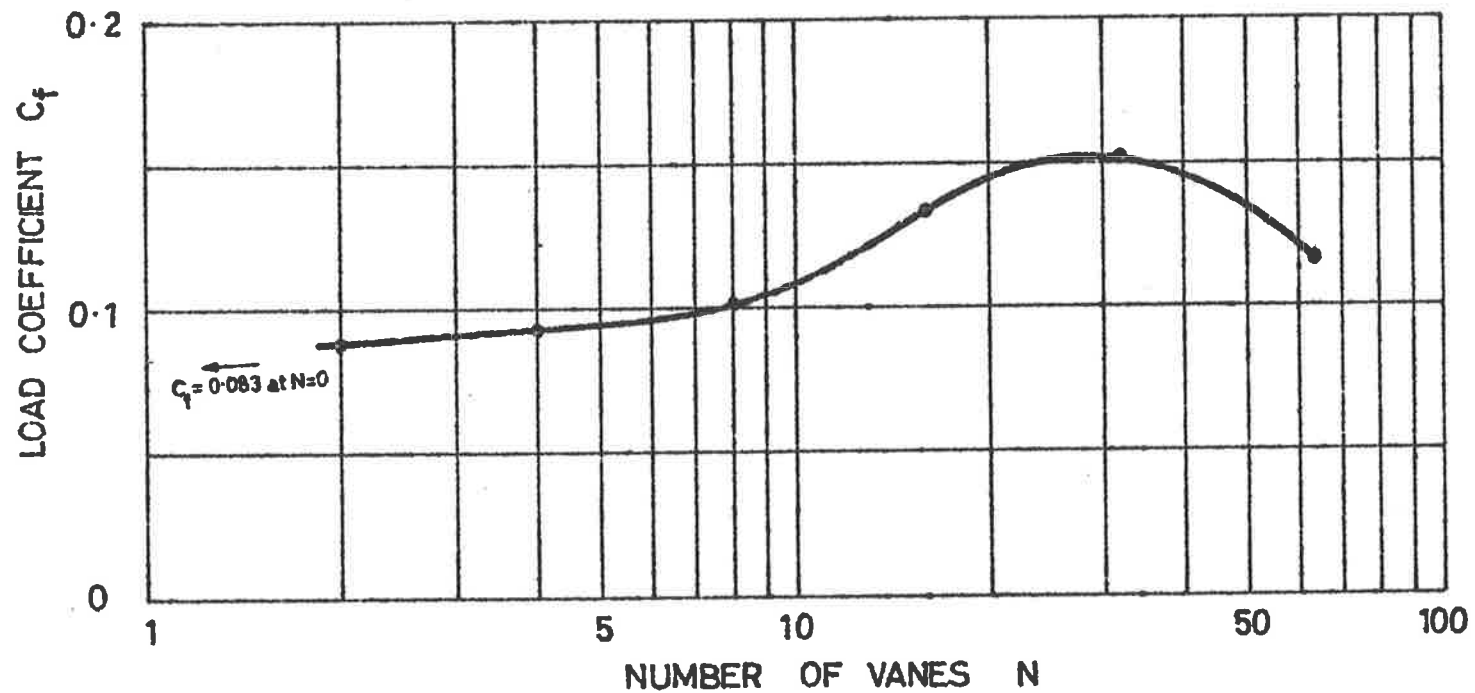
FIGURE 61 Load coefficient against number of vanes — stepped land journal (L=2·0, SLR=0·05, SDR=1·0). Compressible flow (PR=4·4)

sufficient to show that the configuration can produce a significant improvement to the load carrying capacity of the tapered or stepped land forms. Furthermore, it is considered that this journal configuration is worthy of further investigation.

5 CONCLUSIONS

The results of the theoretical analysis, which are closely confirmed by experimental evidence, lead to the conclusions that:-

(1)   The Reynold's equation can be used to evaluate the performance characteristics (load capacity, leakage flow and righting torque) of the bearing configurations discussed in this thesis, provided that, in the compressible flow case, the lubricant flow does not become choked. If it is required to determine these characteristics for choked flow conditions, corrections must be applied to the 'Reynolds' analysis. However, it is considered that bearings would rarely be required to operate in the choked condition in practice.

(2)   The assumption of isothermal flow in the clearance space is valid for both incompressible and compressible flows, except (in the compressible flow case) when choked flow conditions occur.

(3)   The effect of lubricant compressibility is to decrease the load carrying capacity and to increase the leakage flow and the righting torque.

(4)   The effect of the pressure ratio ($PR = \dfrac{P_{INLET}}{P_{OUTLET}}$) with incompressible lubricants is negligible. With compressible lubricants, an increase in the pressure ratio results in a decrease in the load coefficient (C_f) and an increase in the flow and moment coefficients (C_q and C_m) from the values obtained for incompressible flow. At very low pressure ratios ($PR \rightarrow 1$) the values of these coefficients

closely approach the values obtained for incompressible flow.

(5)   The load coefficient (C_f) varies approximately linearly with eccentricity ratio (E), both for incompressible flow and for compressible flow at a given pressure ratio. The radial stiffness of the bearing (K_r) is therefore constant throughout the clearance.

(6)   The maximum load coefficient (C_f) for tapered land bearings with length ratios (L) in the range 0.5 to 2.0 is developed at a taper ratio (T) in the region of 1. The maximum values of the load coefficient, for length ratio L = 1, are:-

(a) C_f = 0.20 for incompressible flow

(b) C_f = 0.16 for compressible flow

The data for the stepped land bearings have not yet been adequately checked by experiment. However, the theory predicts that the maximum load coefficient will be developed when the step length ratio (SLR) is in the range 0.1 to 0.2, with the step depth ratio (SDR) in the range 1.0 to 2.0. The maximum values of the load coefficient, for length ratio L = 1, are:-

(c) C_f = 0.28 for incompressible flow

(d) C_f = 0.20 for compressible flow

(7)   The angular stiffness (K_a) of both tapered and stepped land bearings is less than that of a parallel land configuration. However, the parallel land bearing has no radial load carrying capacity.

(8)   The load carrying capacity of both tapered and stepped land configurations can be improved by adding flow straightening vanes

to the lands. For bearings with length ratio $L = 2.0$, improvements in the load capacity of the order of 30% for tapered land and 80% for stepped land configurations were recorded.

(9) The tapered and stepped land bearing configurations are characterised by ease of manufacture (these bearings have been moulded in plastic), operation (an industrial compressed air supply was used to operate prototype instruments fitted with these bearings), and maintenance (the component parts are simple, and require no specialised servicing equipment). It is considered therefore that bearings of these types are suitable for industrial applications.

6 BIBLIOGRAPHY

1 GRASSAM, N.S. and POWELL, J.W. "Gas Lubricated Bearings", Butterworths, 1964. 309p.

2 MANNAM, J. "Further Aspects of Hydraulic Lock", Proc. Instn Mech. Engrs. 1959, Vol. 173 (No. 28)

3 PINKUS, O. and STERNLICHT, B. "Theory of Hydrodynamic Lubrication", Mc.Graw-Hill, 1961. 465p.

4 AUSMAN, J.S. "Advanced Bearing Technology", N.A.S.A. publication No. SP-38, 1964. 511p.

5 OSTERLE, J.F. and HUGHES, W.F. "High Speed Effects in Pneumodynamic Journal Bearing Lubrication", Appl. Sci. Res. 1958 Section A, Vol.7.

6 NATIONAL PHYSICAL LABORATORY "Modern Computing Methods", Notes on Applied Science. No. 16, 1961. H.M. Stationery Office, London. 170p.

7 SCHLICTING, H. "Boundary Layer Theory", Mc.Graw-Hill, 1960. 647p.

8   HIRS, G.G.   "The Design of Partly Grooved, Externally
               Pressurised Journal Bearings" Trans. A.S.M.E.,
               Paper No. 67-LubS-1, Lubrication Symposium,
               June 1967

9   HIRS, G.G.   "Partly Grooved, Externally Pressurised Bearings"
               Proc. Instn Mech. Engrs 1965-66, Vol. 180, Pt. 3K.

10   SOUTHWELL, R.V. "Relaxation Methods of Analysis in Theoretical
               Physics", 1946 (Oxford Engng Science Series).

11   FAIRES, V.M.   "Design of Machine Elements", Macmillan, 1959.
               550p.

APPENDIX I   DERIVATION OF THE GENERALIZED REYNOLDS EQUATION

The theoretical determination of any bearing characteristic must begin with the evaluation of the pressure distribution over the bearing surface. Consequently, an equation describing this pressure field is required. It is therefore necessary to know what type of flow regime (laminar or turbulent, incompressible or compressible) exists in the clearance space. Experimental evidence suggests that, within the normal limits of operation, the flow is laminar. Making this assumption an equation now known as the Reynolds Equation can be derived.

The derivation of the Reynolds Equation can be found in any basic text on lubrication (3). The steps involved and the assumptions made are outlined here as they have some bearing on the original theoretical work undertaken in the section dealing with inertia and choking effects.

With reference to the co-ordinate system shown (I-1) the general Navier-Stokes equations can be written as

$$\rho \cdot \frac{Du}{dt} = \rho \cdot G_x - \frac{\partial p}{\partial x} + \frac{\partial}{\partial x} \mu [2\frac{\partial u}{\partial x} - \frac{2}{3}(\frac{\partial u}{\partial x} + \frac{\partial v}{\partial y} + \frac{\partial w}{\partial z})] \ \ldots$$

$$\ldots + \frac{\partial}{\partial y}[\mu(\frac{\partial u}{\partial y} + \frac{\partial v}{\partial x})] + \frac{\partial}{\partial z}[\mu(\frac{\partial w}{\partial x} + \frac{\partial u}{\partial z})] \qquad \ldots \text{(I-1a)}$$

$$\rho \cdot \frac{Dv}{dt} = \rho \cdot G_y - \frac{\partial p}{\partial y} + \frac{\partial}{\partial y} \mu [2\frac{\partial v}{\partial y} - \frac{2}{3}(\frac{\partial u}{\partial x} + \frac{\partial v}{\partial y} + \frac{\partial w}{\partial z})] \ \ldots$$

$$\ldots + \frac{\partial}{\partial z}[\mu(\frac{\partial v}{\partial z} + \frac{\partial w}{\partial y})] + \frac{\partial}{\partial x}[\mu(\frac{\partial u}{\partial y} + \frac{\partial v}{\partial x})] \qquad \ldots \text{(I-1b)}$$
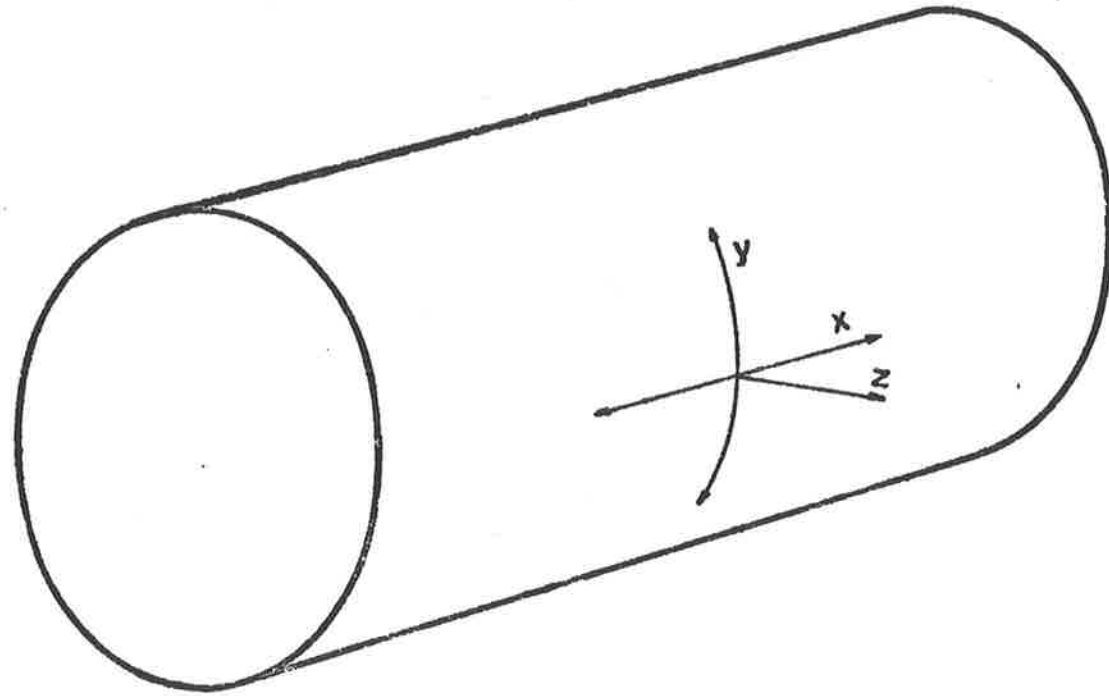
FIGURE I-1   The coordinate system on the bearing surface.

$$\rho \cdot \frac{Dw}{dt} = \rho \cdot G_z \; - \frac{\partial p}{\partial z} + \frac{\partial}{\partial z} \; \mu [2 \frac{\partial w}{\partial z} - \frac{2}{3}(\frac{\partial u}{\partial x} + \frac{\partial v}{\partial y} + \frac{\partial w}{\partial z})] \; \ldots$$

$$\ldots \; + \frac{\partial}{\partial x}[\mu(\frac{\partial w}{\partial x} + \frac{\partial u}{\partial z})] + \frac{\partial}{\partial y}[\mu(\frac{\partial v}{\partial z} + \frac{\partial w}{\partial y})] \qquad \ldots (I-1c)$$

where x, y, z are the mutually perpendicular co-ordinates,

u, v, w are the velocities in the direction of the respective

co-ordinate axes,

p is the local pressure

ρ is the local density

μ is the local viscosity

t is the time variable

G_x , G_y , G_z , are the components of the external force field

per unit mass

$\frac{Du}{dt}$, $\frac{Dv}{dt}$, $\frac{Dw}{dt}$ are the total derivatives giving the three components

of acceleration of the fluid.

Use is also made of the continuity equation, which, with no

sources or sinks present in the field, is given by

$$\frac{d\rho}{dt} + \frac{\partial(\rho u)}{\partial x} + \frac{\partial(\rho v)}{\partial y} + \frac{\partial(\rho w)}{\partial z} = 0 \qquad \ldots (I-2)$$

The differential equation originally derived by Reynolds was
restricted to incompressible fluids. The equation formulated here
has been broadened to include the effects of compressibility and
dynamic loading. The assumptions involved in reducing equations (1)

to the Reynolds equation are:

(1)   The height of the fluid film, z, is very small compared to the span and length, x, y. Thus the curvature of the film of journal bearings may be ignored, and rotational velocities replace translational velocities.

(2)   There is no variation of pressure across the film. Thus

$$\frac{\partial p}{\partial z} = 0$$

(3)   The flow is laminar. No vortex flow and no turbulence occur anywhere in the film.

(4)   No external forces act on the film. Therefore

$$G_x = G_y = G_z = 0$$

(5)   Fluid inertia is small compared with viscous shear. Therefore

$$\frac{Du}{dt} = \frac{Dv}{dt} = \frac{Dw}{dt} = 0$$

(6)   There is no slip at the bearing surfaces.

(7)   Compared with the two velocity gradients $\frac{\partial u}{\partial z}$ and $\frac{\partial w}{\partial z}$ all other velocity gradients can be considered negligible. Derivatives of terms other than $\frac{\partial u}{\partial z}$ and $\frac{\partial w}{\partial z}$ will also therefore be negligible.

All derivatives with the exception of $\frac{\partial^2 u}{\partial z^2}$ and $\frac{\partial^2 w}{\partial z^2}$ can therefore be omitted.

Assumptions 1 to 7, used with equations (1), yield

$$\frac{1}{\mu}\cdot\frac{\partial p}{\partial x} = \frac{\partial^2 u}{\partial z^2} \qquad \ldots(\text{I-3})$$

$$\frac{1}{\mu}\cdot\frac{\partial p}{\partial y} = \frac{\partial^2 v}{\partial z^2} \qquad \ldots(\text{I-4})$$

which, upon integration, and with the use of the relevant boundary conditions, yield expressions for the velocity components u and v. viz.

$$u = \frac{1}{2\mu}\cdot\frac{\partial p}{\partial x}\cdot z(z - h) \qquad \ldots(\text{I-5})$$

$$v = \frac{1}{2\mu}\cdot\frac{\partial p}{\partial y}\cdot z(z - h) + \frac{h - z}{h}\cdot V_1 + \frac{z}{h}\cdot V_2 \qquad \ldots(\text{I-6})$$

When combined with the continuity equation, which for time-invariant lubrication can be written

$$\frac{\partial(\rho v)}{\partial y} + \frac{\partial(\rho u)}{\partial x} + \frac{\partial(\rho w)}{\partial z} = 0 \qquad \ldots(\text{I-7})$$

the generalised Reynolds equation can be derived, viz.

$$\frac{\partial}{\partial x}\left(\frac{\rho h^3}{\mu}\cdot\frac{\partial p}{\partial x}\right) + \frac{\partial}{\partial y}\left(\frac{\rho h^3}{\mu}\cdot\frac{\partial p}{\partial y}\right) = 6(V_1 - V_2)\cdot\frac{\partial(\rho h)}{\partial y} + 12\rho W \qquad \ldots(\text{I-8})$$

where V_U = surface velocity in the circumferential direction

where W = surface velocity in the normal direction.

Of the terms on the R.H.S. the first is the contribution of the velocities of the bearing surfaces along the film, while the second is due to the relative normal velocity of the surfaces.

For a static (non-rotating journal) bearing, $V_1 = V_2 = 0$. For steady loading $W = 0$. Under these conditions equation (I-8) reduces to

$$\frac{\partial}{\partial x}\left(\frac{\rho h^3}{\mu}\cdot\frac{\partial p}{\partial x}\right) + \frac{\partial}{\partial y}\left(\frac{\rho h^3}{\mu}\cdot\frac{\partial p}{\partial y}\right) = 0 \qquad \ldots(\text{I-9})$$

It is this form of the Reynolds equation that is used as the basis of the analysis given in this thesis.

APPENDIX II   EXPRESSION FOR THE LOCAL CLEARANCE

II.1   Journal and Bearing Axes Parallel

Consider a cross-section of a bearing-journal configuration
at a distance x from the exit annulus (Figure II.1)
then

$$(O'A)^2 + (AB)^2 = (O'B)^2$$

and therefore

$$(r.\cos\theta - e)^2 + (r.\sin\theta)^2 = (r - -.t\frac{x}{l}c + h)^2 \qquad ...(II-1)$$

Neglecting second order terms in c, e, h and θ in equation (II-1)
yields an expression for the local clearance, h, viz,

$$h = c + \frac{x}{l}.t - e.\cos\theta \qquad ...(II-2)$$

Dividing equation (II-2) by c gives

$$\frac{h}{c} = 1 + \frac{x}{l}.\frac{t}{c} - \frac{e}{c}.\cos\theta$$

which can be expressed in non-dimensional form as
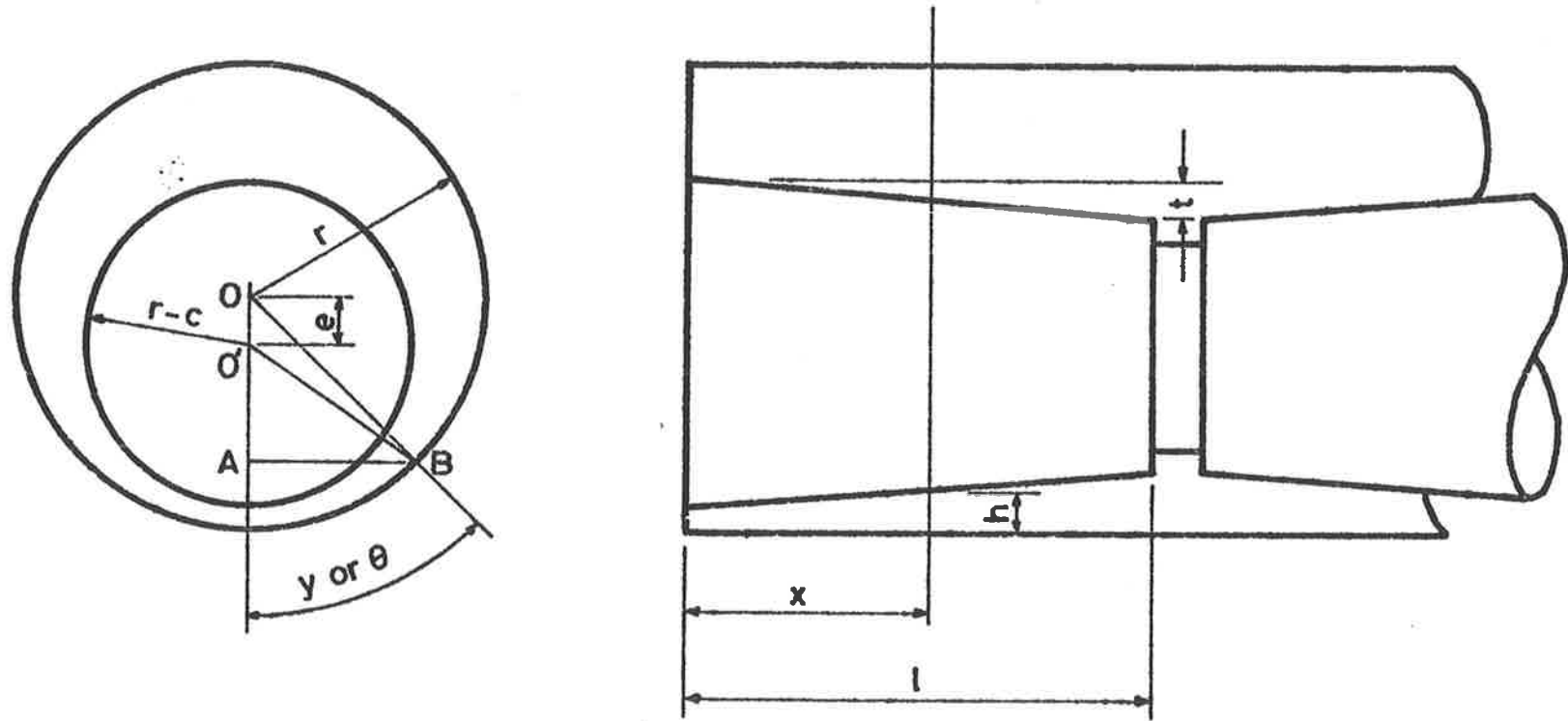
FIGURE II.1   Diagrammatic   representation   of   the   journal   and   bearing.

$$H = 1 + X.T. - E.\cos(2\pi Y) \qquad\qquad ...(II-3)$$

II.2 Journal and Bearing Axes Misaligned

With reference to Figure II-2, the displacement (δ) at a distance x from the exit end of the land, located at θ from the position of minimum clearance, is given by

$$\delta = (1 - x).\tan\phi.\cos\theta$$

An expression for the non-tilted, concentric condition is obtained by substituting $e = 0$ in equation (II-2), viz.

$$h_c = c + \frac{x}{l}.t$$

The film thickness for the tilted condition (h) is given by

$$h_t = h_c - \delta$$

and substituting for h_c and δ yields

$$h_t = c + \frac{x}{l}.t - (1 - x).\tan\phi.\cos\theta \qquad\qquad ...(II-4)$$

The Angularity Ratio (A) may be defined as
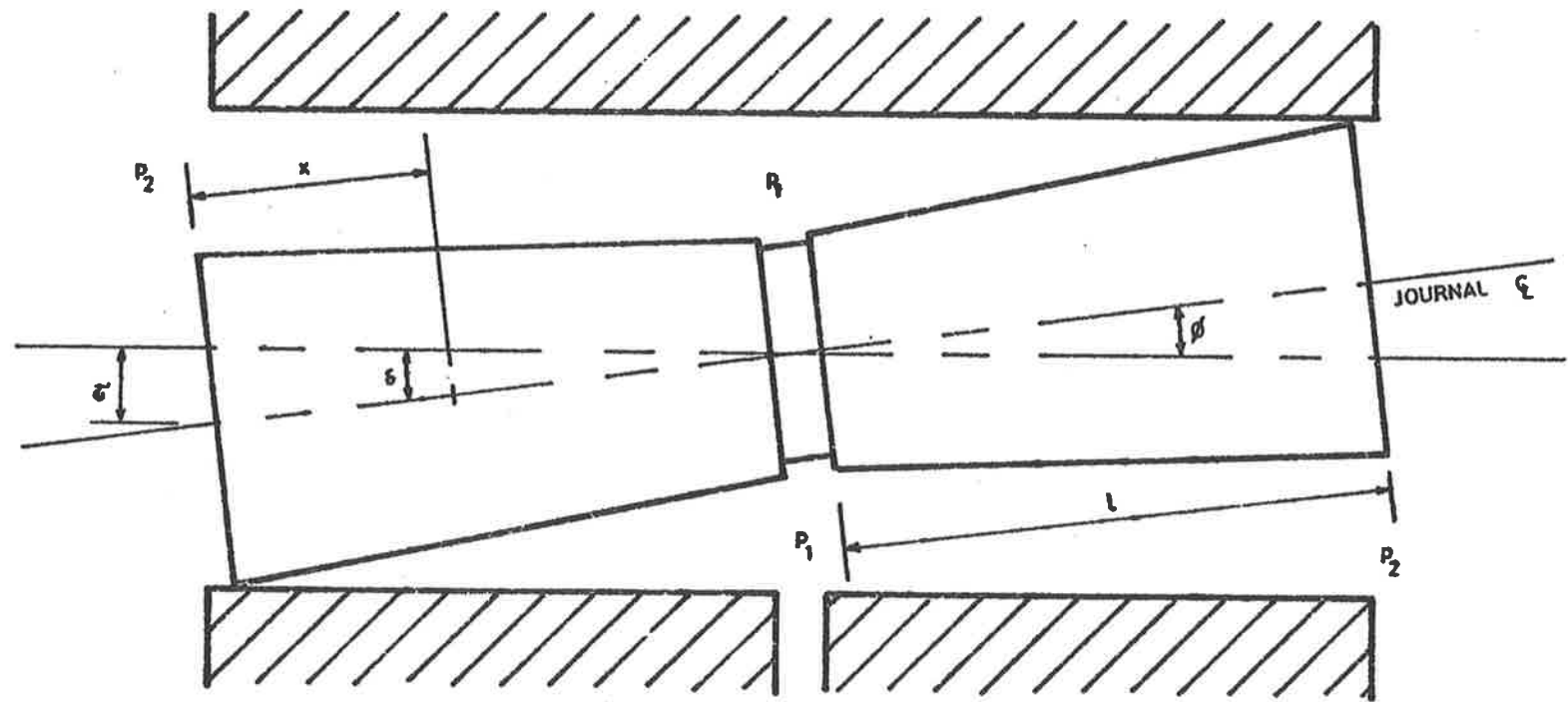
FIGURE II-2   Fully tilted tapered land journal bearing.

$$A = \frac{e_t}{c} \qquad \qquad \ldots(II-5)$$

where e_t is the eccentricity at the end of the land for the tilted condition (see Figure II-2).

The tangent of the angle of tilt ($\tan\phi$) is given by

$$\tan\phi = \frac{e_t}{l}$$

and substituting for e_t from equation (II-5) yields

$$\tan\phi = \frac{A.C}{l}$$

Substituting for $\tan\phi$ in equation (II-4) gives

$$h_t = c + \frac{x}{l}.t - \frac{(l-x).A.c}{l}\cos\theta \qquad \qquad \ldots(II-6)$$

In terms of the dimensionless groups previously defined (Nomenclature, p3), equation (II-6) can be written as

$$H_t = 1 + X.T - A(1 - X).\cos(2\pi Y) \qquad \qquad \ldots(II-7)$$

APPENDIX III   LOAD, FLOW AND MOMENT CO-EFFICIENTS

III.1   Load Coefficient

To obtain an expression for the load capacity (F) of the bearing, consider an element of the surface (Figure III.1) of area Δx by Δy, located at an angle $\theta = \frac{Y}{r}$ to the load line. The load (f) carried by such an element is given by

$$f = p.\cos\left(\frac{Y}{r}\right).\Delta x.\Delta y \qquad \qquad ...(III-1)$$

An expression for the total load, F, carried by one land of the journal is obtained by integrating equation III-1, i.e.,

$$F = \int\limits_{0}^{\pi r}\int\limits_{0}^{1} p.\cos\left(\frac{Y}{r}\right).dx.dy \qquad \qquad ...(III-2)$$

Expressed in dimensionless terms, equation (III-2) can be written as

$$F = \Delta p.1.2\pi r\int\limits_{0}^{1}\int\limits_{0}^{1} P.\cos(2\pi Y).dX.dY \qquad \qquad ...(III-3)$$

Hence, by re-arrangement of equation (III-3), a load coefficient can be defined as

$$C_f = \frac{F}{\Delta p.1.d} = \pi\int\limits_{0}^{1}\int\limits_{0}^{1} P.\cos(2\pi Y).dX.dY \qquad \qquad ...(III-4)$$
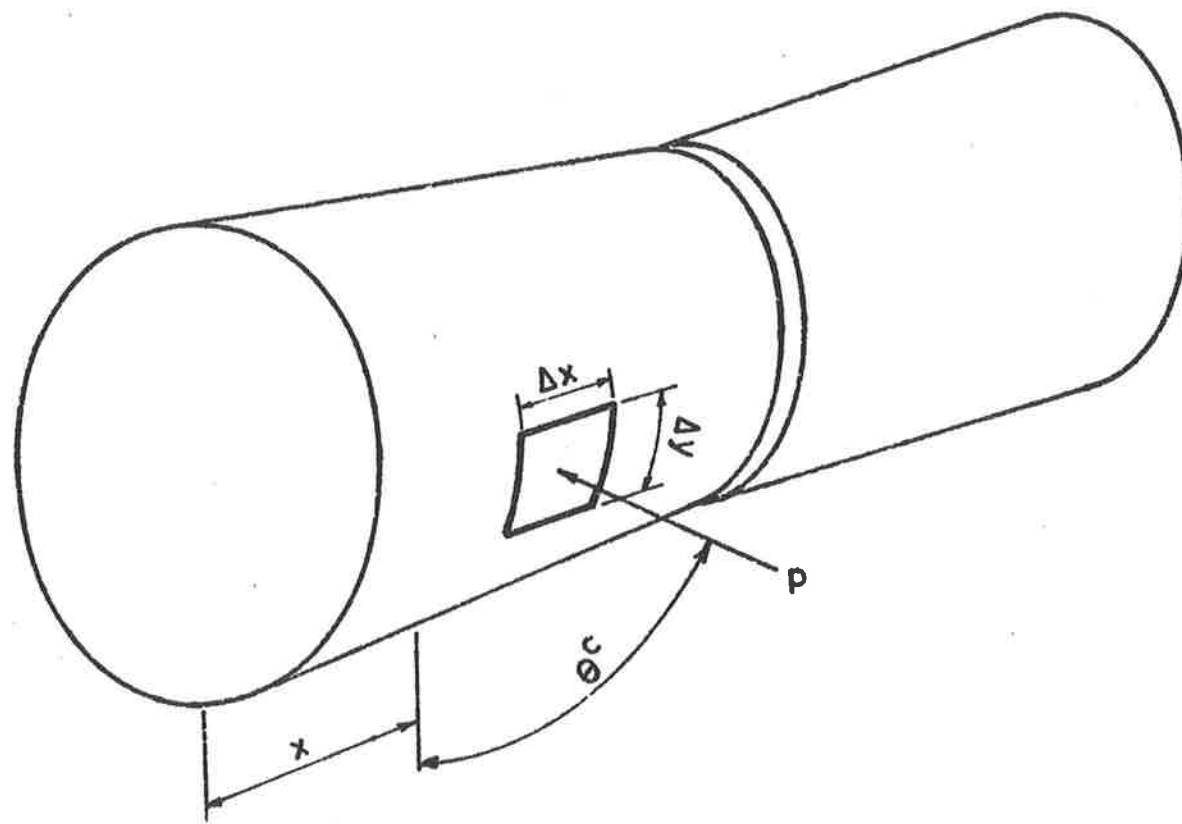
FIGURE III-1   Elemental load-carrying area.

III.2   Flow Coefficient

The leakage flow through an element of the exit annulus (Figure III-2) of width Δy and height Δz is given by

$$q = u.\Delta y.\Delta z \Big|_{x=0} \qquad \qquad \ldots (III-5)$$

where u is the x-component of the flow velocity, given (3) by

$$u = \frac{1}{2\mu}.\frac{\partial p}{\partial x}.(z^2 - zh) \qquad \qquad \ldots (III-6)$$

where h is the local film thickness, defined in Appendix II. Substituting for u from equation (III-6) in equation (III-5) and integrating over the film thickness gives

$$q_h = \frac{1}{2\mu}.\frac{\partial p}{\partial x}.\Delta y. \int_0^h (z^2 - zh)dz \Big|_{x=0}$$

$$= \frac{h^3}{12\mu}.\frac{\partial p}{\partial x}.\Delta y \Big|_{x=0} \qquad \qquad \ldots (III-7)$$

An expression for the total flow through the annulus is obtained by integrating equation (III-7), viz.,

$$Q = \int_0^{2\pi r} q_h.dy \Big|_{x=0}$$

$$= \frac{1}{12\mu}. \int_0^{2\pi r} h^3.\frac{\partial p}{\partial x}.dy \Big|_{x=0} \qquad \qquad \ldots (III-8)$$
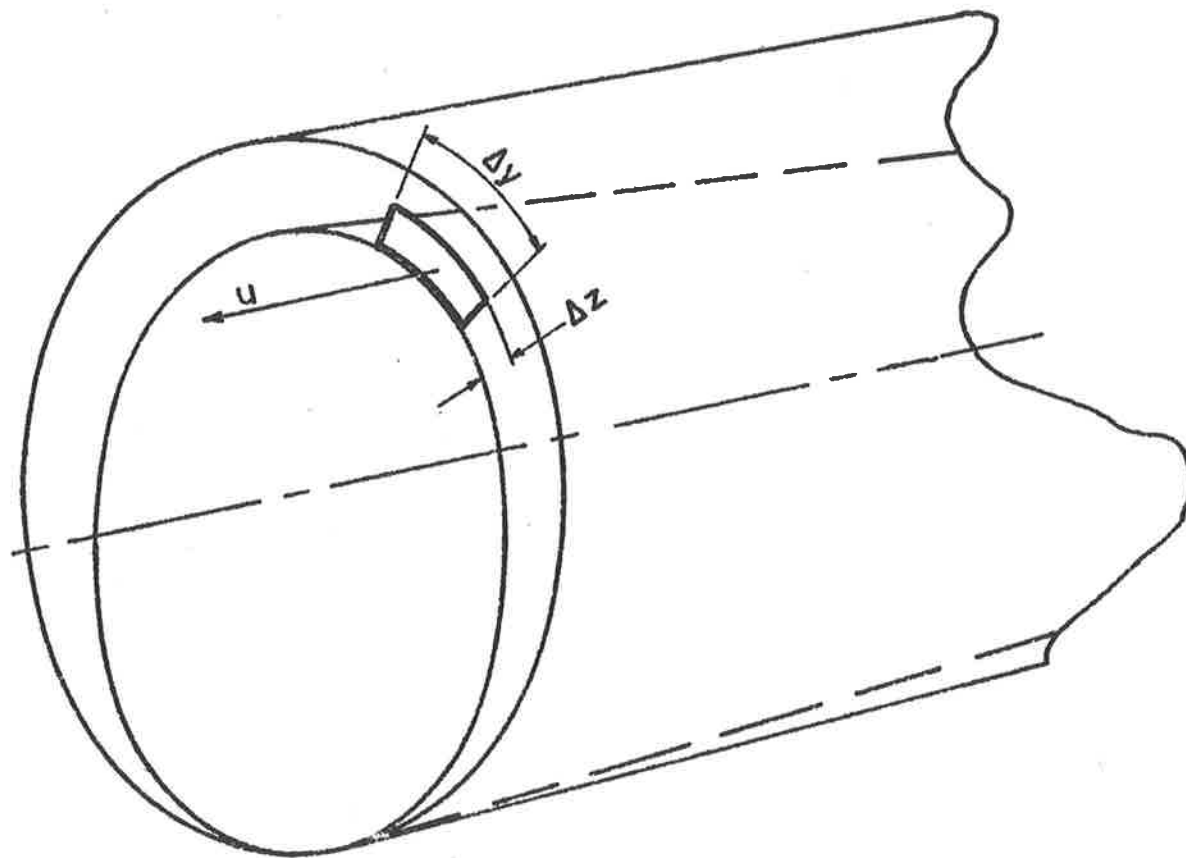
FIGURE III-2 Elemental flow area.

Expressed in dimensionless terms equation (III-8) can be written as

$$Q = \frac{\Delta p . \pi . d . c^3}{12 \mu . l} . \int_0^1 H^3 \frac{\partial P}{\partial X} . dY \bigg|_{X = 0} \qquad \ldots (III-9)$$

Hence, by re-arrangement of equation (III-9), a flow coefficient can be defined as

$$C_q = \frac{Q . \mu . l}{\Delta p . d . c^3} = \frac{\pi}{12} \int_0^1 H^3 \frac{\partial P}{\partial X} . dY \bigg|_{X = 0} \qquad \ldots (III-10)$$

Note: The term $\frac{\partial P}{\partial X}$ in equation (III-10) may be evaluated numerically using a five point approximation (6) given by

$$\left(\frac{\partial P}{\partial X}\right)_0 = \frac{1}{12\delta} . (-25 P_0 + 48 P_1 - 36 P_2 + 16 P_3 - 3 P_4) + \xi \qquad \ldots (III-11)$$

where δ is the finite difference interval,

    X is the position at which the determination is required,

    P_0 , P_1 , P_2 , P_3 , P_4 are the pressures at successive points

                X_0, X_1, X_2, X_3, X_4, separated by the

                interval δ, and

    ξ is an error term of the fifth order.

Note also that the mass flow (m) is given by

$$m = \rho . \int_{0}^{h} u.dz \qquad\qquad ...(III-12)$$

Substituting for u from equation (III-6), p149

$$m = \rho . \int_{0}^{h} \frac{1}{2\mu} . \frac{\partial p}{\partial x} . (z^2 - zh).dz$$

and hence

$$m = \frac{\rho h^3}{12\mu} . \frac{\partial p}{\partial x} \qquad\qquad ...(III-13)$$

Re-arranging equation (III-13) gives an expression for the pressure gradient $(\frac{\partial p}{\partial x})$ in terms of the mass flow (m), viz.

$$\frac{\partial p}{\partial x} = \frac{12\mu m}{\rho h^3} \qquad\qquad ...(III-14)$$

Equation (III-14) is used in the Predictor-corrector method of solution for the pressure distribution (Section 3.2.5).

III.3   Moment Coefficient

The moment acting on an element of surface at location x, y, of area Δx by Δy, and located at $\theta = \frac{y}{r}$ to the moment plane (Figure III-1), is given by

$$m = p.\cos\left(\frac{Y}{r}\right).\Delta x.\Delta y.(1 - x) \qquad \qquad ...(III-15)$$

An expression for the total moment, M, acting to right one land
of the journal is obtained by integrating equation (III-15), i.e.,

$$M = \int_0^{2\pi r}\int_0^l (1 - x).p.\cos\left(\frac{Y}{r}\right).dx.dy \qquad \qquad ...(III-16)$$

Expressed in dimensionless terms, equation (III-16) can be
written as

$$M = \Delta p.l^2.d.\pi \int_0^1\int_0^1 (1 - X).P.\cos(2\pi Y).dX.dY \qquad \qquad ...(III-17)$$

Hence, by re-arranging equation (III-17), a moment coefficient
can be defined as

$$C_m = \frac{M}{\Delta p.l^2.d} = \pi \int_0^1\int_0^1 (1 - X).P.\cos(2\pi Y).dX.dY \qquad \qquad ...(III-18)$$

APPENDIX IV   INTEGRATION OF EQUATION (18)

The equation to be integrated is equation (18), p13, viz.

$$F = \Delta p.l.d.\pi \int_0^1 \int_0^1 \left[P_2 + \left(\frac{(1 + T - E.\cos(2\pi Y))^2}{T(T + 2(1 - E.\cos(2\pi Y)))} \right) \cdots \right.$$
$$\left. \cdots \left(1 - \frac{(1 - E.\cos(2\pi Y))^2}{(1 + X.T - E.\cos(2\pi Y))^2} \right) \right] .\cos(2\pi Y).dX.dY \qquad \ldots(IV-1)$$

integrating with respect to x, and re-arranging,

$$F = \Delta p.l.d.\pi \int_0 \left[P_2 + \frac{1 + T - E.\cos(2\pi Y)}{T + 2(1 - E.\cos(2\pi Y))} \right] .\cos(2\pi Y).dY \qquad \ldots(IV-2)$$

Changing the limits of the integral, and re-arranging,

$$F = \Delta p.l.d.\pi.2 \int_0^{\frac{1}{2}} P_2.\cos(2\pi Y).dY \cdots$$
$$\cdots + \Delta p.l.d.\pi.2 \int_0^{\frac{1}{2}} \frac{T + (1 - E.\cos(2\pi Y)}{T + 2(1 - E.\cos(2\pi Y)} .\cos(2\pi Y).dY \qquad \ldots(IV-3)$$

The first term in equation (IV-3) is odd, and on integration reduces to zero. Equation (IV-3) can therefore be written as

$$F = \Delta p.l.d.\pi.2 \int_0^{\frac{1}{2}} \frac{T + (1 - E.\cos(2\pi Y)}{T + 2(1 - E.\cos(2\pi Y))} .\cos(2\pi Y).dY \qquad \ldots(IV-4)$$

Expanding equation (IV-4),

$$F = \Delta p.l.d.\pi. \int_0^{\frac{1}{2}} \cos(2\pi Y).dY \quad ...$$

$$... \quad + \Delta p.l.d.\pi \int_0^{\frac{1}{2}} \frac{T}{T + 2(1 - E.\cos(2\pi Y))}.\cos(2\pi Y).dY$$

$$...(IV-5)$$

The first term in equation (IV-5) is odd, and on integration reduces to zero. Equation (IV-5) can therefore be written as

$$F = \Delta p.l.d.\pi.T \int_0^{\frac{1}{2}} \frac{\cos(2\pi Y)}{T + 2(1 - E.\cos(2\pi Y))}.dY$$

which can be expanded to give

$$F = \Delta p.l.d.\pi.T \left[\int_0^{\frac{1}{2}} \frac{T + 2}{T + 2(1 - E.\cos(2\pi Y))}.dY - \int_0^{\frac{1}{2}} dY \right] \quad ...(IV-6)$$

Evaluating the integrals of equation (IV-) results in an expression for the load capacity, viz.

$$F = \frac{\Delta p.l.d.\pi.T}{4E} \left[\frac{T + 2}{\sqrt{(T + 2)^2 - 4E^2}} - 1 \right] \quad ...(IV-7)$$

APPENDIX V DIFFERENCE SOLUTION OF THE REYNOLDS EQUATION

The equation to be solved is equation (12), p11, viz.,

$$\frac{\partial}{\partial x}\left(h^3 \cdot \frac{\partial p}{\partial x}\right) + \frac{\partial}{\partial y}\left(h^3 \frac{\partial p}{\partial y}\right) = 0 \qquad \ldots (V-1)$$

Making the substitutions

$$p = \Delta p \cdot P + p_2$$

$$h = cH$$

$$x = lX$$

$$y = 2\pi r Y$$

gives

$$\frac{\partial}{\partial(X.l)}\left(c^3 \cdot H^3 \cdot \frac{\partial(P.\Delta p + p_2)}{\partial(Xl)}\right) + \frac{\partial}{\partial(2\pi rY)}\left(c^3 \cdot H^3 \cdot \frac{\partial(P.\Delta p + p_2)}{\partial(2\pi rY)}\right) = 0$$

$$\ldots (V-2)$$

which on re-arrangement gives

$$\frac{\partial}{\partial X}\left(H^3 \cdot \frac{\partial P}{\partial X}\right) + \left(\frac{L}{2\pi}\right)^2 \cdot \frac{\partial}{\partial Y}\left(H^3 \frac{\partial P}{\partial Y}\right) = 0 \qquad \ldots (V-3)$$

where $L = \frac{l}{r}$

Using an identity given by Southwell (10) which, in terms of the variables of equation (V-3) is

$$2\frac{\partial}{\partial X}\left(H'\frac{\partial P}{\partial X}\right) = \frac{\partial^2(H'.P)}{\partial X^2} + H'\frac{\partial^2(P)}{\partial X^2} - P\frac{\partial^2(H')}{\partial X^2} \qquad \ldots(V-4)$$

Equation (V-4) transforms into

$$\left[\frac{\partial^2}{\partial X^2} + \left(\frac{L}{2\pi}\right)^2 \frac{\partial^2}{\partial Y^2}\right](H'.P) + H'\left[\frac{\partial^2}{\partial X^2} + \left(\frac{L}{2\pi}\right)^2 \frac{\partial^2}{\partial Y^2}\right]P \ldots$$

$$\ldots -P\left[\frac{\partial^2}{\partial X^2} + \left(\frac{L}{2\pi}\right)^2 \frac{\partial^2}{\partial Y^2}\right](H') = 0 \qquad \ldots(V-5)$$

The finite difference operators, assuming a square mesh of interval δ, may be written as

$$\frac{\partial^2\phi}{\partial X^2} = \frac{\phi_x - 2\phi_0 + \phi_w}{\delta^2} \qquad \ldots(V-6a)$$

$$\frac{\partial^2\phi}{\partial Y^2} = \frac{\phi_{-Y} - 2\phi_0 + \phi_{+Y}}{\delta^2} \qquad \ldots(V-6b)$$

Equation (V-5) expressed in finite difference form becomes

$$\left[(H_{-1}^3 + 2H_0^3 + H_{+1}^3) + \left(\frac{L}{2\pi}\right)^2 \cdot (H_{-1}^3 + 2H_0^3 + H_{+1}^3)\right] \cdot P_0$$

$$= (H_{+1}^3 + H_0^3) \cdot P_{+1} + (H_{-1}^3 + H_0^3) \cdot P_{-1} \ldots$$

$$\ldots + \left(\frac{L}{2\pi}\right)^2 \cdot \left[(H_{+1}^3 + H_0^3) \cdot P_{+1} + (H_{-1}^3 + H_0^3) \cdot P_{-1}\right] \qquad \ldots (V-7)$$

Equation (V-7) was applied by dividing the XY area into a 10 x 20 grid and the numerical solution was obtained by a cyclic sequential relaxation of the Gauss-Seidel type, using over-relaxation to increase the rate of convergence (6). The assumption of a pressure distribution symmetrical about the load line reduced by half the field over which the relaxation was applied.

The computation was programmed in FORTRAN compiler language for a CDC 6400 computer. The input data for each problem were the bearing radius, length and clearance, and the lubricant density, viscosity, supply and exhaust pressures. The program produced the pressure distribution load and flow coefficients, actual load and flow, and velocity and Reynolds number distributions. Samples of the programs written for the several sections of the theory are contained in Appendix VII.

APPENDIX VI   SOLUTION OF THE 'INERTIA' EQUATION

Equation

$$\frac{\partial P}{\partial X} = \frac{P}{Hc} \cdot \frac{6ml(Tc - 10\mu)}{5h^2 P_\rho (\frac{P}{p_0})^{\frac{1}{n}} - \frac{6m^2}{n}} \qquad \qquad \ldots(VI-1)$$

can be solved by the Runge Kutta predictor method (6). If a function is of the form

$$y' = f(x,y)$$

then an expression for the function value (y) at location (x + δ) is given by

$$y(x_0 + \delta) = y(x_0) + \frac{1}{6}(K_0 + 2K_1 + 2K_2 + K_3) \qquad \ldots(VI-2)$$

where

$$K_0 = \delta.f(x_0, y_0)$$
$$K_1 = \delta.f(x_0 + \tfrac{1}{2}\delta, \ y_0 + \tfrac{1}{2}K_0)$$
$$K_2 = \delta.f(x_0 + \tfrac{1}{2}\delta, \ y_0 + \tfrac{1}{2}K_1)$$
$$K_3 = \delta.f(x_0 + \delta, \ y_0 + K_2)$$

and δ = the increment in the x variable.

The procedure for the application of equation (VI-2) to obtain the solution of equation (VI-1) was

(1)   Set an initial value of m.

(2)   Start at the exit boundary where the pressure is known $(P = P_2)$ and by successive application of equation (VI-2), calculate the pressure at successive intervals of x until the pressure at the inlet boundary has been obtained.

(3)   The pressure at the inlet boundary is also known $(P = P_1)$ and so the error in the predicted value of P can be obtained.

(4)   The assumed value of m can then be modified in relation to the magnitude and sign of the error in the pressure at inlet.

(5)   The cycle is repeated until the error in P_{INLET} is reduced to an acceptable level.

A test program was developed to determine the best choice of the initial value of the mass flow (m), and of the direction and magnitude of the change in m required for a given error in P_{INLET}

This was then incorporated into the main program which contained the Runge-Kutta iteration for the pressure distribution along axial streamlines equispaced around the circumference.

APPENDIX VII   COMPUTER PROGRAMS

This Appendix contains samples of the computer programs written for the several sections of this investigation. The programs presented herein are:-

VII.1   Taper bearing: two-dimensional, incompressible flow.

VII.2   Taper bearing: two-dimensional, compressible flow.

VII.3   Taper bearing: one-dimensional, compressible flow with
                       inertia and choking effects considered.

VII.4   Step bearing: one-dimensional, incompressible flow.

VII.1

Taper bearing program 1

Two-dimensional, incompressible flow.
Fluid inertia effects neglected.
Gauss-Seidel relaxation, with the
bearing half-surface divided into
a 10 by 10 finite difference mesh.
Simpson's rule used to evaluate
integrals for load and flow.

```
      PROGRAM TPRBRG (INPUT,TAPE60=INPUT, OUTPUT,TAPE61=OUTPUT)
      DIMENSION P(11,13),H(11,13),A(11,13),B(11,13),C(11,13),D(11,13),
     1T(13)
   10 FORMAT(14H TAPER BEARING)
   20 FORMAT(I5 4F7.4)
   30 FORMAT///10H FILE NO =,I5//15H LENGTH RATIO =,F7.4/6H TAPER,
     18H RATIO =,F7.4/21H ECCENTRICITY RATIO =,F7.4)
   40 FORMAT(/19H TORQ COEFFICIENT = F7.4/19H FLOW COEFFICIENT =,F7.4
     1///15H PRESSURE FIELD)
   50 FORMAT(/13H            Y=,11F6.3)
   60 FORMAT(4H X =,F5.2,4H P =,11F6.3)
   70 FORMAT(12H NO.CYCLES =,I4,6H SUM =,E12.5)
      DO100 I=1,11
      X=I-1
      X=X*0.1
      DO100 J=1,13
  100 P(I,J)=X
      WRITE(61,10)
  110 READ(60,20)N,RL,RT,RE
      IF(EOF,60)410,115
  115 WRITE(61,30)N,RL,RT,RE
      DO130 I=1,11
```

```
      X=(I-1)*0.1
      DO120 J=2,12
      Y=J-2
120   H(I,J)=1.0+X*RT-RE*COSF(Y*0.31415927)
      H(I,J)=H(I,J)**3
      H(I,1)=H(I,3)
130   H(I,13)=H(I,11)
      RL=RL*RL*0.10132118
      DO140 I=1,11
      DO140 J=1,13
      A(I,J)=0.0
      B(I,J)=0.0
      C(I,J)=0.0
140   D(I,J)=0.0
      DO150 I=2,10
      DO150 J=2,12
      X=H(I+1,J)+2.0*H(I,J)+H(I-1,J)+RL*(H(I,J+1)+2.0*H(I,J)+H(I,J-1))
      A(I,J)=(H(I+1,J)+H(I,J))/X
      B(I,J)=(H(I-1,J)+H(I,J))/X
      C(I,J)=(RL*(H(I,J+1)+H(I,J)))/X
150   D(I,J)=(RL*(H(I,J-1)+H(I,J)))/X
      X=0.0
```

```
        W=1.0
170 SUM=0.0
        K=K+1
        DO190 I=2.10
        DO180 J=2,12
        X=A(I,J)*P(I+1,J)+B(I,J)*P(I-1,J)+C(I,J)*P(I,J+1)
        X=(X+D(I,J)*P(I,J-1)-P(I,J))*W
        SUM=SUM+X*X
        P(I,J)=P(I,J)+X
180 P(I,13)=P(I,11)
190 P(I,1)=P(I,3)
        W=1.5
        IF(SUM-1.0E-12)200,170,170
200 DO230 J=2,12
        Y=J-2
        T(J)=0.0
        DO220 I=2,10,2
        T(J)=T(J)+P(I-1,J)+P(I,J)+P(I+1,J)*4.0
220 CONTINUE
230 T(J)=T(J)*COSF(Y*0.31415927)
        W=0.0
        DO235 J=3,11,2
```

```
235 W=W+T(J-1)+4.0*T(J)+T(J+1)
    W=W*3.1415927/900.0
    DO240 J=2,12
    T(J)=-25.0*P(1,J)+48.0*P(2,J)-36.0*P(3,J)+16.0*P(4,J)-3.0*P(5,J)
240 T(J)=T(J)*H(1,J)
    X=0.0
    DO250 J=3,11,2
250 X=X+T(J-1)+4.0*T(J)+T(J+1)
    X=X*3.1415927/432.0
    WRITE(61,40)W,X
    DO260 J=2,12
    Y=J-2
260 T(J)=Y*0.1
    WRITE(61,50)(T(J),J=2,12)
    W=0.0
    DO390 I=1,11
    W=I-1
    W=W*0.1
390 WRITE(61,60)W,(P(I,J),J=2,12)
    WRITE(61,70)K SUM
    GOTO110
410 STOP
    END
```

VII.2

Taper bearing program 2

Two-dimensional, compressible flow.

Fluid inertia effects neglected.

A modification of program 1, using

the P to P^2 transformation.

The program has also been expanded

to allow for computation of dynamic

(rotating journal) characteristics.

```
      PROGRAM BEARNG (INPUT,TAPE60=INPUT, OUTPUT,TAPE61=OUTPUT)
      DIMENSION H(12,23),G(12,23),A(12,23),B(12,23),C(12,23),D(12,23),P(12,23),
     1PTEMP(12,23),S(12,23),T(23),U(23),DIFF(12,23),Q(23)
   10 FORMAT(26H1AERODYNAMIC TAPER BEARING)
   20 FORMAT(I5,2I3)
   30 FORMAT(7E10.4)
   40 FORMAT(///9H FILE NO.,I5)
   50 FORMAT(//19H BEARING DIMENSIONS,//7H LENGTH,14X,F7.3,4H IN.,
     1/9H DIAMETER,12X,F7.3,4H IN.,/13H RADIAL TAPER,8X,F7.3,4H IN.,
     2/17H RADIAL CLEARANCE,4X,F7.3,4H IN.)
   60 FORMAT(//21H OPERATING CONDITIONS,//13H ECCENTRICITY,10X,E10.4,
     14H IN.,/14H JOURNAL SPEED,9X,E10.4,7H R.P.M.,/15H INLET PRESSURE,
     28X,E10.4,14H LB/SQ.IN.ABS.,/16H OUTLET PRESSURE,7X,E10.4,4H LB/,
     311H SQ.IN.ABS.,/12H GAS DENSITY,11X,E10.4,20H LB/CU.IN. AT S.T.P.,
     4/14H GAS VISCOSITY,9X,E10.4,32H LB-SEC/SQ.IN. (REYNS) AT S.T.P.,
     5/17H POLYTROPIC INDEX,6X,E10.4)
   70 FORMAT(//25H DIMENSIONLESS PARAMETERS,//13H LENGTH RATIO 8X,F7.3,
     1/12H TAPER RATIO,9X,F7.3 /19H ECCENTRICITY RATIO,2X,F7.3,
     2/20H COMPRESSIBILITY NO.,3X,E10.4)
   75 FORMAT(//17H RELAXATION GRID ,I3,3H  X,I3)
   80 FORMAT(//24H BEARING CHARACTERISTICS,//17H LOAD COEFFICIENT,4X,
     1F7.3/17H FLOW COEFFICIENT,4X,F7.3,/15H ATTITUDE ANGLE,6X,F7.3,
     28H DEGREES,///15H PRESSURE FIELD)
```

```
 90 FORMAT(/10H        Y=,11F8.3)
 95 FORMAT(/13H NO. CYCLES =,I5)
 96 FORMAT(6H SUM =,E10.4)
100 FORMAT(3H X=,F4.1,3H P=,11F8.3)
110 READ(60,20)N,L,M
    IF(EOF,60)310,115
115 READ(60,30)BL,BD,BT,BC,BE,BS,BPI
    READ(60,30)BPO,DENS,VISC,POLY
    WRITE(61,10)
    WRITE(61,40)N
    WRITE(61,50)BL,BD,BT,BC
    WRITE(61,60)BE,BS,BPI,BPO,DENS,VISC,POLY
    DP=BPI-BPO
    RL=2.0*BL/BD
    RT=BT/BC
    RE=BE/BC
    RK=6.0*VISC*BS*3.1415927*BD*BL/(60.0*BC*BC)
    WRITE(61,70)RL,RT,RE,RK
    WRITE(61,75)L,M
    DO130 I=1,11
    DO120 J=2,22
    X=(I-1)*0.1
    P(I,J)=BPO/DP+X
```

```
        Y=J-2
        H(I,J)=1.0+X*RT-RB*COSF(Y*0.31415927)
120 G(I,J)=H(I,J)**3
        P(I,1)=P(I,3)
        P(I,23)=P(I,21)
        H(I,1)=H(I,3)
        H(I,23)=H(I,21)
        G(I,1)=G(I,3)
130 G(I,23)=G(I,21)
        DO140 J=2,22
        P(12,J)=P(10,J)
        H(12,J)=H(10,J)
140 G(12,J)=G(10,J)
        RL=RL*RL*0.1013212
        DO145 I=1,12
        DO145 J=1,23
145 P(I,J)=P(I.J)**2
        W=1.0
        K=0
        DO141 I=2,10
        DO141 J=2.22
        S(I,J)=G(I+1.J)+2.0*G(I J)+G(I-1,J)+RL*(G(I J+1)+2.0*G(I J)+G(I J-1))
        A(I,J)=(G(I+1,J)+G(I,J))/S(I,J)
```

```
      B(I,J)=(G(I-1,J)+G(I,J))/S(I,J)
      C(I,J)=(G(I,J+1)+G(I,J))*RL/S(I,J)
141   D(I,J)=(G(I,J-1)+G(I,J))*RL/S(I,J)
150   K=K+1
      SUM=0.0
      DO190 I=2,10
      DO190 J=2,21
      PTEMP(I,J)=A(I,J)*P(I+1,J)+B(I,J)*P(I-1,J)+C(I,J)*P(I,J+1)
     1+D(I,J)*P(I,J-1)
      DIFF(I,J)=W*PTEMP(I,J)-W*P(I,J)
      P(12,J)=P(10 J)
190   SUM=SUM+DIFF(I,J)**2
      DO200 I=2,10
      DO200 J=2,21
      P(I,J)=P(I,J)+DIFF(I,J)
      P(I,1)=P(I,21)
      P(I,22)=P(I,2)
200   P(I,23)=P(I,3)
      IF(SUM.LT.1.0E-12)210.150
210   DO215 I=1,12
      DO215 J=1,23
215   P(I,J)=SQRT(P(I,J))
```

```
      DO230 J=2,22
      Y=J-2
      T(J)=0.0
      DO220 I=2,20,2
220   T(J)=T(J)+P(I-1,J)+4.0*P(I,J)+P(I+1,J)
      U(J)=T(J)*SINF(Y*0.314159)
230   T(J)=T(J)*COSF(Y*0.314159)
      W=0.0
      V=0.0
      DO240 J=3,21,2
      W=W+T(J-1)+4.0*T(J)+T(J+1)
240   V=V+U(J-1)+4.0*U(J)+U(J+1)
      TANGT=V/W
      ANGLE=ATANF(TANGT)*57.296
      W=SQRT(W*W+V*V)
      W=W*0.00087266
      DO250 J=2,22
      T(J)=-25.0*P(1,J)+48.0*P(2,J)-36.0*P(3,J)+16.0*P(4,J)-3.0*P(5,J)
      Q(J)=T(J)*DP
250   T(J)=T(J)*G(1,J)
      X=0.0
      DO260 J=3,21,2
```

```
260 X=X+T(J-1)+4.0*T(J)+T(J+1)
    X=X*0.0036361
3   WRITE(61,80)W,X,ANGLE
399 FORMAT(1H )
    WRITE(61,399)
400 FORMAT(24H REAL LOAD PER BEARING =,F8.3,3HLB.)
    RLOAD=2*W*BL*BD
    WRITE(61,400)RLOAD
401 FORMAT(24H REAL FLOW PER BEARING =,F8.3,8HS.C.F.M.)
    RFLOW=X*BC**3*BD/VISC/BL/14.4
    WRITE(61,401)RFLOW
    WRITE(61,499)
499 FORMAT(56H     Y    VELOCITY,F.P.S.   FRICTION FACTOR   REYNOLDS NUMBER
   1)
    DO501 J=2,12
    Y=(J-2)*0.1
    VELOC=BC*BC*H(1,J)*H(1,J)*Q(J)/172.8/BL/VISC
     FRICT=4.0*BC*H(1,J)*Q(J)/BL/VELOC/DENS/172.8
     REY=BC*H(1,J)*VELOC*12.0*DENS/386.0*P(I,J)/BPO/VISC*DP
501 WRITE(61,500)Y,VELOC,FRICT,REY
500 FORMAT(X,F4.1,4X,E11.4,6X,E11.4,6X,E11.4)
    GOTO110
```

```
310 STOP
    END
```

VII.3

Taper bearing program 3

One-dimensional, compressible flow.
Fluid inertia effects and flow choking
at the exit annulus are considered.
Runge-Kutta iteration, with the bearing
surface divided into a 40 by 20 mesh.
Load and flow evaluation as for
programs 1 and 2.

```
      PROGRAM INRTIA (INPUT,TAPE60=INPUT, OUTPUT,TAPE61=OUTPUT)
      DIMENSION H(42,23),HS(42,23),G(42,23),P(22,23),T(23),U(23),Q(23),
     1VEL(23),K(23)
10 FORMAT(26H1AERODYNAMIC TAPER BEARING)
20 FORMAT(I5,2I3)
30 FORMAT(7E10.4)
40 FORMAT(///9H FILE NO.,I5)
50 FORMAT(//19H BEARING DIMENSIONS,//7H LENGTH,14X,F7.3,4H IN.,
     1/9H DIAMETER,12X,F7.3,4H IN.,/13H RADIAL TAPER,8X,F7.3,4H IN.,
     2/17H RADIAL CLEARANCE,4X,F7.3,4H IN.)
60 FORMAT(//21H OPERATING CONDITIONS,//13H ECCENTRICITY,10X,E10.4,
     14H IN.,/14H JOURNAL SPEED,9X,E10.4,7H R.P.M.,/15H INLET PRESSURE,
     28X,E10.4,14H LB/SQ.IN.ABS.,/16H OUTLET PRESSURE,7X,E10.4,4H LB/,
     311H SQ.IN.ABS.,/12H GAS DENSITY,11X,E10.4,20H LB/CU.IN. AT S.T.P.,
     4/14H GAS VISCOSITY,9X,E10.4,32H LB-SEC/SQ.IN. (REYNS) AT S.T.P.,
     5/17H POLYTROPIC INDEX,6X,E10.4)
70 FORMAT(//25H DIMENSIONLESS PARAMETERS,//13H LENGTH RATIO 8X,F7.3,
     1/12H TAPER RATIO,9X,F7.3 /19H ECCENTRICITY RATIO,2X,F7.3,
     2/20H COMPRESSIBILITY NO.,3X,E10.4)
75 FORMAT(//17H RELAXATION GRID ,I3,3H  X,I3)
80 FORMAT(//24H BEARING CHARACTERISTICS,//17H LOAD COEFFICIENT,4X,
     1F7.3/17H FLOW COEFFICIENT,4X,F7.3,/15H ATTITUDE ANGLE,6X,F7.3,
     28H DEGREES,///15H PRESSURE FIELD)
```

```
 90 FORMAT(/10H        Y=,11F8.3)
 95 FORMAT(/13H NO. CYCLES =,I5)
 96 FORMAT(6H SUM =,E10.4)
100 FORMAT(3H X=,F4.1,3H P=,11F8.3)
110 READ(60,20)N,L,M
    IF(EOF,60)310,115
115 READ(60,30)BL,BD,BT,BC,BE,BS,BPI
    READ(60,30)BPO,DENS,VISC,POLY
    WRITE(61,10)
    WRITE(61,40)N
    WRITE(61,50)BL,BD,BT,BC
    WRITE(61,60)BE,BS,BPI,BPO,DENS,VISC,POLY
    DP=BPI-BPO
    RL=2.0*BL/BD
    RT=BT/BC
    RE=BE/BC
    RK=6.0*VISC*BS*3.1415927*BD*BL/(60.0*BC*BC)
    WRITE(61,70)RL,RT,RE,RK
    WRITE(61,75)L,M
    DO120 I=1,21
    X=(I-1)/20.0
    DO119 J=2,22
119 P(I,J)=BPO+X*DP
```

```
      P(I,1)=P(I,3)
120 P(I,23)=P(I,21)
      DO130 I=1,41
      X=I-1
      X=X/40.0
      DO125 J=2,22
      Y=J-2
      H(I,J)=1.0+X*RT-RB*COSF(Y*0.31415927)
      HS(I,J)=H(I,J)**2
125 G(I,J)=H(I,J)**3
      H(I,1)=H(I,3)
      H(I,23)=H(I,21)
      HS(I,1)=HS(I,3)
      HS(I,23)=HS(I,21)
      G(I,1)=G(I,3)
130 G(I,23)=G(I,21)
      DENS=DENS/386.0
      W=1.0
      BCS=BC**2
      B1=SQRT(BPO*DENS*BCS/10.0)
      DO200 J=2,12
      K(J)=0
```

```
      BP2=BP0
150 CONTINUE
      P(1,J)=BP2
      B2=B1
141 CONTINUE
      B2S=B2**2
      Z=6.0*B1*BL*(BC*RT*B2-10.0*VISC)/BC
      DO170 I=2,21
      AO=P(I-1,J)*Z/H(2*I-3,J)/(P(I-1,J)*DENS*(P(I-1,J)/BP2)**POLY*BCS*
     1HS(2*I-3,J)*5.0-6.0*B2S)/POLY
      IF((P(I-1,J)+AO/2.0).GT.0.0)GOTO160
      B1=B1/1.9
      GOTO150
160 A1=(P(I-1,J)+AO/2.0)*Z/H(2*I-2,J)/((P(I-1,J)+AO/2.0)*DENS*((P(I-1,
     1J)+AO/2.0)/BP2)**POLY*BCS*HS(2*I-2,J)*5.0-6.0*B2S)/POLY
      IF((P(I-1,J)+A1/2.0).GT.0.0)GOTO161
      B1=B1/1.9
      GOTO150
161 A2=(P(I-1,J)+A1/2.0)*Z/H(2*I-2,J)/((P(I-1,J)+A1/2.0)*DENS*((P(I-1,
     1J)+A1/2.0)/BP2)**POLY*BCS*HS(2*I-2,J)*5.0-6.0*B2S)/POLY
      IF((P(I-1,J)+A2)GT.0.0)GOTO162
```

```
      B1=B1/1.9
      GOTO150
162 A3=(P(I-1,J)+A2)*Z/H(2*I-1,J)/((P(I-1,J)+A2)*DENS*((P(I-1,J)+A2)/B
   1B2)**POLY*BCS*HS(2*I-1 J)*5.0-6.0*B2S)/POLY
170 P(I,J)=P(I-1,J)+(A0+2*A1+2*A2+A3)/6.0
      Q(J)=-25.0*P(1,J)+48.0*P(2,J)-36.0*P(3,J)+16.0*P(4,J)-3.0*P(5,J)
      VELOC=BC*BC*H(1,J)*H(1,J)*Q(J)/172.8/BL/VISC
      IF(K(J).GT.5)174,173
174 IF(VELOC.GT.1100.0)171,172
171 BP2=1.01*BP2
      GOTO173
172 IF(ABS(BPI-P(21,J)).LT.BPI/1000.0)GOTO200
173 CONTINUE
      K(J)=K(J)+1
      IF(K(J).GT.200)GOTO200
      DIF=BPI-P(21,J)
      F=(BPI+W*DIF)/BPI
      IF(F.GT.2.0)GOTO180
      IF(F.LT.0.0)GOTO190
      B1=B1*F
```

```
      GOTO150
180 F=2.0
      B1=B1*F
      GOTO150
190 F=0.1
      B1=B1*F
      GOTO150
200 CONTINUE
      DO270 J=2,12
      Y=J-2
      Y=Y*0.05
270 T(J)=Y
      WRITE(61,90)(T(J),J=2,12)
      DO290 I=1,21
      W=I-1
      W=W/20.0
290 WRITE(61,100)W,(P(I,J),J=2,12)
      DO300 J=3,11
      DO300 I=1,21
300 P(I,24-J)=P(I,J)
```

```
      DO230 J=2,22
      Y=J-2
      T(J)=0.0
      DO220 I=2,20,2
220   T(J)=T(J)+P(I-1,J)+4.0*P(I,J)+P(I+1,J)
      U(J)=T(J)*SINF(Y*0.314159)
230   T(J)=T(J)*COSF(Y*0.314159)
      W=0.0
      V=0.0
      DO240 J=3,21,2
      W=W+T(J-1)+4.0*T(J)+T(J+1)
240   V=V+U(J-1)+4.0*U(J)+U(J+1)
      TANGT=V/W
      ANGLE=ATANF(TANGT)*57.296
      W=SQRT(W*W+V*V)
      W=W*0.00087266/DP
      DO250 J=2,22
      T(J)=-25.0*P(1,J)+48.0*P(2,J)-36.0*P(3,J)+16.0*P(4,J)-3.0*P(5,J)
      Q(J)=T(J)
250   T(J)=T(J)*G(1,J)
      X=0.0
      DO260 J=3,21,2
```

```
260 X=X+T(J-1)+4.0*T(J)+T(J+1)
    X=X*0.0036361
3   WRITE(61,80)W,X,ANGLE
399 FORMAT(1H )
    WRITE(61,399)
400 FORMAT(24H REAL LOAD PER BEARING =,F8.3,3HLB.)
    RLOAD=2*W*BL*BD
    WRITE(61,400)RLOAD
401 FORMAT(24H REAL FLOW PER BEARING =,F8.3,8HS.C.F.M.)
    RFLOW=X*BC**3*BD/VISC/BL/14.4
    WRITE(61,401)RFLOW
    WRITE(61,499)
499 FORMAT(56H     Y    VELOCITY,F.P.S.  FRICTION FACTOR  REYNOLDS NUMBER
   1)
    DO501 J=2,12
    Y=(J-2)*0.1
    VELOC=BC*BC*H(1,J)*H(1,J)*Q(J)/172.8/BL/VISC
    FRICT=4.0*BC*H(1 J)*Q(J)/BL/VELOC/DENS/172.8/386.0
    REY=BC*H(1,J)*VELOC*12.0*DENS*P(1,J)/BPO/VISC
501 WRITE(61,500)Y,VELOC,FRICT,REY
500 FORMAT(X,F4.1,4X,E11.4,6X,E11.4,6X,E11.4)
    GOTO110
```

310 STOP
    END

VII.4

Step bearing program 1

One-dimensional, incompressible flow.
Evaluation of the analytical expressions
derived in Section 3.4.1
The two-dimensional case was computed by
applying the expressions for the stepped
clearance $(H(I,J))$ used in this program
to programs VII.1 and VII.2, and relaxing
as before.

```
      PROGRAM STPBRG (INPUT,TAPE60=INPUT,  OUTPUT,TAPE61=OUTPUT)
      DIMENSION H1(23),H2(23),P(82,23),T(23),U(23)
10 FORMAT(25H1HYDROSTATIC STEP BEARING)
20 FORMAT(I5,2I3)
30 FORMAT(7E10.4)
40 FORMAT(///9H FILE NO.,I5)
50 FORMAT(//19H BEARING DIMENSIONS,//7H LENGTH,14X,F7.3,4H IN.,
   1/9H DIAMETER,12X,F7.3,4H IN.,/13H RADIAL  STEP,8X,F7.3,4H IN.,
   2/17H RADIAL CLEARANCE,4X,F7.3,4H IN.)
60 FORMAT(//21H OPERATING CONDITIONS,//13H ECCENTRICITY,10X,E10.4,
   14H IN.,/14H JOURNAL SPEED,9X,E10.4,7H R.P.M.,/15H INLET PRESSURE,
   28X,E10.4,14H LB/SQ.IN.ABS.,/16H OUTLET PRESSURE,7X,E10.4,4H LB/,
   311H SQ.IN.ABS.,/12H GAS DENSITY,11X,E10.4,20H LB/CU.IN. AT S.T.P.,
   4/14H GAS VISCOSITY,9X,E10.4,32H LB-SEC/SQ.IN. (REYNS) AT S.T.P.,
   5/17H POLYTROPIC INDEX,6X,E10.4)
70 FORMAT(//25H DIMENSIONLESS PARAMETERS,//13H LENGTH RATIO 8X,F7.3,
   1/12H  STEP RATIO,9X,F7.3 /19H ECCENTRICITY RATIO,2X,F7.3,
   2/20H COMPRESSIBILITY NO.,3X,E10.4)
75 FORMAT(//17H RELAXATION GRID ,I3,3H  X,I3)
80 FORMAT(//24H BEARING CHARACTERISTICS,//17H LOAD COEFFICIENT,4X,
   1F7.3/17H FLOW COEFFICIENT,4X,F7.3,/15H ATTITUDE ANGLE,6X,F7.3,
   28H DEGREES,///15H PRESSURE FIELD)
85 FORMAT(20H STEP LENGTH RATIO =,F7.4)
```

```
   90 FORMAT(/10H          Y=,11F8.3)
   95 FORMAT(/13H NO. CYCLES =,I5)
   96 FORMAT(6H SUM =,E10.4)
  100 FORMAT(3H X=,F4.1,3H P=,11F8.3)
  110 READ(60,20)N,L,M
      IF(EOF,60)310,115
  115 READ(60,30)BL,BD,BT,BC,BE,BS,BPI
      READ(60,30)BPO,DENS,VISC,POLY,SLR
      WRITE(61,10)
      WRITE(61,40)N
      WRITE(61,50)BL,BD,BT,BC
      WRITE(61,60)BE,BS,BPI,BPO,DENS,VISC,POLY
      DP=BPI-BPO
      RL=2.0*BL/BD
      RS=BT/BC
      RE=BE/BC
      RK=6.0*VISC*BS*3.1415927*BD*BL/(60.0*BC*BC)
      WRITE(61,70)RL,RT,RE,RK
      WRITE(61,75)L,M
      DO15 J=2,12
      P(81,J)=64.7
   15 P(81,24-J)=P(81,J)
      DO120 J=2,22
```

```
      Y=J-2
      H1(J)=1.0-RE*COSF(Y*0.31415927)
120   H2(J)=H1(J)+RS
      K=80.0*SLR+0.025
      K=K+1
      SL1=SLR
      SL2=1.0-SLR
      DO140 J=2,22
      RH3=(H2(J)/H1(J))**3
      DO130 I=1,K
      X=(I-1)/80.0
130   P(I,J)=BP0+(P(81,J)-BP0)*RH3/(RH3*SL1+SL2)*X
      DO140 I=K,81
      X=1.0-(I-1)/80.0
140   P(I,J)=P(81,J)-(P(81,J)-BP0)/(RH3*SL1+SL2)*X
      DO300 J=3,11
      DO300 I=1,81
300   P(I,24-J)=P(I,J)
      DO230 J=2,22
      Y=J-2
      T(J)=0.0
      DO220 I=2,80,2
```

```
220 T(J)=T(J)+P(I-1,J)+4.0*P(I,J)+P(I+1,J)
    U(J)=T(J)*SINF(Y*0.31415927)
230 T(J)=T(J)*COSF(Y*0.31415927)
    W=0.0
    V=0.0
    DO240 J=3,21,2
    W=W+T(J-1)+4.0*T(J)+T(J+1)
240 V=V+U(J-1)+4.0*U(J)+U(J+1)
    TANGT=V/W
    ANGLE=ATANF(TANGT)*57.296
    W=SQRT(W*W+V*V)
    W=W*0.00021817
    DO900 J=2,22
900 G(1,J)=H1(J)**3
    DO250 J=2,22
    T(J)=-25.0*P(1,J)+48.0*P(2,J)-36.0*P(3,J)+16.0*P(4,J)-3.0*P(5,J)
250 T(J)=T(J)*G(1,J)
    X=0.0
    DO260 J=3,21,2
260 X=X+T(J-1)+4.0*T(J)+T(J+1)
    X=X*0.0036361
    WRITE(61,85)SLR
```

```
      WRITE(61,80)W,X,ANGLE
      WRITE(61,399)
399 FORMAT(1H )
400 FORMAT(24H REAL LOAD PER BEARING =,F8.3,3HLB.)
      RLOAD=2*W*BL*BD
      WRITE(61,400)RLOAD
401 FORMAT(24H REAL FLOW PER BEARING =,F8.3,8HS.C.F.M.)
      RFLOW=X*BC**3*BD/VISC/BL/14.4
      WRITE(61,401)RFLOW
310 STOP
      END
```

APPENDIX VIII   **VISCOSITY – TEMPERATURE CHARTS**

This Appendix contains

(1)   Chart VIII-1   for SAE 10W oil
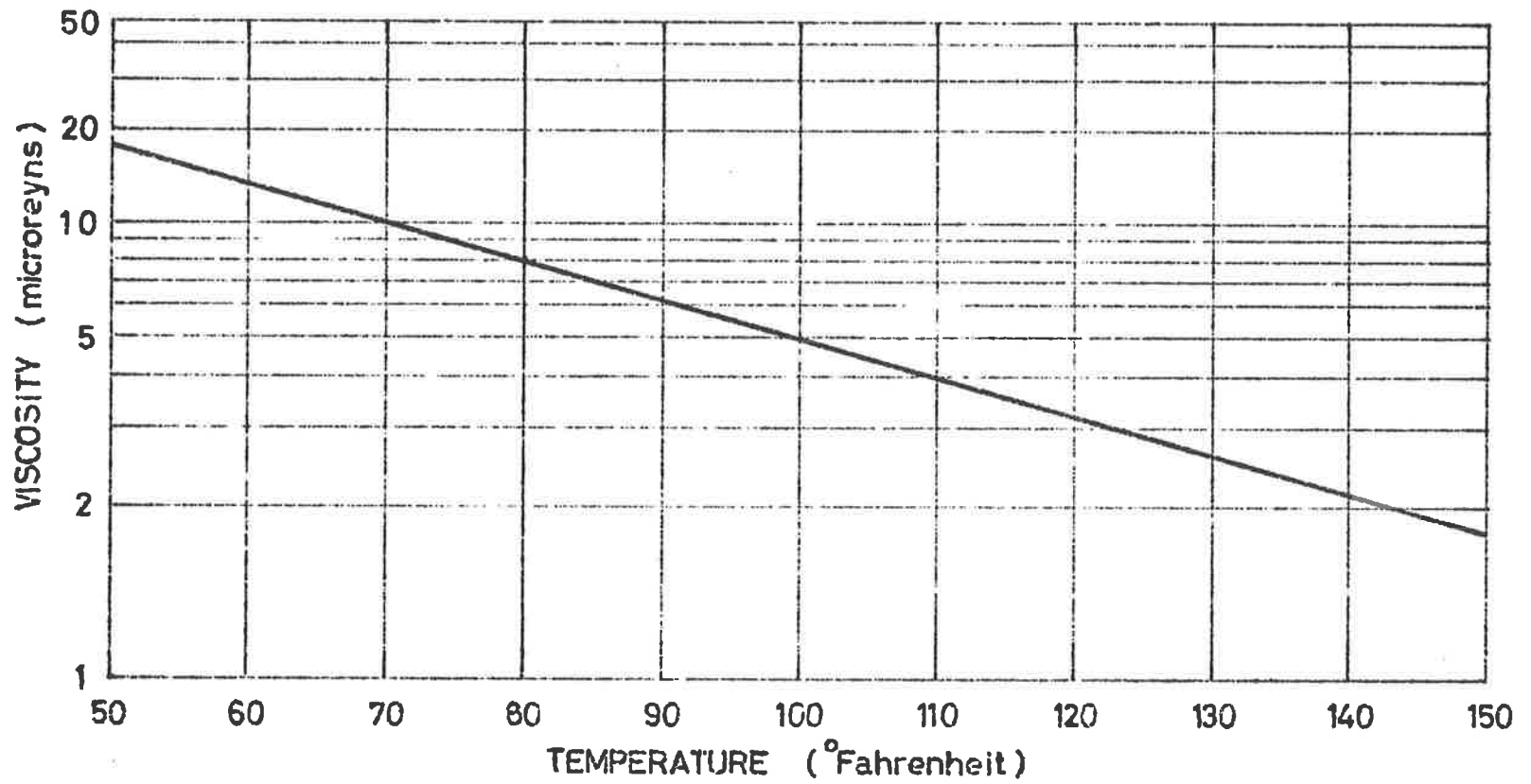
(2)   Chart VIII-2   for air

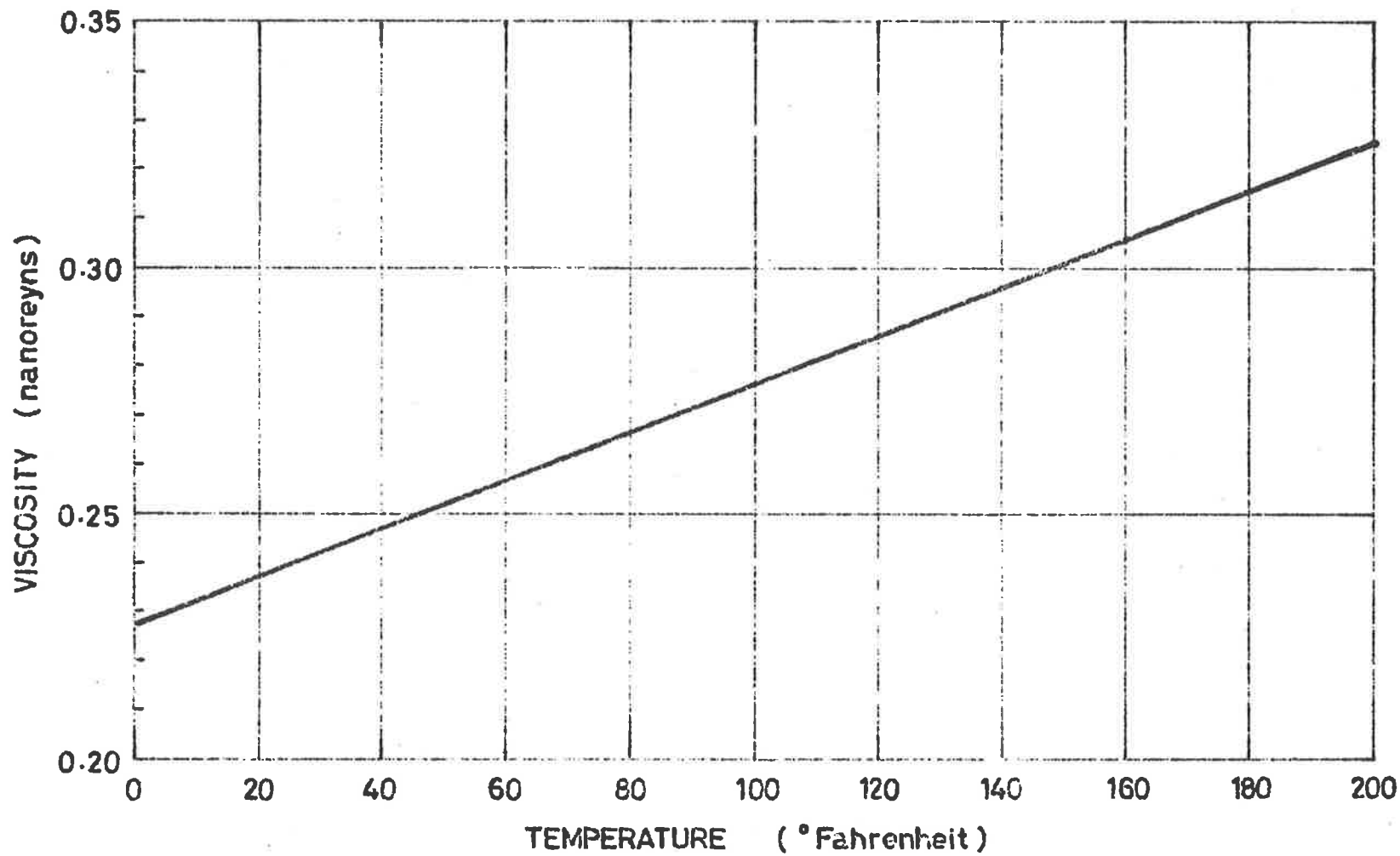FIGURE VIII-1 Viscosity – Temperature chart for SAE 10W oil (ref. 11).

FIGURE VIII-2   Viscosity - temperature chart for air (ref. 7).

APPENDIX IX   THE DISPLACEMENT TRANSDUCER

      The design of the displacement transducer was not a part of this project, and is not claimed as the work of the author. However, it was considered that, for completeness, the basic circuits of the instrument (which was built locally for this project) should be included here.

      The information contained in this Appendix is taken from an article by J.L.Hoffman published in the October, 1962 issue of the ISA Transactions.

IX.1   Description

The instrument is described as being suitable for clearance measurement of high speed rotating journal bearings. It consists of small, non-contacting, eddycurrent transducers, serving as distance detectors, which sense shaft position and vibration amplitude.

By means of a time-sharing system, signals from the pickups are fed to an oscilloscope along with a calibration signal. These appear in polar form as a journal trace (a point) and a clearance circle. Thus, continuous inspection and study of the journal-to-bearing relationship is possible.

Measurements of radial journal motion as well as rotating clearance values may be read directly on a digital indicating dial.

The transducers were shown to display linear characteristics to within 2% for displacements up to 0.020in., and to better than 1% where the displacements did not exceed 0.003in.

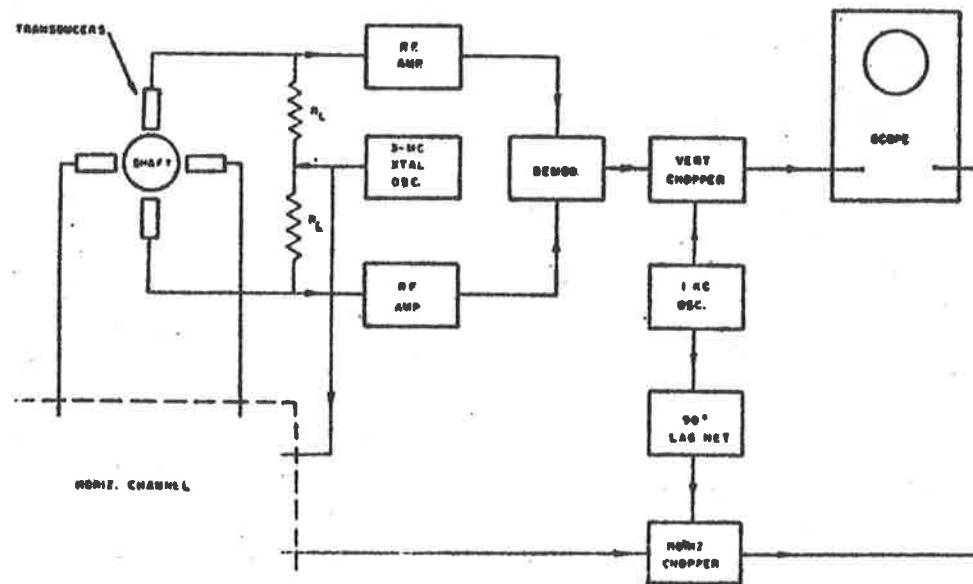The system response is essentially uniform from 0 to 18,000 cycles per second.

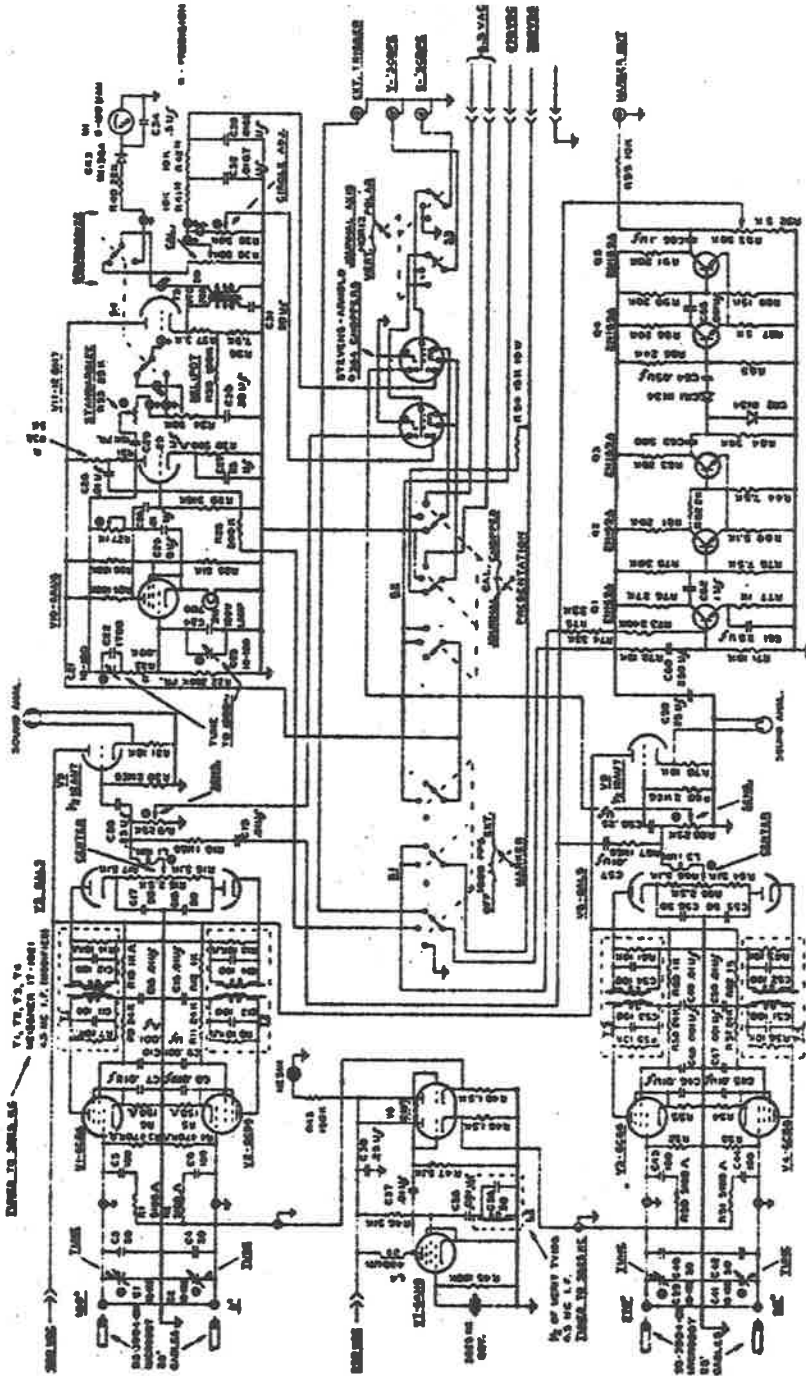FIGURE IX.1   System diagram (vertical channel only)

FIGURE IX.2 Instrument circuit diagram

PUBLICATIONS

During the course of this research project, several sections of the work have been published. The papers accepted for publication include:-

1 MANNAM, J., FOWLER, J.H. & CARPENTER, A.L. "Tapered Lands Hydrostatic Bearings"- Lubrication & Wear Convention, Proc. I.Mech.E., Vol. 179, 1964-65, Part 3J.

2 CARPENTER, A.L. & MANNAM, J. "Internally Compensated, Externally Pressurised Gas Bearings"- Third Australasian Conference on Hydraulics & Fluid Mechanics, Sydney, 1968.

3 CARPENTER, A.L. & MANNAM, J. "Tapered Land Bearings"- Fourth Biannual Gas Bearing Symposium, University of Southampton, 1969